

e-ISSN 1308-8459

Official Publication of the Turkish Society of Anatomy and Clinical Anatomy

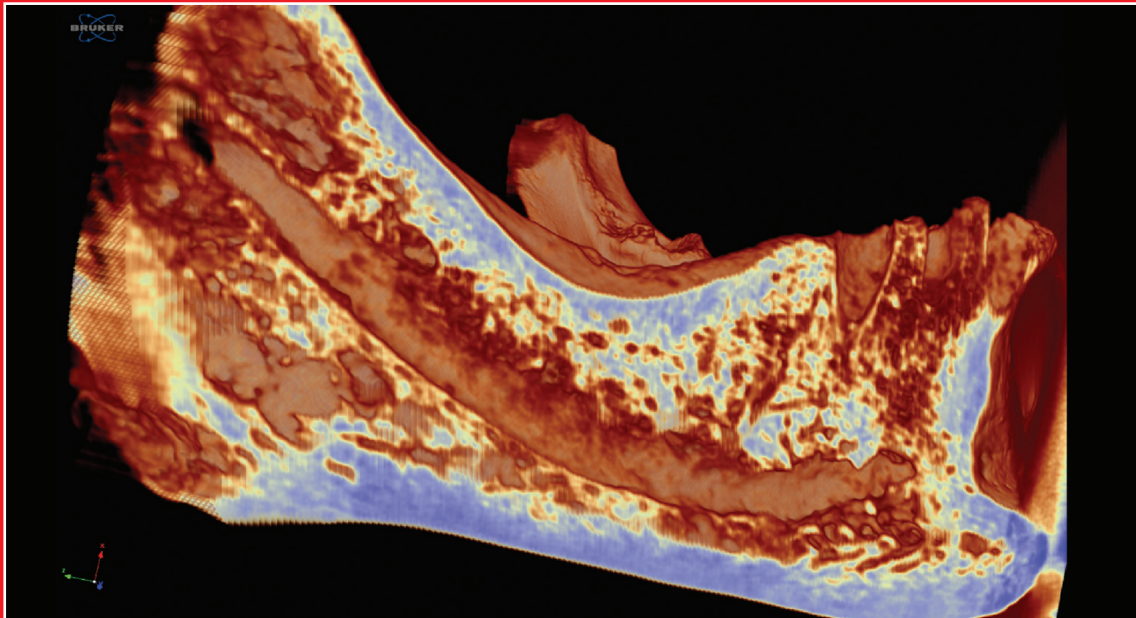
<http://dergipark.org.tr/en/pub/anatomy>

anatomy

An International Journal of Experimental and Clinical Anatomy

Volume 16 / Issue 1 / April 2022

Published three times a year



Official Publication of the Turkish Society of Anatomy and Clinical Anatomy

Aim and Scope

Anatomy, an international journal of experimental and clinical anatomy, is a peer-reviewed journal published three times a year with an objective to publish manuscripts with high scientific quality from all areas of anatomy. The journal offers a forum for anatomical investigations involving gross, histologic, developmental, neurological, radiological and clinical anatomy, and anatomy teaching methods and techniques. The journal is open to original papers covering a link between gross anatomy and areas related with clinical anatomy such as experimental and functional anatomy, neuroanatomy, comparative anatomy, modern imaging techniques, molecular biology, cell biology, embryology, morphological studies of veterinary discipline, and teaching anatomy. The journal is currently indexing and abstracting in TUBITAK ULAKBIM Turkish Medical Index, Proquest, EBSCO Host, Index Copernicus and Google Scholar.

Publication Ethics

Anatomy is committed to upholding the highest standards of publication ethics and observes the principles of Journal's Publication Ethics and Malpractice Statement which is based on the recommendations and guidelines for journal editors developed by the Committee on Publication Ethics (COPE), Council of Science Editors (CSE), World Association of Medical Editors (WAME) and International Committee of Medical Journal Editors (ICMJE). For detailed information please visit the online version of the journal which is available at <https://dergipark.org.tr/tr/pub/anatomy>

Authorship

All persons designated as authors should have participated sufficiently in the work to take public responsibility for the content of the manuscript. Authorship credit should be based on substantial contributions to (1) conception and design or analysis and interpretation of data, (2) drafting of the manuscript or revising it for important intellectual content and, (3) final approval of the version to be published. The Editor may require the authors to justify assignment of authorship. In the case of collective authorship, the key persons responsible for the article should be identified and others contributing to the work should be recognized with proper acknowledgment.

Copyright

Copyright © 2022, by the Turkish Society of Anatomy and Clinical Anatomy, TSACA. All rights reserved. No part of this publication may be reproduced, stored or transmitted in any form without permission in writing from the copyright holder beforehand, exceptionally for research purpose, criticism or review. The publisher and the Turkish Society of Anatomy and Clinical Anatomy assume no liability for any material published in the journal. All statements are the responsibility of the authors. Although all advertising material is expected to conform ethical standards, inclusion in this publication does not constitute a guarantee or endorsement of the quality or value of such product or of the claims made of it by its manufacturer. Permission requests should be addressed to the publisher.

Publisher

Deomed Publishing
Gür Sok. No:7/B Kadıköy, İstanbul, Turkey
Phone: +90 216 414 83 43 (Pbx) / Fax: +90 216 414 83 42
www.deomed.com / e-mail: medya@deomed.com

Publication Information

Anatomy (e-ISSN 1308-8459) as an open access electronic journal is published by Deomed Publishing, İstanbul, for the Turkish Society of Anatomy and Clinical Anatomy, TSACA. Due the Press Law of Turkish Republic dated as June 26, 2004 and numbered as 5187, this publication is classified as a periodical in English language.

Ownership

On behalf of the Turkish Society of Anatomy and Clinical Anatomy, Ahmet Kağan Karabulut, MD, PhD; Konya

Editor-in-Chief

Nihal Apaydin, MD
Department of Anatomy,
Faculty of Medicine, Ankara University,
06100, Sıhhiye, Ankara, Turkey
Phone: 0090 312 595 82 48
e-mail: napaydin@gmail.com; napaydin@medicine.ankara.edu.tr

Administrative Office

Güven Mah. Güvenlik Cad. Onlar Ap. 129/2 Aşağı Ayrancı, Ankara
Phone: +90 312 447 55 52-53

Submission of Manuscripts

Manuscripts should be submitted at our manuscript submission and information portal <https://dergipark.org.tr/en/pub/anatomy>

Categories of Articles

- **Original Articles** describe substantial original research that falls within the scope of the Journal.
- **Teaching Anatomy** section contains regular or all formats of papers which are relevant to comparing teaching models or to introducing novel techniques, including especially the own experiences of the authors.
- **Reviews** section highlights current development in relevant areas of anatomy. The reviews are generally invited; other prospective authors should consult with the Editor-in-Chief.
- **Case Reports** include new, noteworthy or unusual cases which could be of help for basic notions and clinical practice.
- **Technical Note** articles cover technical innovations and developments with a specific technique or procedure or a modification of an existing technique. They should be sectioned like an original research article but not exceed 2000 words.
- **Viewpoint** articles give opinions on controversial topics or future projections, some of these are invited.
- **Historical View** category presents overview articles about historical sections from all areas of anatomy.
- **Terminology Zone** category is a platform for the articles which discuss some terminological controversies or opinions.

The categories above are peer-reviewed. They should include abstract and keywords. There are also categories including Letters to the Editor, Book Reviews, Abstracts, Obituary, News and Announcements which do not require a peer review process.

For detailed instructions concerning the submission of manuscripts, please refer to the Instructions to Authors.

Advertising and Reprint Requests

Please direct to publisher. e-mail: medya@deomed.com

Honorary Editor

Doğan Akşit, Ankara, Turkey

Founding Editors

Salih Murat Akkın, Gaziantep, Turkey

Hakan Hamdi Çelik, Ankara, Turkey

Former Editors-in-Chief and Advising Editors

Salih Murat Akkın (2007–2013)

Gaziantep, Turkey

Gülgün Şengül (2014–2019)

Izmir, Turkey

Editor-in-Chief

Nihal Apaydın, Ankara, Turkey

Editors

Ceren Günenç Beşer, Ankara, Turkey

Zeliha Kurtoğlu Olgunus, Mersin, Turkey

Luis Puelles, Murcia, Spain

Gülgün Şengül, Izmir, Turkey

Shane Tubbs, Birmingham, AL, USA

Emel Ulupınar, Eskişehir, Turkey

Associate Editors

Vaclav Baca, Prague, Czech Republic

Çağatay Barut, Istanbul, Turkey

Jon Cornwall, Dunedin, New Zealand

Ayhan Cömert, Ankara, Turkey

Mirela Eric, Novi Sad, Serbia

Georg Feigl, Graz, Austria

Quentin Fogg, Melbourne, Australia

David Kachlik, Prague, Czech Republic

Marko Korschake, Innsbruck, Austria

Scott Lozanoff, Honolulu, HI, USA

Levent Sarıkçıoğlu, Antalya, Turkey

Cristian Stefan, Boston, MA, USA

İlkan Tatar, Ankara, Turkey

Trifon Totlis, Thessaloniki, Greece

Executive Board of Turkish Society of Anatomy and Clinical Anatomy

Piraye Kervancıoğlu (President)

Çağatay Barut (Vice President)

Nadire Ünver Doğan (Vice President)

İlke Ali Gürses (Secretary General)

Ceren Günenç Beşer (Treasurer)

Esat Adıgüzel (Member)

Selçuk Tunalı (Member)

Scientific Advisory Board

Peter H. Abrahams
Cambridge, UK

Halil İbrahim Açar
Ankara, Turkey

Marian Adamkov
Martin, Slovakia

Esat Adıgüzel
Denizli, Turkey

Mustafa Aktekin
Istanbul, Turkey

Abduelmenem Alashkham
Edinburgh, UK

Mahindra Kumar Anand
Gujarat, India

Serap Arbak
Istanbul, Turkey

Alp Bayramoğlu
Istanbul, Turkey

Brion Benninger
Lebanon, OR, USA

Susana Biasutto
Cordoba, Argentina

Dragica Bobinac
Rijeka, Croatia

David Bolender
Milwaukee, WI, USA

Eric Brenner
Innsbruck, Austria

Mustafa Büyükmumcu
Konya, Turkey

Richard Halti Cabral
Sao Paulo, Brazil

Safiye Çavdar
Istanbul, Turkey

Katharina D'Herde
Ghent, Belgium

Fabrice Duparc
Rouen, France

Behice Durgun
Adana, Turkey

İzzet Duyar
Istanbul, Turkey

Mete Ertürk
Izmir, Turkey

Reha Erzurumlu
Baltimore, MD, USA

Ali Fırat Esmen
Ankara, Turkey

António José Gonçalves Ferreira
Lisboa, Portugal

Christian Fontaine
Lille, France

Figen Gövs Gökmen
Izmir, Turkey

Rod Green
Bendigo, Australia

Bruno Grignon
Nancy Cedex, France

Nadir Gülekon
Ankara, Turkey

Mürvet Hayran
Izmir, Turkey

David Heylings
Norwich, UK

Lazar Jelev
Sofia, Bulgaria

Samet Kapakin
Erzurum, Turkey

Ahmet Kağan Karabulut
Konya, Turkey

S. Tuna Karahan
Ankara, Turkey

Simel Kendir
Ankara, Turkey

Piraye Kervancıoğlu
Gaziantep, Turkey

Hee-Jin Kim
Seoul, Korea

Necdet Kocacıyık
Ankara, Turkey

Cem Kopuz
Samsun, Turkey

Mustafa Ayberk Kurt
Istanbul, Turkey

Marios Loukas
Grenada, West Indies

Veronica Macchi
Padua, Italy

Ali Mirjalili
Auckland, New Zealand

Bernard Moxham
Cardiff, Wales, UK

Konstantinos Natsis
Thessaloniki, Greece

Lia Lucas Neto
Lisbon, Portugal

Helen Nicholson
Dunedin, New Zealand

Davut Özbağ
Malatya, Turkey

P. Hande Özdinler
Chicago, IL, USA

Adnan Öztürk
Istanbul, Turkey

Mehmet Hakan Öztürk
Mersin, Turkey

Friedrich Paulsen
Erlangen, Germany

Wojciech Pawlina
Rochester, MN, USA

Tuncay Veysel Peker
Ankara, Turkey

Vid Persaud
Winnipeg, MB, Canada

David Porta
Louisville, KY, USA

Jose Ramon Sanudo
Madrid, Spain

Tatsuo Sato
Tokyo, Japan

Mohammadali M. Shoja
Birmingham, AL, USA

Ahmet Sinav
Istanbul, Turkey

Takis Skandalakis
Athens, Greece

Isabel Stabile
Malta

Vildan Sümbüloğlu
Gaziantep, Turkey

(Biostatistics)

Muzaffer Şeker
Konya, Turkey

Erdoğan Şendimir
Bursa, Turkey

İbrahim Tekdemir
Ankara, Turkey

Hironubu Tokuno
Tokyo, Japan

Mehmet İbrahim Tuğlu
Manisa, Turkey

Selçuk Tunalı
Ankara, Turkey

Uğur Türe
Istanbul, Turkey

Aysun Uz
Ankara, Turkey

Mehmet Üzel
Istanbul, Turkey

Ivan Varga
Bratislava, Slovakia

Tuncay Varol
Manisa, Turkey

Stephanie Woodley
Otago, New Zealand

Bülent Yalçın
Ankara, Turkey

Gazi Yaşargil
Istanbul, Turkey

Hiroshi Yorifuji
Gunma, Japan

Anatomy, an international journal of experimental and clinical anatomy, is the official publication of the Turkish Society of Anatomy and Clinical Anatomy, TSACA. It is a peer-reviewed e-journal that publishes scientific articles in English. For a manuscript to be published in the journal, it should not be published previously in another journal or as full text in congress books and should be found relevant by the editorial board. Also, manuscripts submitted to Anatomy must not be under consideration by any other journal. Relevant manuscripts undergo conventional peer review procedure (at least three reviewers). For the publication of accepted manuscripts, author(s) should reveal to the Editor-in-Chief any conflict of interest and transfer the copyright to the Turkish Society of Anatomy and Clinical Anatomy, TSACA.

In the Materials and Methods section of the manuscripts where experimental studies on humans are presented, a statement that informed consent was obtained from each volunteer or patient after explanation of the procedures should be included. This section also should contain a statement that the investigation conforms with the principles outlined in the appropriate version of 1964 Declaration of Helsinki. For studies involving animals, all work must have been conducted according to applicable national and international guidelines. Prior approval must have been obtained for all protocols from the relevant author's institutional or other appropriate ethics committee, and the institution name and permit numbers must be provided at submission.

Anatomical terms used should comply with Terminologia Anatomica by FCAT (1998).

No publication cost is charged for the manuscripts but reprints and color printings are at authors' cost.

Preparation of manuscripts

During the preparation of the manuscripts, uniform requirements of the International Committee of Medical Journal Editors, a part of which is stated below, are valid (see ICMJE). Uniform requirements for manuscripts submitted to biomedical journals. Updated content is available at www.icmje.org. The manuscript should be typed double-spaced on one side of a 21x29.7 cm (A4) blank sheet of paper. At the top, bottom and right and left sides of the pages a space of 2.5 cm should be left and all the pages should be numbered except for the title page.

Manuscripts should not exceed 15 pages (except for the title page). They must be accompanied by a cover letter signed by corresponding author and the Conflicts of Interest Disclosure Statement and Copyright Transfer Form signed by all authors. The contents of the manuscript (original articles and articles for Teaching Anatomy category) should include: 1- Title Page, 2- Abstract and Keywords, 3- Introduction, 4- Materials and Methods, 5- Results, 6- Discussion (Conclusion and/or Acknowledgement if necessary), 7- References

Title page

In all manuscripts the title of the manuscript should be written at the top and the full names and surnames and titles of the authors beneath. These should be followed with the affiliation of the author. Manuscripts with long titles are better accompanied underneath by a short version (maximum 80 characters) to be published as running head. In the title page the correspondence address and telephone, fax and e-mail should be written. At the bottom of this page, if present, funding sources supporting the work should be written with full names of all funding organizations and grant numbers. It should also be indicated in a separate line if the study has already been presented in a congress or likewise scientific meeting. Other information such as name and affiliation are not to be indicated in pages other than the title page.

Abstract

Abstract should be written after the title in 100–250 words. In original articles and articles prepared in IMRAD format for Teaching Anatomy category the abstract should be structured under sections Objectives, Methods, Results and Conclusion. Following the abstract at least 3 keywords should be added in alphabetical order separated by semicolons.

References

Authors should provide direct references to original research sources. References should be numbered consecutively in square brackets, according to the order in which they are first mentioned in the manuscript. They should follow the standards detailed in the NLM's Citing Medicine, 2nd edition (Citing medicine: the NLM style guide for authors, editors, and publishers [Internet]. 2nd edition. Updated content is available at www.ncbi.nlm.nih.gov/books/NBK7256). The names of all contributing authors should be listed, and should be in the order they appear in the original reference. The author is responsible for the accuracy and completeness of references. When necessary, a copy of a referred article can be requested from the author. Journal names should be abbreviated as in *Index Medicus*. Examples of main reference types are shown below.

- **Journal articles:** Author's name(s), article title, journal title (abbreviated), year of publication, volume number, inclusive pages
 - *Standard journal article:* Sargon MF, Celik HH, Aksit MD, Karaagaoglu E. Quantitative analysis of myelinated axons of corpus callosum in the human brain. *Int J Neurosci* 2007;117:749–55.

- *Journal article with indication article published electronically before print:* Sengul G, Fu Y, Yu Y, Paxinos G. Spinal cord projections to the cerebellum in the mouse. *Brain Struct Funct* Epub 2014 Jul 10. DOI 10.1007/s00429-014-0840-7.

- **Books:** Author's name(s), book title, place of publication, publisher, year of publication, total pages (entire book) or inclusive pages (contribution to a book or chapter in a book)

– Entire book:

- *Standard entire book:* Sengul G, Watson C, Tanaka I, Paxinos G. Atlas of the spinal cord of the rat, mouse, marmoset, rhesus and human. San Diego (CA): Academic Press Elsevier; 2013. 360 p.

- *Book with organization as author:* Federative Committee of Anatomical Terminology (FCAT). *Terminologia anatomica*. Stuttgart: Thieme; 1998. 292 p.

- *Citation to a book on the Internet:* Bergman RA, Afifi AK, Miyauchi R. Illustrated encyclopedia of human anatomic variation. Opus I: muscular system [Internet]. [Revised on March 24, 2015] Available from: <http://www.anatomyatlases.org/AnatomicVariants/AnatomyHP.shtml>

– Contribution to a book:

- *Standard reference to a contributed chapter:* Potten CS, Wilson JW. Development of epithelial stem cell concepts. In: Lanza R, Gearhart J, Blau H, Melton D, Moore M, Pedersen R, Thomson J, West M, editors. *Handbook of stem cell*. Vol. 2, Adult and fetal. Amsterdam: Elsevier; 2004. p. 1–11.

- *Contributed section with editors:* Johnson D, Ellis H, Collins P, editors. *Pectoral girdle and upper limb*. In: Standing S, editor. *Gray's anatomy: the anatomical basis of clinical practice*. 29th ed. Edinburgh (Scotland): Elsevier Churchill Livingstone; 2005. p. 799–942.

– Chapter in a book:

- *Standard chapter in a book:* Doyle JR, Botte MJ. Surgical anatomy of the hand and upper extremity. Philadelphia (PA): Lippincott Williams and Wilkins; 2003. Chapter 10, Hand, Part 1, Palmar hand; p. 532–641.

Illustrations and tables

Illustrations and tables should be numbered in different categories in the manuscript and Roman numbers should not be used in numbering. Legends of the illustrations and tables should be added to the end of the manuscript as a separate page. Attention should be paid to the dimensions of the photographs to be proportional with 10x15 cm. Some abbreviations out of standards can be used in related illustrations and tables. In this case, abbreviation used should be explained in the legend. Figures and tables published previously can only be used when necessary for a comparison and only by giving reference after obtaining permission from the author(s) or the publisher (copyright holder).

Author Contribution

Each manuscript should contain a statement about the authors' contribution to the Manuscript. Please note that authorship changes are no longer possible after the final acceptance of an article.

List each author by the initials of names and surnames and describe each of their contributions to the manuscript using the following terms:

- Protocol/project development
- Data collection or management
- Data analysis
- Manuscript writing/editing
- Other (please specify briefly using 1 to 5 words)

For example: NBA: Project development, data collection; AS: Data collection, manuscript writing; STR: Manuscript writing

Funding: information that explains whether and by whom the research was supported.

Conflicts of interest/Competing interests: include appropriate disclosures.

Ethics approval: include appropriate approvals or waivers. Submitting the official ethics approval by whom the research was approved, including the approval date, number or code is necessary.

If the submission uses cadaveric tissue, please acknowledge the donors in an acknowledgement at the end of the paper.

Control list

- Length of the manuscript (max. 15 pages)
- Manuscript format (double space; one space before punctuation marks except for apostrophes)
- Title page (author names and affiliations; running head; correspondence)
- Abstract (100–250 words)
- Keywords (at least three)
- References (relevant to *Index Medicus*)
- Illustrations and tables (numbering; legends)
- Conflicts of Interest Disclosure Statement and Copyright Transfer Form
- Cover letter

All manuscripts must contain the following declaration sections. These should be placed before the reference list at the end of the manuscript.

The effect of tooth loss on the cancellous bone pattern of the mandible and on the superior bony wall of the mandibular canal: a micro-CT study

Ferhat Geneci¹ , Mert Ocak² , Bilge İpek Torun¹ , Handan Soysal³ 

¹Department of Anatomy, Faculty of Medicine, Ankara Yıldırım Beyazıt University, Ankara, Türkiye

²Department of Anatomy, Faculty of Dentistry, Ankara University, Ankara, Türkiye

³Department of Anatomy, Faculty of Dentistry, Ankara Yıldırım Beyazıt University, Ankara, Türkiye

Abstract

Objectives: The aim of this study was to examine the effect of tooth loss on the cancellous bone pattern of the mandible and on the superior bony wall of the mandibular canal.

Methods: Twenty-four dry mandibles without any physical deformation were scanned with high-resolution micro-CT device. The second premolar, first, second, and third molar regions on the mandibular canal, the presence of the bony superior wall of the mandibular canal and the cancellous bone pattern of the mandible were examined on micro-CT images. The images were classified into three groups, Type I (trabecular pattern), Type II (osteoporotic pattern), and Type III (dense/irregular pattern). The presence of the bony superior wall of the mandibular canal was noted as absent or present.

Results: While 133 (91%) of the dentulous sections were showing Type I trabecular cancellous bone pattern; 25 (54%) of the edentulous sections were of Type I. The superior wall was visible in 90 (62%) of the dentulous regions and in 41 (89%) of the edentulous areas. The cancellous bone pattern of the mandible of the majority of dentulous and edentulous areas had a regular trabecular structure. Dense and irregular trabecular structure were encountered only in edentulous areas.

Conclusion: We suggest that there is a very strong relationship between the superior bony wall of the mandibular canal and the cancellous bone pattern of the mandible. We conclude that the trabecular structure of the mandible could change following tooth loss and this have an effect on the change of the structure and the presence of the superior wall of the mandibular canal.

Keywords: mandible; mandibular canal; micro-CT; tooth loss; trabeculae

Anatomy 2022;16(1):1-6 ©2022 Turkish Society of Anatomy and Clinical Anatomy (TSACA)

Introduction

The mandibular canal (MC) is a bony canal beginning from the mandibular foramen and contains the inferior alveolar nerve (IAN) together with the inferior alveolar artery and vein.^[1] The other term used especially by clinicians for the MC is the inferior alveolar canal. These two terms describe the same structure.^[2]

In recent studies, many small accessory canals have been reported to accompany this canal. It has long been recognized that the branching pattern of IAN shows variations as well and multiple foramina or ducts may originate

from the MC.^[3-5] Accessory canals can be detected radiologically or during surgical procedures. In cases where the accessory MC is seen, the possibility of the presence of accessory mental foramen increases.^[3,6-8] Haas et al.^[9] reported two types of accessory MCs as; bifid MC (BMC) and its variant, trifid MC (TMC). In the BMC type, the MC is divided into two, in the TMC type, the accessory MC is divided into two, and there are three canals in total.^[3] Apart from these, accessory mental foramen and lingual foramen are of other anatomical variations.^[10]

IAN is vulnerable to iatrogenic injuries, so knowing the course of MC and IAN is very important for surgical

procedures.^[11] The risk of injury to the IAN is relatively high during implant placement, tooth extraction and other surgical procedures. In such a case, permanent damage may occur in structures such as palate, teeth, lips, and tongue innervated by IAN.^[12] It is very important to determine the trabecular quality of the jawbone and the neighborhood of the anatomical structures before implant applications and jaw surgeries. For this reason, imaging of the region with cone-beam computed tomography (CBCT) is recommended before these operations.^[13]

Based on gross anatomical observations, Iwanaga et al.^[13] classified the cancellous part of the mandible as type I (trabecular pattern), type II (osteoporotic) and type III (dense-irregular pattern). Another study conducted by Iwanaga et al.^[10] revealed that edentulous sections in both men and women were generally of type I trabecular pattern. The results also suggested that the superior wall of the MC may not be visible where the cancellous bone was osteoporotic and the dentulous areas were mostly of Type I. However, Type I was suggested to be the least common cancellous bone type in edentulous areas.^[13] There are strong evidences in the literature that, the IAN loses its branches to the teeth, after the teeth are lost. In addition to this, as the bone remodels, the superior wall of the MC loses its trabecular structure and the superior wall becomes smoother. However, it was also shown by Iwanaga et al.^[13] that the type 2 osteoporotic spongy pattern present in 30% of edentulous areas in women, and the superior wall of the MC was not smooth.

As the literature reveals some discrepancies related with the relation of the tooth loss and the cancellous bone pattern of the mandible; the aim of this study was to examine the effect of tooth loss on the trabecular structure of the mandible and its effect on the superior wall of the MC. Thus, we aimed to evaluate which one (tooth loss or loss of trabecular tissue) has more effect on the superior wall of the MC and to provide a prediction for the possibility of injury to the MC to the surgeons working at this region.

Materials and Methods

This study has been performed on 24 dry adult mandibles obtained from Ankara University Faculty of Dentistry and Ankara Yıldırım Beyazıt University Faculty of Medicine. The dry bones were belonging to Anatolian people of unknown sex and age and did not have any physical deformation.

The dry bones were scanned with a micro-CT device (Bruker micro-CT, Kontich, Belgium) with following configuration and parameters: 1 mm aluminum filter, 80

keV, 125 μ A, 10 μ m resolution, exposure=47ms, rotation=180° and rotation step=0.400°. The three-dimensional reconstruction data was obtained by using NRecon reconstruction software (version 1.6.9.4; Bruker micro-CT). All measurements were carried out with CTAn software (version 1.17.7.2; Bruker micro-CT) and 3D images were created with CTVol software (version 2.3).

After all samples were scanned with micro-CT and their two-dimensional images were obtained in the axial plane with Nrecon software. Care was taken to avoid any artifacts in any sample so that it would not affect the measurements. 3D images were created with Ctvox software using images reconstructed with Nrecon. Scoring for the presence or absence of the superior wall of the MC was performed using these 3D images.

The body of mandibles were divided into four regions according to the tooth fitting on the MC (second premolar, first, second, and third molars). The superior wall of the MC in the region of each tooth was scored by two observers as visible or invisible. And total of 192 tooth regions (4 tooth regions on the right and 4 on the left, multiplied by 24) were scored and grouped according to the appearance of the cancellous bone pattern of the mandible on 3D images in the relevant region. The grouping was as follows; Type I: trabecular pattern; type II: osteoporotic; and type III: dense-irregular patterns as previously defined by Iwanaga et al.^[13] (**Figure 1**).

Microsoft Excel, 15.33 version (Microsoft Corporation, Redmond, WA, USA) was used for the statistical analysis. Statistical significance was defined as $p < 0.05$. The relationship between the observed characteristics were documented by using chi-square test.

Results

The MCs of all dry bones were in the form of a single canal, originating from the mandibular foramen and ending in the mental foramen. Accessory mental foramen was not encountered in any of the specimens.

A total of 192 tooth regions were examined in this study. Of these 192 regions; 146 were dentulous and 46 were edentulous. In some jaws, the third molars were impacted or not fully erupted. These regions were included in the dentulous areas in the study. While the appearance of the cancellous bone pattern of the mandible was Type I (trabecular) in 133 (91%) of the dentulous sections, 13 (9%) were Type II (osteoporotic). Type III was not found in the dentulous sections. Of the edentulous sections, 25 (54%) were Type I (trabecular), 5 (11%) were

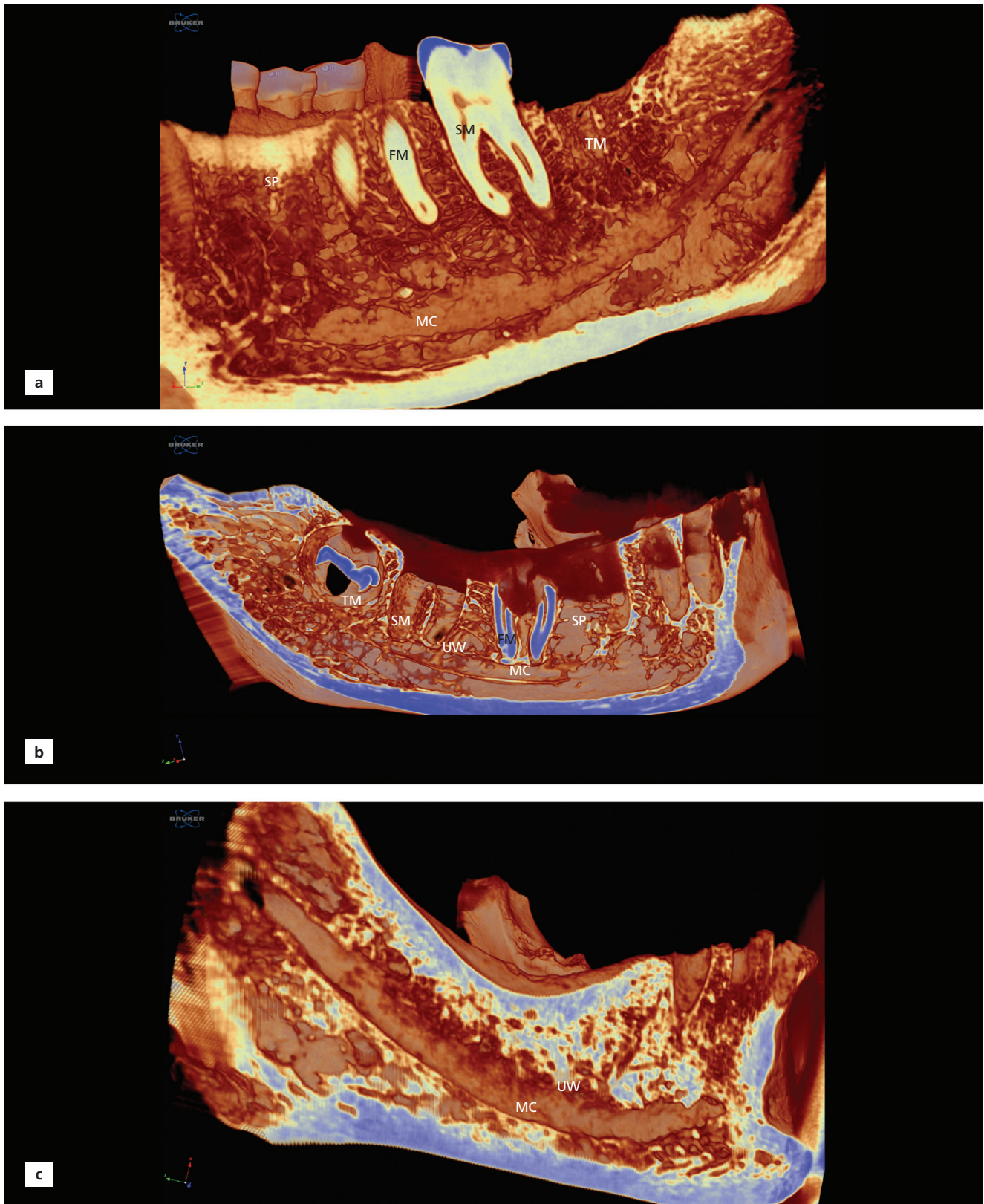


Figure 1. Cancellous bone pattern of the mandibles on micro-CT images of the mandibles. (a) type I trabecular pattern; (b) type II osteoporotic pattern; (c) type III dense-irregular pattern (edentulous). FM: first molar; MC: mandibular canal; SM: second molar; SP: second premolar; TM: third molar; UW: superior wall of the mandibular canal.

Table 1

Cancellous bone pattern of dentulous and edentulous areas and superior wall of mandibular canal.

	Type I	Type II	Type III	Visible superior wall	Non-visible superior wall
Dentulous sections	133 (91%)	13 (9%)	0	90 (62%)	56 (38%)
Edentulous sections	25 (54%)	5 (11%)	16 (34%)	41 (89%)	5 (11%)

Type II (osteoporotic), and 16 (34%) were Type III (dense-irregular). While type I was present in the majority in both dentulous and edentulous regions, it was seen that it was much more dominant in dentulous regions. Interestingly, while Type III was not found in the dentulous regions, approximately one third of the edentulous regions were found to be type III. It was observed that alveolar processes have disappeared in mandibles that have lost all their teeth. In these mandibles the body has become thinner and the trabecular structure of these thin bodies has become denser. This caused Type III to be more common in edentulous areas. The relationship between the dentulous and edentulous parts and the trabecular structure was found to be statistically significant ($p=0.000$) (**Table 1**).

The superior bony wall of the MC was classified as present or absent. The superior wall of the MC was visible in 131 (68%) of all the regions, and was not visible in 61 (32%). While the superior wall was visible in 113 (72%) of the type I regions, was not visible in 45 (28%). In addition to this, while the superior wall was not visible in 16 (89%) of the type II regions, it was visible only in 2 (11%). The superior wall was visible in all type III regions. The relationship between the trabecular formation and the visibility of the superior wall was found to be significant according to the chi-square test ($p=0.000$). The superior wall was visible in 90 (62%) of the dentulous regions and in 41 (89%) of the edentulous region, whereas, the superior wall was not visible in 56 (38%) of the dentulous regions and not visible in 5 (11%) of the edentulous regions. The relationship between the dentulous and edentulous regions, and the visibility of the superior wall was found to be significant according to the chi-square test ($p=0.001$) (**Table 2**).

Discussion

Present literature reveals some discrepancies related with the relation of the tooth loss and the cancellous bone pattern of the mandible and the presence or absence of the superior wall of the MC in cases with tooth loss. Bertl et al.^[14] determined that 65% of the superior wall and 81% of the lower wall of the MC are covered with bone. Schwarz et al.^[15] found that the walls of the MC are mostly of trabecular type. Iwanaga et al.^[16] examined 80 tooth regions of 20 dry mandibles with CBCT and classified the superior wall of the MC. The images of 5 samples could not be examined due to artifacts, and the superior wall of the MC could not be visualized in the CBCT images of 5 of the remaining 75 images. They observed that superior wall of MCs with osteoporotic trabeculae was less visible in CBCT, and the detection rate of superior wall of the MCs with smooth trabecular formation was higher than other groups. The difference between the two groups was found to be statistically significant.^[10] Accordingly, they reported that, as the trabeculae weakens, the incidence of MC in CBCT decreases. We also visualized the superior wall of the MC in relation with the cancellous bone pattern of the mandibles with micro-CT. We made all our evaluations visually by taking virtual sections from 3D images with Ctvox software. We paid particular attention to the absence of artifacts in the images, re-scanned the samples, and reconstructed the obtained data if needed. Thanks to the high resolution of micro-CT, we were able to see even small canals that emerged from the MC in dry bones with dense trabecular formation. Likewise in the study of Iwanaga et al.^[10] we found that the higher the trabecular density, the higher the probability of the superior wall to be seen. As

Table 2

Superior wall of mandibular canal according to cancellous bone pattern.

	Type I	Type II	Type III
Visible superior wall	113 (72%)	2 (11%)	16 (100%)
Non-visible superior wall	45 (28%)	16 (89%)	0

the trabecular formation weakens, the bony boundaries of the MC became unclear.

Iwanaga et al.^[16] investigated why the MC was sometimes clearly seen on radiological images and sometimes not. As a result of the study, they stated that mostly dentulous regions are type I and edentulous regions are type IV (smooth pattern).^[16] In a serial of studies made on mandibles, Iwanaga et al.^[10,13,16] determined that wall formation of the MC in edentulous areas could be seen more clearly with CBCT. The difference between the dentulous and edentulous areas was thought to be due to the remodeling of the area after the tooth is lost.^[10,16] While the tooth is present, IAN passes through the trabeculae-like superior wall of the MC to innervate the tooth. When the tooth is extracted, the IAN does not need to cross the superior wall of the MC, as it loses the branches that innervate the tooth, and the superior wall of the MC loses its trabecular pattern and becomes smooth.^[10,17,18] In our study, the superior wall was clearly visible in most edentulous areas, while the trabecular structure was dense and irregular. The trabeculae were regular in most of the dentulous areas (Type I) and in addition, the majority had a superior wall formation. We found that the superior wall of the MC can be seen more clearly, while the edentulous areas have a dense and irregular trabecular formation with remodeling. However, the superior wall was clearly visible in dentulous areas as long as the trabecular formation was not weak, and this was considerably higher (62%) in dentulous areas. We found that there was a very strong correlation between the superior wall formation of the MC and the trabecular density.

Conclusion

Implant applications and other surgical operations related to the jaw are of frequent interventions in dentistry and there is always a risk of damage to the MC and thus to IAN. Therefore, it is important to have an idea about the trabecular formation of the jaw and the superior wall of the MC. As a result of our study, we concluded that there is a very strong connection between the trabecular formation of the mandible and the superior bony wall of the MC. The superior wall of the MC becomes more pronounced as the trabecular density increases in the dentulous and edentulous regions. In addition, we observed that the trabeculae was denser in edentulous regions and the superior bony wall of the MC was more prominent.

Acknowledgments

The authors would like to express their sincere gratitude to the donors and their families.

Conflict of Interest

The authors declare no conflict of interest.

Author Contributions

FG: protocol/project development, data analysis; MO: data analysis; BİT: manuscript writing/editing; HS: manuscript writing/editing

Ethics Approval

The study was approved by Ethical Committee of Ankara Yıldırım Beyazıt University (No:2019-169) and carried out in accordance with the Helsinki declaration of principles.

Funding

The authors declare no financial support.

References

1. Cunningham CA, Fernandez-Miranda JC. The skull. In: Standring S, editor. Gray's anatomy: the anatomical basis of clinical practice. 42nd ed. Edinburgh (Scotland): Elsevier Churchill Livingstone; 2021. p. 558–60.
2. Iwanaga J, Matsushita Y, Decater T, Ibaragi S, Tubbs RS. Mandibular canal vs. inferior alveolar canal: evidence-based terminology analysis. *Clin Anat* 2021;34:209–17.
3. Ngeow WC, Chai WL. The clinical anatomy of accessory mandibular canal in dentistry. *Clin Anat* 2020;33:1214–27.
4. Barker BC, Lockett BC. Multiple canals in the rami of a mandible. *Oral Surg Oral Med Oral Pathol* 1972;34:384–9.
5. Olivier E. The inferior dental canal and its nerve in the adult. *British Dental Journal* 1928; 49:356–8.
6. Mallya SM, Lam EWN. White and Pharoah's oral radiology: principles and interpretation. 7th ed. St. Louis, MO: Elsevier Mosby; 2014. p. 636.
7. Kaufman E, Serman NJ, Wang PD. Bilateral mandibular accessory foramina and canals: a case report and review of the literature. *Dentomaxillofac Radiol* 2000;29:170–5.
8. Eshak M, Brooks S, Abdel-Wahed N, Edwards PC. Cone beam CT evaluation of the presence of anatomic accessory canals in the jaws. *Dentomaxillofac Radiol* 2014;43:20130259.
9. Haas LF, Dutra K, Porporatti AL, Mezzomo LA, De Luca Canto G, Flores-Mir C, Correa M. Anatomical variations of mandibular canal detected by panoramic radiography and CT: a systematic review and meta-analysis. *Dentomaxillofac Radiol* 2016;45:20150310.
10. Iwanaga J, Katafuchi M, Matsushita Y, Kato T, Horner K, Tubbs RS. Anatomy of the mandibular canal and surrounding structures. Part I: morphology of the superior wall of the mandibular canal. *Ann Anat* 2020;232:151580.

11. Kilic C, Kamburoglu K, Ozen T, Balcioglu HA, Kurt B, Kutoglu T, Ozan H. The position of the mandibular canal and histologic feature of the inferior alveolar nerve. *Clin Anat* 2010;23:34–42.
12. Lahoud P, Diels S, Niclaes L, Aelst SV, Willems H, Gerven AV, Quirynen M, Jacobs R. Development and validation of a novel artificial intelligence driven tool for accurate mandibular canal segmentation on CBCT. *J Dent* 2022;116:103891.
13. Iwanaga J, Shiromoto K, Kato T, Tanaka T, Ibaragi S, Tubbs RS. Anatomy of the mandibular canal and surrounding structures. Part II: cancellous pattern of the mandible. *Ann Anat* 2020;232:151583
14. Bertl K, Heimel P, Reich KM, Schwarze UY, Ulm C. A histomorphometric analysis of the nature of the mandibular canal in the anterior molar region. *Clin Oral Investig* 2014;18:41–7.
15. Schwarz MS, Rothman SL, Rhodes ML, Chafetz N. Computed tomography: part I. Preoperative assessment of the mandible for endosseous implant surgery. *Int J Oral Maxillofac Implants* 1987;2:137–41.
16. Iwanaga J, Anand MK, Jain MN, Nagata M, Matsushita Y, Ibaragi S, Kusakawa J, Tubbs RS. Microsurgical anatomy of the superior wall of the mandibular canal and surrounding structures: suggestion for new classifications for dental implantology. *Clin Anat* 2020;33:223–31.
17. Gowgiel JM. The position and course of the mandibular canal. *J Oral Implantol* 1992;18:383–5.
18. Polland KE, Munro S, Reford G, Lockhart A, Logan G, Brocklebank L, McDonald SW. The mandibular canal of the edentulous jaw. *Clin Anat* 2001;14:445–52.

ORCID ID:

F. Geneci 0000-0002-5039-4664;
M. Ocak 0000-0001-6832-6208;
B. I. Torun 0000-0002-0155-7447;
H. Soysal 0000-0001-7550-6362







Correspondence to: Ferhat Geneci, PhD

Department of Anatomy, Faculty of Medicine,
Ankara Yıldırım Beyazıt University, Ankara, Türkiye
Phone: +90 530 458 07 95
e-mail: fgeneci@yahoo.com

Conflict of interest statement: No conflicts declared.

This is an open access article distributed under the terms of the Creative Commons Attribution-NonCommercial-NoDerivs 4.0 Unported (CC BY-NC-ND4.0) Licence (<http://creativecommons.org/licenses/by-nc-nd/4.0/>) which permits unrestricted noncommercial use, distribution, and reproduction in any medium, provided the original work is properly cited. *How to cite this article:* Geneci F, Ocak M, Torun Bİ, Soysal H. The effect of tooth loss on the cancellous bone pattern of the mandible and on the superior bony wall of the mandibular canal: a micro-CT study. *Anatomy* 2022;16(1):1–6.

The relationship between the body mass index and the subcutaneous adipose tissue

Bilge İpek Torun¹ , Mehtap Balaban² , Ferhat Geneci¹ , Şükrü Cem Hatipoğlu³ 

¹Department of Anatomy, Faculty of Medicine, Ankara Yıldırım Beyazıt University, Ankara, Türkiye

²Department of Radiology, Faculty of Medicine, Ankara Yıldırım Beyazıt University, Ankara, Türkiye

³Department of Radiology, Ankara City Hospital, Ankara, Türkiye

Abstract

Objectives: The aim of the study was to investigate the relationship between the body mass index and ultrasound-measured subcutaneous adipose tissue (SCAT) thickness, in order to propose an alternative non-invasive and inexpensive method to measure the subcutaneous fat. We also evaluated the liver size and the existence of hepatosteatosi, and investigated whether there was a relationship between liver measurements and body mass index (BMI), and the SCAT measurements.

Methods: Height, weight, arm SCAT, umbilical SCAT, thigh SCAT, umbilical preperitoneal fat (PPF) and craniocaudal liver size of 72 volunteers were measured and liver parenchymal echogenicity was evaluated with ultrasound. Correlations between BMI and the SCAT, the PPF, and liver measurements were evaluated statistically.

Results: BMI was mostly well correlated with umbilical SCAT ($r=0.650$, $p<0.001$). The arm SCAT ($r=0.549$, $p<0.001$) and the thigh SCAT ($r=0.470$, $p\leq 0.001$) followed it. The umbilical PPF was only correlated with the umbilical SCAT. There was no relationship between arm, or thigh SCAT values and existence of hepatosteatosi, but existence of hepatosteatosi was related with umbilical SCAT ($p=0.008$), and umbilical PPF ($p=0.009$) values.

Conclusion: As an alternative method to skinfold measurement, SCAT measurement with ultrasound can be used to evaluate body fat status.

Keywords: fat; hepatosteatosi; obesity; weight

Anatomy 2022;16(1):7–12 ©2022 Turkish Society of Anatomy and Clinical Anatomy (TSACA)

Introduction

Body mass index (BMI) is the most common method used to classify individuals as overweight, obese and thin.^[1–3] BMI is used to determine obesity-related disease risks in both adults and children.^[4] Skinfold thickness has long been used as the subcutaneous fat measurement method, on the grounds that half of the total body fat is collected in the subcutaneous fat deposits and this is related to the total amount of fat.^[5,6] Since the amount of subcutaneous fat is an indicator of total body fat, it has been widely used to determine total body fat.^[7,8] The skinfold technique is commonly used because it is noninvasive, relatively easy to administer, and inexpensive.^[9]

In this study we aimed to investigate the relationship between the body mass index and ultrasound-measured subcutaneous adipose tissue (SCAT), in order to propose

an alternative non-invasive and inexpensive method to measure the subcutaneous fat. We also evaluated the liver size and the existence of hepatosteatosi, and investigated whether there was a relationship between liver measurements and BMI, and the SCAT measurements.

Materials and Methods

Seventy-two volunteers (41 women, 31 men), aged between 20 and 76 were included in this study. Those with physical problems, diabetes, severe liver, kidney and heart diseases, those who were treated with diuretics, those who were treated for cancer, and those who were on a special diet program to gain or lose weight were excluded from the study.

Measurements of the subjects were made in the morning on an empty stomach and without excessive fluid intake

(between 8–10 am) and height measurements were made with bare feet. Weight was measured barefoot and wearing light clothing. Length measurement was made with a wall tape measure sensitive to centimeter, and weight measurement was made with a scale sensitive to 0.1 kilograms. In order to avoid errors that may occur in the body compositions to be measured, the subjects were asked to rest for half an hour and avoid exercise before starting the measurement.

Measurements with ultrasound were made with 5–11 MHz linear (for the SCAT measurements) and 1–6 MHz convex (for the deeper measurements) probes (LOGIQ S7

Expert, GE, Medical Systems). SCAT measurements were done while the volunteers were lying supine, and while limbs were extended in anatomic position, from three regions: mid-arm (arm SCAT), umbilical (umbilical SCAT), and mid-thigh (thigh SCAT). Mid-arm was determined as the mid-point between the uppermost point of the glenohumeral joint and antecubital fossa (**Figure 1a**). Mid-thigh was determined as the mid-point between the anterior superior iliac spine and the base of patella (**Figure 1b**). Limb measurements were done on the right side. Umbilical measurements were done on the midline, 5 cm above the umbilicus (**Figure 1c**). The thickness (antero-

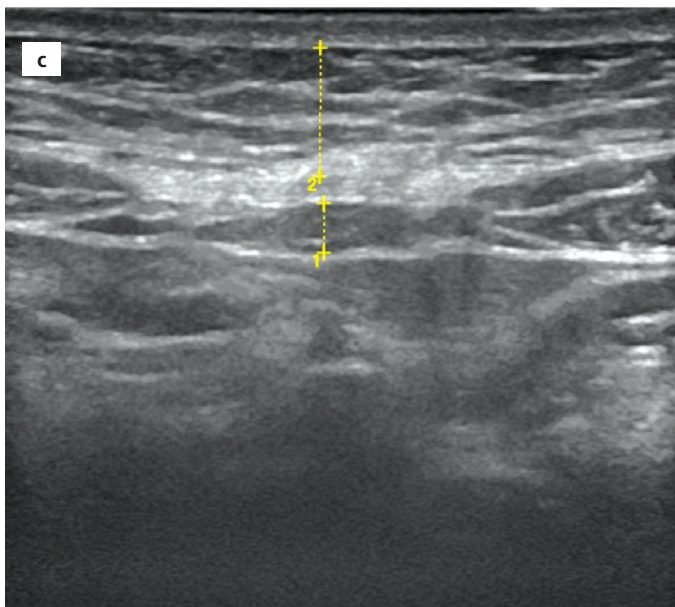
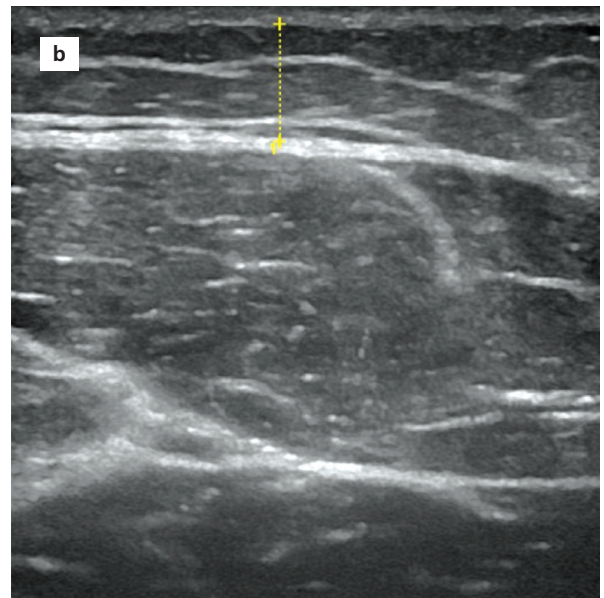
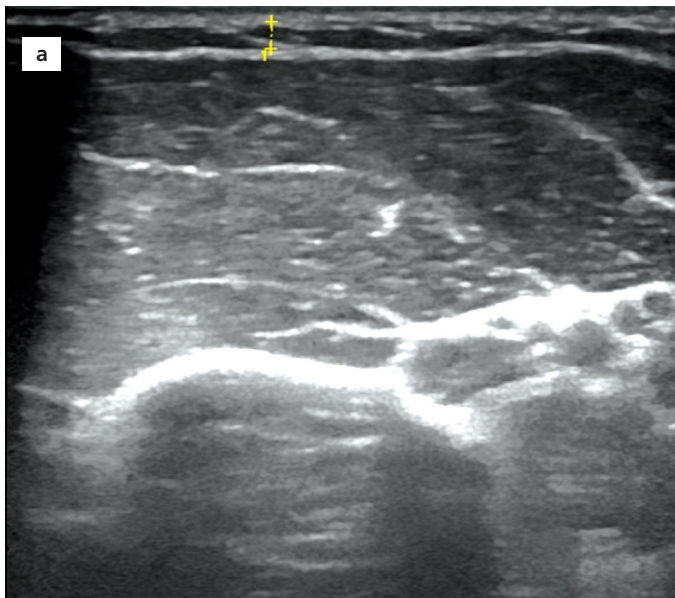


Figure 1. Ultrasound measurements on images. (a) measurement of the subcutaneous adipose tissue of the arm; (b) measurement of the subcutaneous adipose tissue of the thigh; (c) measurement of the umbilical preperitoneal fat (1) and umbilical subcutaneous adipose tissue (2).

posterior diameter) of the subcutaneous fat tissue (hypodermis) in the transverse view was measured as the arm SCAT anterior to the biceps muscle, the thigh SCAT anterior to the rectus femoris muscle, and the umbilical SCAT anterior to the rectus abdominis muscle. The thickness of the adipose tissue between the deep fascia and the peritoneum was measured as umbilical preperitoneal fat (PPF). In the right upper quadrant of the abdomen, cranio-caudal liver size and parenchymal echogenicity, in terms of steatosis, were evaluated with a 1–6 Mhz convex probe, while the patient was in inspiration.

The correlations between BMI and the SCAT, the PPF, and liver measurements were analyzed using SPSS (Statistical Package for Social Sciences) for Windows (Version 22, Chicago, IL, USA). Kolmogorov-Smirnov and Shapiro-Wilk tests were used to check normality. The Student's t-test was used to compare normally distributed pairs, the Wilcoxon signed-rank test was used to compare non-normally distributed pairs, and chi-square test was used to compare categorical variables. Pearson correlation analysis was used to test the relationship between normally distributed variables, and Spearman correlation analysis was used to test the relationship between non-normally distributed variables. For all analyses; $p < 0.05$ was considered as statistically significant.

Results

The characteristics of the volunteers and the results of the measurements are summarized in **Table 1**, and the correlations between the measurements are summarized in **Table 2**.

Ultrasound examination showed that 68.1% of the volunteers (49 out of 72) did not have hepatosteatois, 16.7% (12 out of 72) had grade I hepatosteatois, 15.3%

(11 out of 72) had grade II hepatosteatois. Hepatomegaly was detected in two of the volunteers (2.8%).

BMI was mostly well correlated with umbilical SCAT ($r=0.650$, $p < 0.001$). The arm SCAT (well correlated) ($r=0.549$, $p < 0.001$) and the thigh SCAT (fairly correlated) ($r=0.470$, $p \leq 0.001$) followed it. The umbilical PPF was only correlated with the umbilical SCAT. There was an excellent correlation between arm SCAT and thigh SCAT, and good correlation between arm SCAT and umbilical SCAT. Interestingly, arm SCAT showed correlation with age even if it was weak. There was no relationship between arm, or thigh SCAT values and existence of hepatosteatois, but existence of hepatosteatois was related with umbilical SCAT ($p=0.008$), and umbilical PPF ($p=0.009$) values. Since hepatomegaly was detected in only two volunteers, which was not statistically sufficient to correlate with any measure.

Except for the height, none of the measurements showed any statistically significant gender difference (**Table 3**).

Discussion

Obesity is a metabolic disease which can cause many health problems and related deaths.^[10] It is a health problem that increases the risk of coronary artery disease, hypertension, type II diabetes, obstructive pulmonary disease, osteoarthritis and some types of cancer, and significantly reduces life expectancy.^[11] BMI is generally the first step and the most ideal method for measuring obesity, but it is considered as a rough guide. Because the fat rates in different people do not correspond to the same level of obesity.

World Health Organization (WHO) interprets BMI for adults as follows: <18.5 : underweight, 18.5 – 24.9 : nor-

Table 1

The characteristics of the volunteers and the results of the measurements.

	Mean or median* \pm SD	Range: min–max or 95% CI†
Age (years)	40.00 \pm 13.23	20–76 years
Height (cm)	167.94 \pm 10.39	150.00–200.00
Weight (kg)	76.06 \pm 14.82	48.00–113.00
BMI	26.96 \pm 4.68	16.34–40.27
Arm SCAT (mm)	2.80* \pm 2.44	0.20–15.10
Thigh SCAT (mm)	11.65 \pm 5.61	10.33–12.97†
Umbilical SCAT (mm)	18.33 \pm 7.39	16.59–20.07†
Umbilical PPF (mm)	4.55* \pm 3.49	0.90–17.40

*Arm SCAT and umbilical PPF were given as median value since they were not distributed normally. †95% CI was given for means of normally distributed parameters. BMI: body mass index; CI: confidence interval; PPF: preperitoneal fat; SCAT: subcutaneous adipose tissue; SD: standard deviation.

Table 2
Correlations between measurements.

		Arm SCAT	Thigh SCAT	Umbilical SCAT	Umbilical PPF
Age	r-value	0.296			
	p-value	0.012*	0.423	0.078	0.545
Height	r-value	-0.397	-0.451		
	p-value	<0.001	<0.001	0.627	0.653
Weight	r-value	0.252		0.554	0.430
	p-value	0.033*	0.287	<0.001	<0.001
BMI	r-value	0.549	0.470	0.650	0.420
	p-value	0.001	<0.001	<0.001	<0.001
Arm SCAT	r-value		0.724	0.555	
	p-value		<0.001	<0.001	0.070
Thigh SCAT	r-value	0.724		0.383	
	p-value	<0.001		<0.001	0.310
Umbilical SCAT	r-value	0.555	0.383		0.334
	p-value	<0.001	<0.001		0.004*
Umbilical PPF	r-value			0.334	
	p-value	0.070	0.310	0.004*	

*p<0.05. BMI: body mass index; PPF: preperitoneal fat; SCAT: subcutaneous adipose tissue.

mal weight, 25.0–29.9: pre-obesity, and ≥ 30.0 : obesity. BMI is calculated based on the formula: weight (kg) / [height (m)]². BMI, which is one of the most basic methods in determining obesity, is also the first method used by WHO to determine obesity. However, BMI does not take

into account the weight of the increased muscle tissue, the body's water retention and the distribution of adipose tissue. Individuals with similar BMI may have different abdominal fat tissue. Therefore, waist circumference and waist-hip ratio measurements have been seen as an alter-

Table 3
Gender differences.

	Gender	Mean or median*	P-value
Height (cm)	W	161.85	0.003 [†]
	M	176.00	
Weight (kg)	W	70.42	0.301
	M	83.53	
BMI	W	26.95	0.347
	M	26.97	
Arm SCAT (cm)	W	3.50*	0.495
	M	2.00*	
Thigh SCAT	W	14.85	0.251
	M	7.41	
Umbilical SCAT (cm)	W	18.46	0.424
	M	18.17	
Umbilical PPF (cm)	W	3.70*	0.447
	M	6.70*	

*Arm SCAT and umbilical PPF were given as median since they were not distributed normally. [†]p<0.05. BMI: body mass index; M: man; PPF: preperitoneal fat; SCAT: subcutaneous adipose tissue; W: woman

native to BMI, with measurements regularly used in both clinical and research settings.

Anthropometric methods are generally preferred when screening for obesity on populations. The most obvious advantages of anthropometric methods are that they are portable, inexpensive and useful in field studies. BMI, which relates weight to height, is the most widely used and also the simplest measure of body size, and is often used to estimate the prevalence of obesity in a population.^[12] However, it has been subjected to many criticisms that it does not reveal the fat ratio, and BMI value of the individuals in the body with excess muscle mass or water retention is high. For these reasons, alternative methods are sought for BMI. At this point, circumference measurements are preferred because they give direct information about the individual's fatness status.

Skin fold thickness measurement, dual-energy X-ray absorptiometry scans, and assessment of the SCAT with computed tomography are commonly used methods to evaluate the fat distribution of the body.^[9,13] SCAT and visceral adipose tissue measurements with ultrasound have also been used in recent years to evaluate body fat distribution.^[14,15]

It has been reported in the literature that there is a relationship between waist circumference and fatty liver.^[16] In our study, no correlation was found between any SCAT measurements and hepatosteatosis, not even with umbilical SCAT. This is probably because hepatosteatosis is associated with visceral adipose tissue, not SCAT. But still, we found that the umbilical SCAT was the most correlated SCAT with BMI. In clinical practice, abdominal fat is the most widely accepted in the assessment of obesity.^[17]

Some researchers compared the skinfold measurements with ultrasound-measured SCAT values, and dual energy X-ray with CT-measured and ultrasound-measured SCAT values, and found that the measurements were correlated.^[13,18] We also found good correlation between BMI values and all three SCAT measurements. In the light of this information, we suggest that SCAT measurements with ultrasound is an inexpensive, safe and easily applicable method for the evaluation of body fat composition.

Conclusion

As an alternative method to skinfold measurement, SCAT measurement with ultrasound can be used to evaluate body fat status.

Acknowledgments

The authors would like to express their sincere gratitude to the volunteers.

Conflict of Interest

The authors declare no conflict of interest.

Author Contributions

BIT: Project development, data analysis, drafting the article; MB: data collection, data analysis, drafting the article, revising it critically for important intellectual content; FG: data collection, data analysis, drafting the article; ŞCH: data collection, data analysis, drafting the article. All authors approved the final of the version to be published, agree to be accountable for all aspects of the work if questions arise related to its accuracy or integrity.

Ethics Approval

The study was approved by Ethical Committee of Ankara Yildirim Beyazit University (No:2019-33). Informed consent was obtained from all the volunteers and carried out in accordance with the Helsinki declaration of principles.

Funding

The authors declare no financial support.

References

1. Krebs NF, Jacobson MS; American Academy of Pediatrics Committee on Nutrition. Prevention of pediatric overweight and obesity. *Pediatrics* 2003;112:424–30.
2. Fujii K, Demura S. Relationship between change in BMI with age and delayed menarche in female athletes. *J Physiol Anthropol Appl Human Sci* 2003;22:97–104.
3. Booth ML, Hunter C, Gore CJ, Bauman A, Owen N. The relationship between body mass index and waist circumference: implications for estimates of the population prevalence of overweight. *Int J Obes Relat Metab Disord* 2000;24:1058–61.
4. Nakao T, Komiya S. Reference norms for a fat-free mass index and fat mass index in the Japanese child population. *J Physiol Anthropol Appl Human Sci* 2003;22:293–8.
5. Hills AP, Lyell L, NM B. An evaluation of the methodology for the assessment of body composition in children and adolescents. In: Jürimäe T, Hills A, editors. *Body Composition assessment in children and adolescents*. Basel: Karger; 2001. p. 1–13.
6. Freedman DS, Ogden CL, Kit BK. Interrelationships between BMI, skinfold thicknesses, percent body fat, and cardiovascular disease risk factors among U.S. children and adolescents. *BMC Pediatr* 2015;15: 188.
7. Martin AD. Body composition. In: Docherty D, editor. *Measurement in pediatric exercise science*. Canada: Human Kinetics; 1996. p. 87–128.
8. Willmore JH, Costill DL, Kenney L. *Physiology of sport and exercise*. USA: Human Kinetics; 1994. p. 400–21.

9. Hastuti J, Rahmawati NT, Suriyanto RA, Wibowo T, Nurani N, Julia M. Patterns of body mass index, percentage body fat, and skin-fold thicknesses in 7- to 18-year-old children and adolescents from Indonesia. *Int J Prev Med* 2020;11:129.
10. Berghöfer A, Pischon T, Reinhold T, Apovian CM, Sharma AM, Willich SN. Obesity prevalence from a European perspective: a systematic review. *BMC Public Health* 2008;8:200.
11. Heyward VH, Stolarczyk LM. Applied body composition assesment. USA: Human Kinetics; 1996. p. 221.
12. Huxley R, Mendis S, Zheleznyakov E, Reddy S, Chan J. Body mass index, waist circumference and waist: hip ratio as predictors of cardiovascular risk--a review of the literature. *Eur J Clin Nutr* 2010;64:16–22.
13. Gradmark AM, Rydh A, Renström F, De Lucia-Rolfe E, Sleight A, Nordström P, Brage S, Franks PW. Computed tomography-based validation of abdominal adiposity measurements from ultrasonography, dual-energy X-ray absorptiometry and anthropometry. *Br J Nutr* 2010;104:582–8.
14. Pétursdóttir Maack H, Sundström Poromaa I, Lindström L, Mulic-Lutvica A, Junus K, Wikström AK. Ultrasound estimated subcutaneous and visceral adipose tissue thicknesses and risk of pre-eclampsia. *Sci Rep* 2021;11:22740.
15. Kelso A, Vogel K, Steinacker JM. Ultrasound measurements of subcutaneous adipose tissue thickness show sexual dimorphism in children of three to five years of age. *Acta Paediatr* 2019;108:514–21.
16. Jakobsen MU, Berentzen T, Sørensen TI, Overvad K. Abdominal obesity and fatty liver. *Epidemiol Rev* 2007;29:77–87.
17. Ibrahim MM. Subcutaneous and visceral adipose tissue: structural and functional differences. *Obes Rev* 2010;11:11–8.
18. Pérez-Chirinos Buxadé C, Solà-Perez T, Castizo-Olier J, Carrasco-Marginet M, Roy A, Marfell-Jones M, Irurtia A. Assessing subcutaneous adipose tissue by simple and portable field instruments: skin-folds versus A-mode ultrasound measurements. *PLoS One* 2018;13:e0205226.

ORCID ID:

B. I. Torun 0000-0002-0155-7447;
 M. Balaban 0000-0002-6752-6838;
 F. Geneci 0000-0002-5039-4664;
 Ş. C. Hatipoğlu 0000-0001-8961-2481

**Correspondence to:** Bilge Ipek Torun, MD

Department of Anatomy, Faculty of Medicine,
 Ankara Yıldırım Beyazıt University, Ankara, Türkiye
 Phone: +90 312 906 20 83
 e-mail: bilgeipek@yahoo.com

Conflict of interest statement: No conflicts declared.

This is an open access article distributed under the terms of the Creative Commons Attribution-NonCommercial-NoDerivs 4.0 Unported (CC BY-NC-ND4.0) Licence (<http://creativecommons.org/licenses/by-nc-nd/4.0/>) which permits unrestricted noncommercial use, distribution, and reproduction in any medium, provided the original work is properly cited. *How to cite this article:* Torun Bİ, Balaban M, Geneci F, Hatipoğlu ŞC. The relationship between the body mass index and the subcutaneous adipose tissue. *Anatomy* 2022;16(1):7–12.

Sonoelastography findings of the patellar tendon in Osgood-Schlatter disease

Mehrap Balaban¹ , Sinem Sigit İikiz² , İlkay S. İdilman³ 

¹Department of Radiology, Faculty of Medicine, Ankara Yıldırım Beyazıt University, Ankara, Türkiye

²Department of Radiology, Lefkoşa Dr. Burhan Nalbantoğlu State Hospital, Lefkoşa, North Cyprus

³Department of Radiology, Faculty of Medicine, Hacettepe University, Ankara, Türkiye

Abstract

Objectives: There are ultrasonographic findings defined in Osgood-Schlatter disease. However, sonoelastographic findings of the disease have not been previously defined. The aim of this study was to evaluate the B-mode ultrasonography (US), Color Doppler ultrasonography (CDUS), and sonoelastography (SEL) findings of the patellar tendon in patients with Osgood-Schlatter disease (OSD) and compare it with healthy individuals.

Methods: A total of 36 patellar tendons were evaluated in 12 patients with OSD and 10 healthy individuals by US, CDUS, and SEL. Thickness, echogenicity, CDUS, and SEL findings of the distal patellar tendon in each group were evaluated.

Results: A total of 22 individuals (19 males, 3 females) and 36 tendons (9 with acute OSD, 7 with chronic OSD and 20 control healthy tendons) were included in this study. The patellar tendons were statistically significantly thicker in OSD patients in comparison with healthy volunteers (5.68±2.32 mm versus 3.42±0.55 mm) (p=0.001). According to the SEL evaluation, all of the patellar tendons in patients with OSD were of type 2 in contrast with all of the patellar tendons in healthy volunteers were of type 1 (p<0.001).

Conclusion: Distal patellar tendon in patients with OSD was thicker and softer in comparison with healthy volunteers. The intratendinous and/or peritendinous vascularity on CDUS was increased in patients with acute OSD. We suggest that these findings could be associated with tendon degeneration in OSD patients and can be useful in the evaluation of the disease.

Keywords: Osgood-Schlatter disease; patellar tendon; sonoelastography

Anatomy 2022;16(1):13–18 ©2022 Turkish Society of Anatomy and Clinical Anatomy (TSACA)

Introduction

Osgood-Schlatter disease (OSD) is commonly seen in active adolescents and widely accepted as a traction apophysitis of the tibial tuberosity.^[1] Chronic repetitive traction trauma in the apophysial cartilage may cause epiphyseal enlargement and microruptures. This causes avulsion fractures, which are osteochondral fragmentations, and tendinopathy at the attachment site of the distal patellar tendon to the tibial tuberosity.^[1,2] The typical presentation of OSD is pain and tenderness over the tibial tuberosity. The anamnesis and the physical examination of the patient are generally sufficient to make a diagnosis.^[3] However, imaging modalities are commonly needed for the evaluation of tibial tuberosity and additional findings in OSD.^[3] Along with technological development, the fre-

quency of ultrasonography (US) usage for evaluation of the musculoskeletal system has enhanced over time and now is commonly used in daily practice.^[4,5] US have low cost, easier use and accessibility, repeatability, no radiation exposure and it is applicable for all age groups. These features serve as important advantages of this modality.^[6] Also, US takes less time and thus more tolerable for the patients when compared to magnetic resonance imaging (MRI) which makes the US the preferred radiological modality in the evaluation of tendons.^[7] US evaluation can also provide information related to the size, extent, morphological feature of the lesion as well as vascularization of the lesion with color Doppler US (CDUS).

Recently, ultrasound elastography has become available for the assessment of soft tissue, in addition to the standard

B-mode US imaging and CDUS. The principle of sonoelastography (SEL) is based on the displacement of the tissues which depends on the stiffness of the tissue due to the applied compression. This displacement can be calculated and generated on a color map superimposed on the B-mode image.^[8,9] On SEL, information about the stiffness of the lesions as well as tissues can be determined by coding in different colors that represent stiffness levels of the tissues.^[10] The usage of SEL in the musculoskeletal system was limited in the past. However, this number is increasing with the extensive usage of US devices for this purpose.^[11-13]

The US findings of OSD include thickened patellar tendon with pretibial swelling, fluid collection in the infrapatellar bursa, and fragmentation of the ossification center.^[14,15] According to our knowledge, the SEL findings of OSD has not been previously defined. Therefore, in this study, we aimed to evaluate US, CDUS, and SEL findings of patellar tendons in patients with acute and chronic OSD in comparison with healthy individuals.

Materials and Methods

A total of 36 patellar tendons (9 patellar tendons of 7 patients with acute OSD, 7 patellar tendons of 5 patients with chronic OSD, and 20 patellar tendons of 10 healthy individuals) were evaluated. We included the diseased patellar tendons in the patient population and both patellar tendons in the healthy individuals. All acute OSD patients had knee pain and swelling. Chronic OSD was defined as having a history of tendon injury and OSD. Chronic OSD patients had typical US findings and were asymptomatic at the time of imaging. The control group consisted of individuals who were referred for a neck US, in the same age range as the study population, and did not have a history of knee injury or a clinical finding which indicated a tendon disorder. Additional informed consent was obtained from all patients for the identifying data included in the study. All procedures followed were in accordance with the ethical standards.

All patients with acute OSD, chronic OSD, and healthy volunteers underwent US, CDUS and SEL evaluation of the distal patellar tendon. The sonographic examinations were performed with a real-time scanner GE Logiq E9 (GE Healthcare, Milwaukee, Wisconsin, USA) and a linear array transducer with a frequency of 5–11 MHz or Toshiba Aplio 500 (Toshiba Medical Systems Corporation, Tochigi, Japan) with a 7–15 MHz wide-band linear transducer by the same experienced radiologist (M.B., with 11 years of experience in the musculoskeletal US). All patellar tendons were examined in axial and longitudinal planes in the sitting position with the

knee at 30° flexion. The thickness of the tendon was determined by measuring the anteroposterior diameter of the distal patellar tendon in the distal adhesion site in a longitudinal view with B-mode sonography. Longitudinal plane was used for generation of real-time elastographic images of the tendon. Slight compression and decompression was applied for the calculation of local strain, and optimization of the strain was evaluated according to the visual indicator of compression that indicates the average strain in the region of interest between two frames. Real-time calculation was used for the tissue elasticity distribution and results were generated on a color map superimposed on the B-mode image. According to the color map, tissue's relative stiffness was represented as a spectrum ranging from blue (hard) to red (soft), blue – green indicated hard tissue, yellow indicated intermediate tissue, and red indicated soft tissue. Multiple real-time elastographic images of the distal part of each tendon was evaluated and the most representative one demonstrating the tendon boundary and peritendinous layers were chosen for image interpretation. This selection and image interpretation was performed by two radiologists (M.B. and I.S.I.) with consensus. Two main types including type 1; blue and green colors-hard tissue, and type 2; yellow and red within green colors-intermediate and soft tissue was defined. Beyond this definition, 2 subtypes of these types including type 1a; blue predominance, type 1b; green predominance, type 2a; small yellow and red areas within green predominance, and type 2b; green areas within yellow and red predominance were defined. Hereby, the elasticity of the tissue was shown as a spectrum ranging from hard to soft as the type progressed from 1a to 2b.^[11]

The statistical analysis was made by SPSS (Statistical Package for Social Sciences) for Windows (Version 22, Chicago, IL, USA). Categorical data are presented as numbers (percentages), while continuous variables are expressed as mean±standard deviation and range. The normality of the variables was tested by the Shapiro-Wilk test. Categorical data were compared using the Pearson chi-square test/Fisher's exact test and continuous variables were compared using the Mann-Whitney U test. Kruskal-Wallis analysis was performed for comparing the difference in tendon thickness in patients with acute OSD, chronic OSD, and healthy individuals. The degree of association between continuous and ordinal variables was calculated by Spearman's rho coefficient. All tests were two-sided with a level of significance of $p < 0.05$. For the power calculation of this study, post hoc power analysis (for p -value of < 0.05 , Cohen's D of 0.8 for a large effect, and total sample size of 36 for a 2-tailed hypothesis) demonstrated an observed power of 0.998.

Results

A total of 22 individuals (19 males, 3 females) and 36 tendons were included in this study. The mean age of the participants was $21.09 \pm .98$ years (range: 13–34 years). A total of 16 patellar tendons of 12 patients with OSD (11 males, 1 females) including 4 patients with both involved tendons and 20 patellar tendons of 10 individuals with no history of OSD or symptoms that formed healthy volunteer group (8 males, 2 females) were evaluated. Seven patients with 9 patellar tendons had symptomatic acute stage OSD disease, 5 patients with 7 patellar tendons had asymptomatic chronic stage OSD. The mean age of the OSD group was 23.25 ± 7.79 years (range: 13–34 years), and the mean age of the healthy volunteers was 18.5 ± 5.06 years (range: 13–25 years). There was no significant difference in terms of age ($p=0.114$) and gender ($p=0.571$) of OSD patients and healthy volunteers.

A total of 36 patellar tendons (19 right sides, 17 left sides) were evaluated. There was 9 right and 7 left tendons in the OSD group, and 10 right and 10 left tendons in the healthy volunteer group with no side predominance ($p=0.709$). All patellar tendons in patients with acute OSD ($n=9$) had low echogenicity with coarse calcification and increased intratendinous and/or peritendinous vascularity on CDUS. Cortical irregularities on tibial tuberosity and infrapatellar deep bursitis were also detected in patients with acute OSD. All patellar tendons in patients with chronic OSD ($n=7$) included microcalcifications. In this patient population, we did not observe increased intratendinous or peritendinous vascularity on CDUS.

The median tendon thickness of the OSD patients was 4.75 mm (range: 3.1–10.0 mm) and healthy volunteers were 3.3 mm (range: 2.5–4.2 mm). The tendons were statistically significantly thicker in OSD patients ($p=0.001$). The median tendon thickness was higher in the acute OSD patients (7.5 mm; range: 4.5–10.0 mm) and followed by chronic

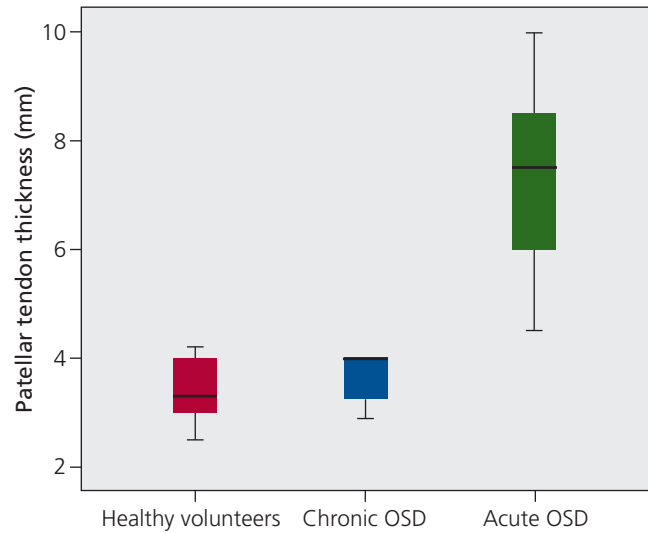


Figure 1. The boxplot shows the distal patellar tendon thickness in patients with acute OSD, chronic OSD, and healthy volunteers. OSD: Osgood-Schlatter disease.

OSD (4 mm; range: 2.9–4.0 mm) and healthy volunteer group (3.3 mm; range 2.5–4.2 mm) ($p<0.001$) (**Figure 1**).

SEL evaluation demonstrated that all of the patellar tendons in patients with OSD had a type 2 structure (16 of 16 tendons) and all of the patellar tendons in healthy volunteers had a type 1 structure (20 of 20 tendons) according to the main elastographic types with a statistically significant difference ($p<0.001$). The elastographic subtypes of the patients were as follows: most of the patellar tendons in patients with acute OSD were of type 2b (8 of 9 acute OSDs) (**Figure 2**) and 1 was of type 2a. All patellar tendons in patients with chronic OSD were of type 2a (**Figure 3**). All healthy volunteers had type 1a tendons (**Figure 4**). There were no type 1b patellar tendons. There were statistically significant differences in patients with

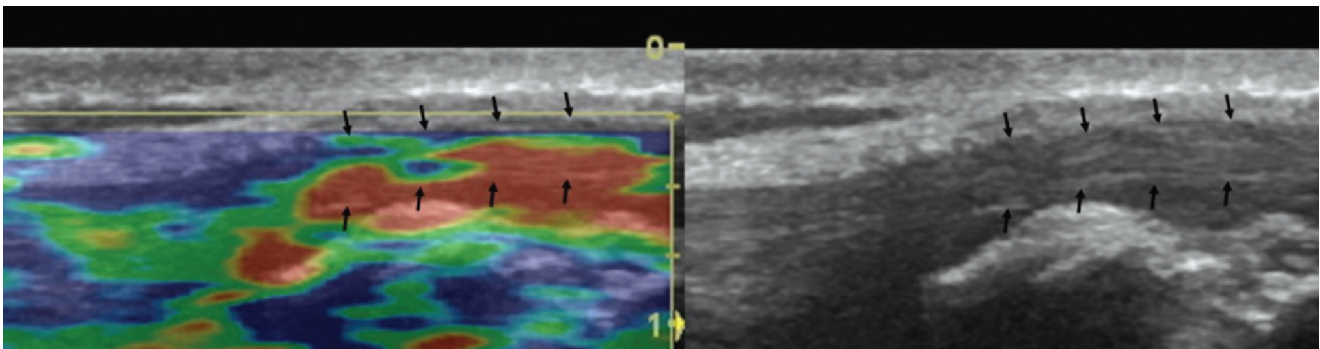


Figure 2. SEL evaluation of the patellar tendon (arrows) demonstrates a type 2b structure in a 15-year-old male patient with acute Osgood-Schlatter disease.

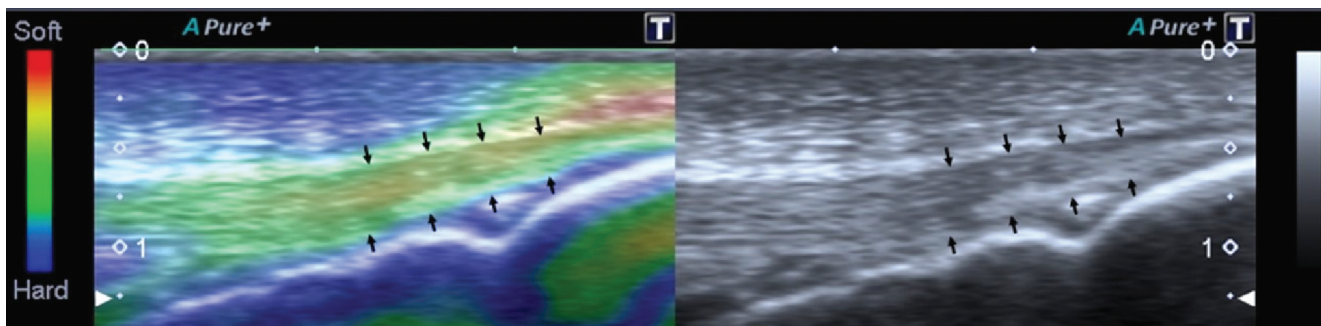


Figure 3. SEL evaluation of the patellar tendon (arrows) demonstrates a type 2a structure in a 30-year-old male patient with chronic Osgood-Schlatter disease.

and without OSD ($p < 0.001$) and in patients with acute OSD, chronic OSD, and healthy volunteers ($p < 0.001$) in terms of elastographic subtypes (Table 1). There was a significant positive correlation between tendon thickness and elastographic subtypes ($r = 0.669$, $p < 0.001$).

Discussion

In this study, we evaluated US and SEL findings of patellar tendons in patients with OSD in comparison with healthy volunteers. We observed that patellar tendons are thicker in patients with OSD which is more obvious in tendons of patients with acute OSD. In the SEL evaluation of the patellar tendons, we observed that all tendons in patients with OSD were of type 2 and all patellar tendons in healthy individuals were of type 1 according to the main elastographic types. When we evaluated the elastographic subtypes, most of the patellar tendons in patients with acute OSD were of type 2b and all patellar tendons in patients with chronic OSD were of type 2a structure with a statistically significant difference in comparison with healthy volunteers.

The thick appearance of epiphyseal cartilage in the distal patellar tendon, cortical irregularities compatible with osteochondrosis, calcific fragmentations, decrease in tendon echogenicity consistent with degenerative changes, and accompanying infrapatellar bursitis are the main findings of OSD in B-mode US examination.^[14] In the acute phase; local hyperemia is evaluated as a marked increase in vascularization by CDUS.^[15] In our patient population, all patellar tendons in patients with acute OSD had low echogenicity compatible with the study of Blankstein et al.^[14] We also observed increased tendon vascularity with CDUS. We also observed infrapatellar deep bursitis in patients with acute OSD. In previous studies, it was reported that healthy patellar tendon thickness is 3–3.5 mm in the middle section and 4–5 mm at the proximal and distal adhesion site.^[15] According to the results of our study, the patellar tendons got thicker in patients with acute OSD when compared to healthy individuals. Likewise, our results showed that, the patellar tendon thickness of patients with acute OSD was statistically significantly higher in comparison with patients with chronic OSD and healthy individuals.

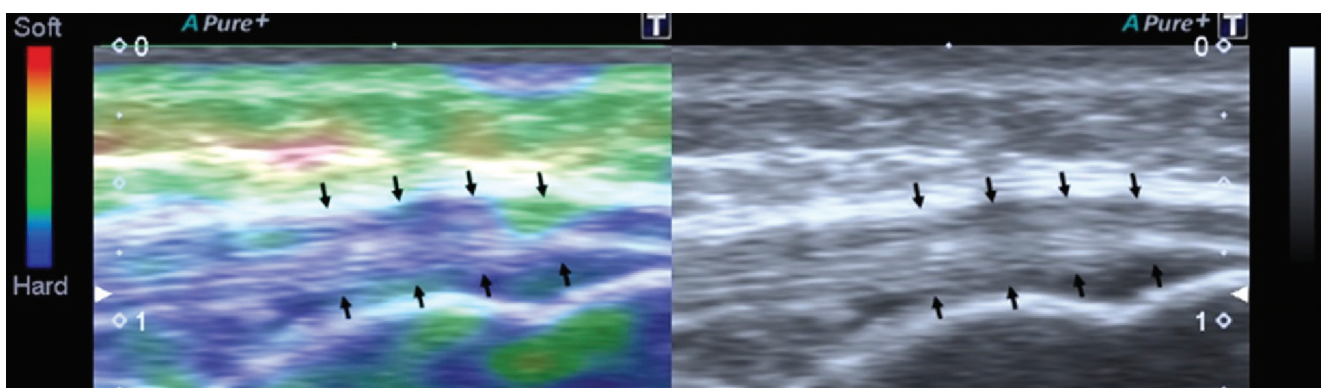


Figure 4. SEL evaluation of the patellar tendon (arrows) demonstrates a type 1a structure in a 14-year-old female healthy volunteer.

Table 1

B- mode US, CDUS and SEL characteristics of the distal patellar tendons in study population.

	Acute OSD (n=9)	Chronic OSD (n=7)	Healthy volunteers (n=20)
The average tendon thickness (mm) (median; range)	7.5; 4.5–10 mm	4; 2.9–4 mm	3.3; 2.5–4.2 mm
B-mod US findings			
Decrease in tendon echogenicity	+	-	-
Micro calcification	-	+	-
Coarse calcification	+	-	-
Cortical irregularities	+	-	-
Infrapatellar deep bursitis	+	-	-
CDUS findings			
Increased intratendinous and/or peritendinous vascularity	+	-	-
SEL subtypes			
	2b (n=8)	2a (n=7)	1a (n=20)
	2a (n=1)		

CDUS: color Doppler US; OSD: Osgood-Schlatter disease; SEL: sonoelastography; US: ultrasound.

Elastography is a new sonographic modality in which the elasticity of different tissue types is evaluated. The basic principle on which SEL is based is the strain (displacement) due to compression applied to viable tissue. This displacement can be calculated with the modified US and reflected on the color scale.^[8,16,17] In our study, we observed a markedly soft appearance of the tendon in symptomatic OSD cases (coding in red color) and a moderately hard appearance (showing a yellow-red color coding in green) in the patients with chronic OSD. This is similar to the previous studies which evaluated SEL findings in tendinopathy. In a series of 214 patients whose clinical examination suggested tendinopathy or underwent surgical treatment but had no sonographic abnormality on the B-mode US, 164 patients had positive findings supporting tendinopathy in SEL.^[18] Another study by Prado-Costa et al.^[19] evaluated tendon damage in 26 cases with different tendons including patellar tendon and observed a decrease in the tendon stiffness in the presence of tendinopathy. In a study by Porta et al.,^[20] it was emphasized that compression-based SEL examination is a useful and easily applicable method in the evaluation of patellar tendon in healthy subjects. In this study, we found that SEL demonstrated hard coding in tendons of healthy individuals and soft coding in tendons with pathological changes. As a result, it was determined that small changes in the elasticity and mechanical characteristics of the distal patellar tendon in patients with OSD can be detected by SEL.

There are some strengths and limitations of the present study. To our knowledge, this is the first study that demonstrates SEL and CDUS findings in addition to US appearance in patients with acute and chronic OSD in comparison with healthy individuals. It can be challenging to differentiate tendon pathologies that has similar findings in B-mode US evaluation. However, the addition of

CDUS and SEL findings to B-mode US may improve both the diagnostic accuracy and the capability of evaluation of the disease course. On the other hand, physicians may use US which is a widely applicable technique with no radiation exposure that is important for the pediatric population for the diagnosis and follow-up of the patients with OSD. The small sample size and retrospective nature of the study are the main limitations. Further prospective studies with larger sample sizes may help demonstrate the role of SEL in the evaluation of chronicity and pain relief in patients with OSD as well as diagnosis.

We demonstrated both B mode US, CDUS and SEL findings of the OSD in comparison with healthy individuals. In B-mode US evaluation, it can be challenging to differentiate different pathologies that has identical findings as discussed in the present study. However, having the knowledge of CDUS and SEL findings of OSD may help clinician to diagnose OSD more confidently. By the way, we think that, SEL will also help to demonstrate the progress of the disease in addition to B mode US and CDUS findings.

Conclusion

Distal patellar tendon in patients with OSD was thicker and softer in comparison with healthy volunteers. The intratendinous and/or peritendinous vascularity on CDUS was increased in patients with acute OSD. We suggest that these findings could be associated with tendon degeneration in OSD patients and can be useful in the evaluation of the disease.

Acknowledgments

The authors would like to express their sincere gratitude to the volunteers.

Conflict of Interest

The authors declare no conflict of interest.

Author Contributions

MB: project development, data collection, data analysis, drafting the article, revising the text; SSI: data collection, data analysis, drafting the article; ISI: data collection, data analysis, drafting the article.

Ethics Approval

The study was approved by Ethical Committee of Ankara Yıldırım Beyazıt University (No:E1/867/2020 date: 30.09.2020). Informed consent was obtained from all the volunteers and carried out in accordance with the Helsinki declaration of principles.

Funding

The authors declare no financial support.

References

- Gholve PA, Scher DM, Khakharia S, Widmann RF, Green DW. Osgood-Schlatter syndrome. *Curr Opin Pediatr* 2007;19:44–50.
- Maher PJ, Ilgen JS. Osgood-Schlatter disease. *BMJ Case Rep* 2013; ber2012007614.
- Circi E, Atalay Y, Beyzadeoglu T. Treatment of Osgood-Schlatter disease: review of the literature. *Musculoskelet Surg* 2017;101:195–200.
- Jacobson JA. Musculoskeletal ultrasound: focused impact on MRI. *AJR Am J Roentgenol* 2009;193:619–27.
- Taljanovic MS, Gimber LH, Becker GW, Becker GW, Latt LD, Klauser AS, Melville DM, Gao L, Witte RS. Shear-wave elastography: basic physics and musculoskeletal applications. *Radiographics* 2017;37:855–70.
- Lin J, Fessell DP, Jacobson JA. An illustrated tutorial of musculoskeletal sonography: part I, introduction and general principles. *AJR Am J Roentgenol* 2000;175:637–45.
- Sarvazyan A, Hall TJ, Urban MW, Fatemi M, Aglyamov SR, Garra BS. An overview of elastography—an emerging branch of medical imaging. *Curr Med Imaging Rev* 2011;7:255–82.
- Park GY, Kwon DR. Application of real-time sonoelastography in musculoskeletal diseases related to physical medicine and rehabilitation. *Am J Phys Med Rehabil* 2011;90:875–886.
- Pesavento A, Perrey C, Krueger M, Ermert H. A time efficient and accurate strain estimation concept for ultrasonic elastography using iterative phase zero estimation. *IEEE Trans Ultrason Ferroelectr Freq Control* 1999;46:1057–67.
- Cho N, Moon WK, Park JS, Park JS, Cha JH, Jang M, Seong MH. Nonpalpable breast masses: evaluation by US elastography. *Korean J Radiol* 2008;9:111–8.
- Balaban M, Idilman IS, Ipek A, İkiz SS, Bektaser B, Gumus M. Elastographic findings of achilles tendons in asymptomatic professional male volleyball players. *J Ultrasound Med* 2016;35:2623–8.
- Evrans B, Idilman I, Ipek A, Polat SB, Cakir B, Ersoy R. Real-time sonoelastography and ultrasound evaluation of the Achilles tendon in patients with diabetes with or without foot ulcers: a cross sectional study. *J Diabetes Complications* 2015;29:1124–9.
- De Zordo T, Lill SR, Fink C, Feuchtner GM, Jaschke W, Bellmann-Weiler R, Klauser AS. Real-time sonoelastography of lateral epicondylitis: comparison of findings between patients and healthy volunteers. *AJR Am J Roentgenol* 2009;193:180–5.
- Blankstein A, Cohen I, Heim M, Diamant L, Salai M, Chechick A, Ganel A. Ultrasonography as a diagnostic modality in Osgood-Schlatter disease. A clinical study and review of the literature. *Arch Orthop Trauma Surg* 2001;121:536–9.
- Waseem N, Arshad N, Saleem K, Ali A, Farooq R, Sultan R. A review on accuracy of doppler ultrasound in various knee joint pathologies. *Saudi J Med Pharm Sci* 2021;7: 107–13.
- Enomoto S, Tsushima A, Oda T, Kaga M. The passive mechanical properties of muscles and tendons in children affected by Osgood-Schlatter disease. *J Pediatr Orthop* 2020;40:e243–e247.
- Varghese T, Ophir J, Konofagou E, Kallel F, Righetti R. Tradeoffs in elastographic imaging. *Ultrason Imaging* 2001;23:216–48.
- Galletti S, Francesco O, Masiero S, Frizziero A, Galletti R, Schiavone C, Salini V, Abate M. Sonoelastography in the diagnosis of tendinopathies: an added value. *Muscles Ligaments Tendons J* 2015; 5:325–30.
- Prado-Costa R, Rebelo J, Monteiro-Barroso J, Preto AS. Ultrasound elastography: compression elastography and shear-wave elastography in the assessment of tendon injury. *Insights Imaging* 2018;9: 791–814.
- Porta F, Damjanov N, Galluccio F, Iagnocco A, Matucci-Cerinic M. Ultrasound elastography is a reproducible and feasible tool for the evaluation of the patellar tendon in healthy subjects. *Int J Rheum Dis* 2014;17:762–6.

ORCID ID:

M. Balaban 0000-0002-6752-6838;
S. Sigit İkiz 0000-0001-5342-9589;
I. S. İdilman 0000-0002-1913-2404









Correspondence to:

Mehtap Balaban, MD
Department of Radiology, Faculty of Medicine,
Yıldırım Beyazıt University, Ankara, Türkiye
Phone: +90 312 906 20 00
e-mail: mehtapbalaban40@hotmail.com

Conflict of interest statement: No conflicts declared.

This is an open access article distributed under the terms of the Creative Commons Attribution-NonCommercial-NoDerivs 4.0 Unported (CC BY-NC-ND4.0) Licence (<http://creativecommons.org/licenses/by-nc-nd/4.0/>) which permits unrestricted noncommercial use, distribution, and reproduction in any medium, provided the original work is properly cited. *How to cite this article:* Balaban M, Sigit İkiz S, İdilman İS. Sonoelastography findings of the patellar tendon in Osgood-Schlatter disease. *Anatomy* 2022;16(1):13–18.

The course of the sciatic nerve in the gluteal region and comparison of two methods used for sciatic nerve blockage

Bilge İpek Torun¹ , Ayşe Surhan Çınar² , Luis Filgueira³ , R. Shane Tubbs⁴⁻⁷ ,
Alparslan Apan⁸ , Aysun Uz^{3,9,10} 

¹Department of Anatomy, Faculty of Medicine, Ankara Yıldırım Beyazıt University, Bilkent, Ankara, Türkiye

²Department of Anesthesiology and Reanimation, Şişli Hamidiye Etfal Training and Research Hospital, University of Health Sciences, Istanbul, Türkiye

³Department of Anatomy, Faculty of Science and Medicine, University of Fribourg, Route Albert-Gockel 1, Fribourg, Switzerland

⁴Department of Neurosurgery, Tulane University, School of Medicine, New Orleans, LA, USA

⁵Department of Neurosurgery and Ochsner Neuroscience Institute, Ochsner Health System, New Orleans, LA, USA

⁶Department of Anatomical Sciences, St. George's University, Grenada

⁷Department of Neurology, Tulane University School of Medicine, New Orleans, LA, USA

⁸Department of Anesthesiology and Reanimation, Faculty of Medicine, University of Giresun, Giresun, Türkiye

⁹Department of Anatomy, Faculty of Medicine, Ankara University, Ankara, Türkiye

¹⁰Department of Neuroscience, Ankara University, Graduate School of Health Science, Ankara, Türkiye

Abstract

Objectives: The aim of this study was to reevaluate the anatomy of the sciatic nerve (SN) in the gluteal region by identifying reliable landmarks in order to suggest a safe insertion point for SN blockage (SNB), and to compare two methods used for SNB.

Methods: Bilateral dissections of the SN were performed on ten embalmed cadavers. The course of the SN in relation to a line drawn between the posterior superior iliac spine (PSIS) and the ischial tuberosity (IT) was determined. The files of 100 patients, 50 of whom had SNB with the Labat's method (group L) and 50 with the parasacral approach (group P), were reviewed retrospectively. The results of the two methods were compared.

Results: The vertical distance between the PSIS to the IT was 13.1±6.5cm. The vertical distance between the intersection points of the inferior border of the piriformis with the medial and lateral margins of the SN were 7.8±0.7 and 9.1±0.6 cm, respectively. Medial and lateral margins of the SN were found to be 1.8±0.5 and 2.9±0.6 cm lateral to the IT. Insertion depth of the needle and time for the intervention were similar for both of the methods, but need for additional nerve blockages were significantly higher in group L than in group P.

Conclusion: We defined a safe insertion point for SNB in the gluteal region, using prominent, fixed bony and easily detectable landmarks. The clinical results of both groups were similar, but need for additional nerve blockages were significantly higher in group L.

Keywords: anatomical landmark; postoperative pain; regional anesthesia; sciatic blockage; gluteal region

Anatomy 2022;16(1):19–25 ©2022 Turkish Society of Anatomy and Clinical Anatomy (TSACA)

Introduction

Peripheral nerve blockage has become increasingly popular for providing peri- and post-operative analgesia, due to lower complication rates in comparison with other anesthetic procedures. Successful application is limited and

depends on knowledge of the regional anatomy, as well as special skills and techniques that are required for efficient peripheral nerve blockages, especially when the nerve is deeply located. Sciatic nerve (SN) blockage (SNB) may be used to anesthetize most of the foot and the knee, as well as the posterior thigh. At the pelvic level, the SN can be

anesthetized by classical posterior (Labat's method) approach, Raj's posterior approach, anterior, lateral, or parasacral approaches.^[1-5] So many approaches have emerged in SNB because there is no single method that is the most effective, safest, and has the least undesirable effects. However, all points defined by published descriptions are insufficient in determining the exact line that corresponds to the underlying nerve.

The use of ultrasound-guided peripheral nerve blockages has become increasingly popular in recent years. However, ultrasound is not always available everywhere, and its use requires certain training and expertise. In this situation, the physician who will apply the blockage should know the anatomical landmarks used to locate the nerve. For these reasons, in-depth knowledge of anatomy is a precondition for performing regional anesthesia.^[6] Defining the main anatomical landmarks for regional anesthesia, detailed knowledge of the proper anatomy is required to define the sonoanatomy.^[7] The SNB, guided by classical anatomy knowledge and traditional nerve stimulation, still maintains its importance recently.

The aim of this study was to reevaluate the regional anatomy of the SN for anesthetic blockage using simply accessible bony landmarks, and to compare the clinical efficacy of two methods used for SNB.

Materials and Methods

Cadaveric Study

Bilateral dissections of the SN were performed on 10 (6 women, 4 men) formaldehyde fixed cadavers (46 to 69 years at death). The use of the human cadaveric material was guided according to the guidelines of the university. Dissections were performed by senior anatomists.

The location and course of the SN was assessed by identifying its relationship with a line drawn from the midpoint of the posterior superior iliac spine (PSIS) to the lowermost point of the ischial tuberosity (IT) (**Figure 1**). The safe area for accessing the SN was determined according to the branching of the regional vascular structures and nerves. The branching of the posterior femoral cutaneous nerve (PCN) was also considered.

The vertical distance between the PSIS and the lowermost point of the IT was measured. The intersection points of the inferior border of the piriformis muscle with the medial (A) and lateral (B) margins of the SN were identified and the vertical distances between the PSIS and A and B points were measured. The horizontal distances between the lateral border of the IT and the medial (C) and the lateral (D) margins of the SN at the level of the lowermost point of the IT were measured (**Figure 2**). The horizontal

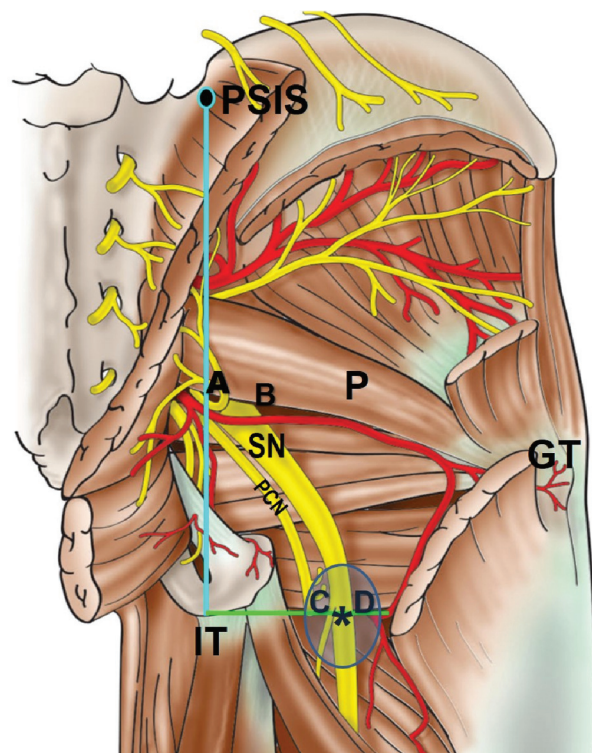


Figure 1. Illustration of the posterior gluteal region. The blue transparent circle is the suggested safe area relatively free from neurovascular structures with asterisk showing the ideal needle insertion point. The vertical distance between PSIS and IT is shown as the blue line. The horizontal distances between IT and the sciatic nerve is shown as the green line. A: the intersection point of the inferior border of the piriformis muscle with the medial margins of SN; B: the intersection point of the inferior border of the piriformis muscle with lateral margins of SN; C: the medial margin of the SN at the level of the lowermost point of IT; D: the lateral margin of the SN at the level of the lowermost point of IT; GT: greater trochanter; IT: ischial tuberosity; P: piriformis muscle; PCN: posterior femoral cutaneous nerve; PSIS: posterior superior iliac spine; SN: sciatic nerve.

distances between A and B points, and C and D points were measured, and considered as the widths of the SN at the level of the exit point from the infrapiriform foramen and at the level of the lowermost point of the IT, respectively. Measurements were performed with ruler and a digital caliper sensitive to one decimal. The neurovascular area was defined as the area surrounding the points A, B, C and D (**Figure 3**). The optimal injection point to reach the SN effectively without injuring any other neurovascular structures was defined according to the measurements.

Clinical Study

A hundred patients, aged between 18 and 69 years, who had ankle and/or foot surgery between January 2015 and January 2018 in our tertiary hospital were included in this study. Fifty of the patients had SNB with the Labat's

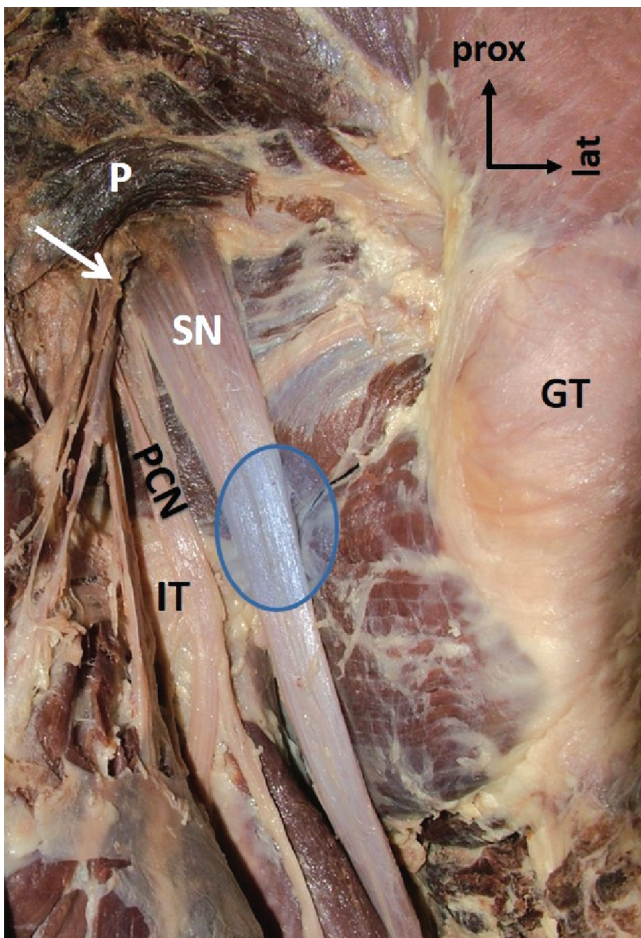


Figure 2. Anatomical dissection of the right sciatic nerve. The arrow indicates the vascular structures emerging from the infrapiriform foramen. Blue transparent circle shows the suggested safe area relatively free from neurovascular structures. GT: greater trochanter; IT: ischial tuberosity; P: piriformis muscle; PCN: posterior femoral cutaneous nerve; SN: sciatic nerve.

method (group L), and 50 of them had SNB with the parasacral approach (group P). The files of the patients were reviewed retrospectively. Patients with a history of neuropathy, neuromuscular disease, or chronic pain syndromes were excluded from the study. All the premedication procedures had been the same for both groups of patients. All patients taken to the operating rooms had been routinely monitored, and vital signs had been checked properly until the end of the operation. Demographic data (age, weight, height, sex), duration of surgery, the depth of the nerve, the number of attempts, and time for successful blockage were obtained from the files of the patients.

The skin at the needle entry site had been infiltrated with 2 mL of 2% lidocaine using a 30-gauge hypodermic needle. SNB had been performed either with Labat's approach, or parasacral approach.

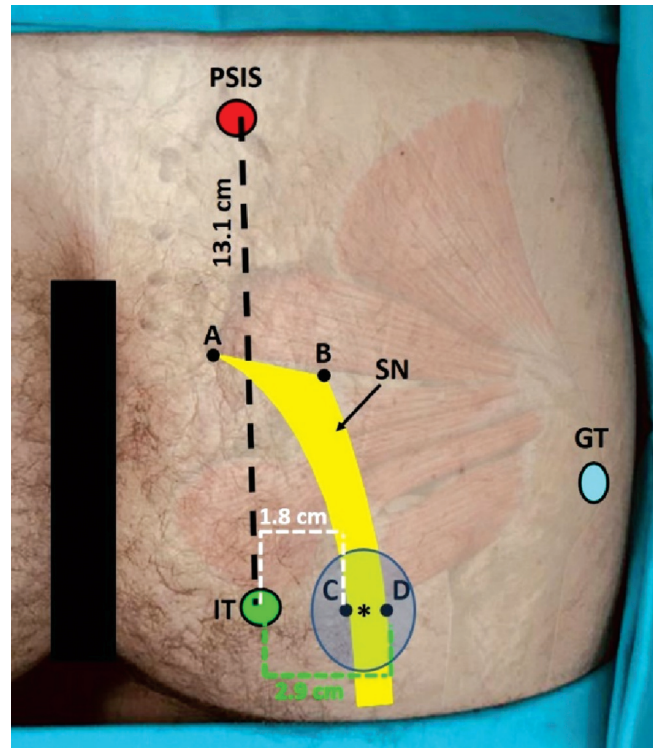


Figure 3. Surface projection of the sciatic nerve on a patient using anatomical landmarks. The blue transparent circle is the suggested safe area relatively free from neurovascular structures with asterisk showing the ideal needle insertion point. A: the intersection points of the inferior border of the piriformis muscle with the medial margins of SN; B: the intersection points of the inferior border of the piriformis muscle with lateral margins of SN; blue circle: the greater trochanter; C: the medial margin of the SN at the level of the lowermost point of IT (ischial tuberosity); D: the lateral margin of the SN at the level of the lowermost point of IT (ischial tuberosity); GT: greater trochanter; green circle: IT (ischial tuberosity); IT: ischial tuberosity; PSIS: posterior superior iliac spine; red circle: PSIS (posterior superior iliac spine); SN: sciatic nerve.

Labat's approach was applied as follows: The PSIS and the GT are marked and a line was drawn between the two structures. A perpendicular line from the midpoint of this line was drawn towards infero-medial. The 5th cm was used as the needle insertion point (Figure 4a).^[4]

Parasacral approach was applied as follows: The PSIS and the IT are marked and a line was drawn between the two structures. The 6th cm from the PSIS was used as the needle insertion point (Figure 4b).^[4]

The following procedures were the same for both methods. To block the SN, a 100-mm short, beveled, 22-gauge stimulating needle (B. Braun, Melsungen, Germany) had been used. The needle had been connected to a nerve stimulator (Stimuplex HNS11, B. Braun, Melsungen, Germany). The initial stimulus had been set at 2 mAmp intensity with 2 Hz frequency. After ankle dor-

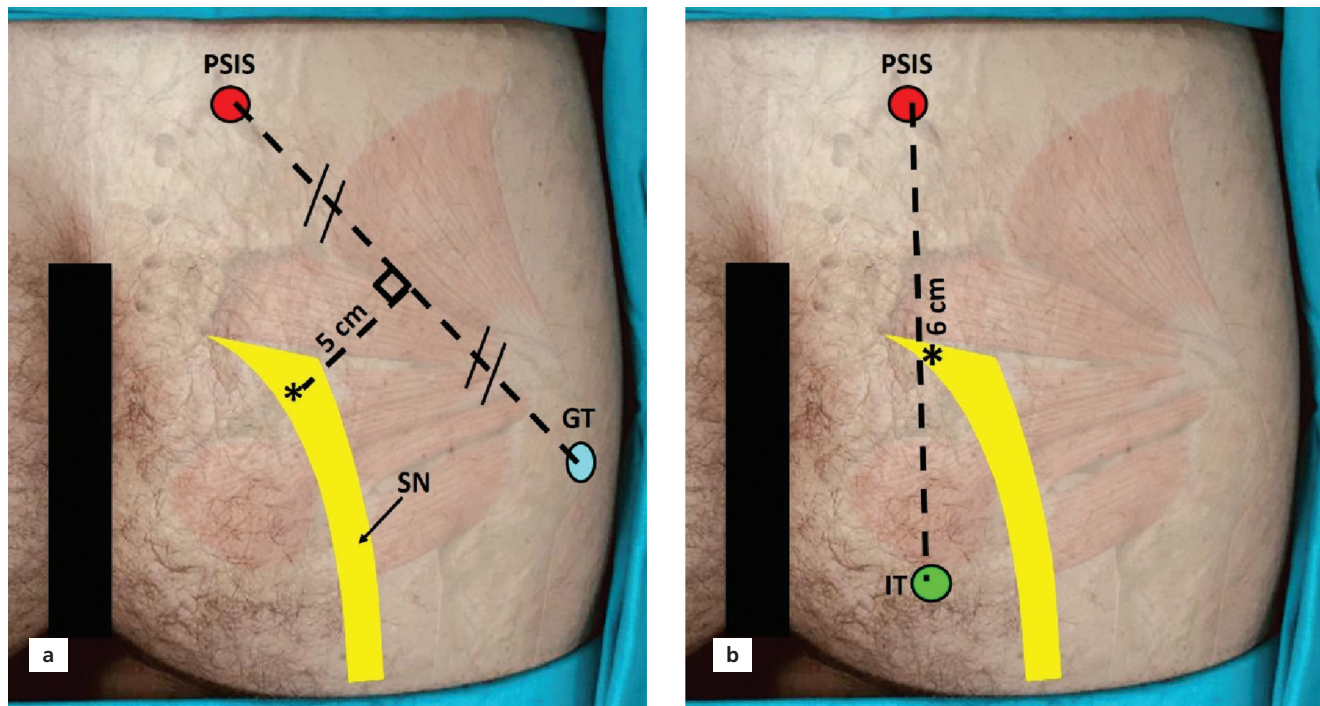


Figure 4. Compared sciatic blockage techniques with asterisk showing the needle insertion point. (a) Labat's approach, (b) Parasacral approach. GT: greater trochanter; IT: ischial tuberosity; PSIS: posterior superior iliac spine; SN: sciatic nerve.

siflexion or eversion with 0.5 mAmp stimulus, gentle aspiration had been performed and 20 mL of a 0.5% solution of bupivacaine (Astra-Zeneca, Orebo, Sweden) had been administered in 5 mL increments. Block had been applied to all patients by senior anesthetists in charge of the orthopedic room. Needle insertion was considered successful if plantar flexion, eversion of the foot, and/or dorsiflexion of the foot had been observed under 0.5 mAmp stimulation. The depth of the location of the SN was measured as the length of the needle from the skin to the point that plantar flexion had been observed. The time for a successful blockage was defined as the time from insertion of the needle into the skin to the observation of muscle contraction with a 0.5 mAmp stimulus. The depth of the nerve, the number of attempts, and time for successful blockage were obtained from the patients' files and considered for this study. The quality of the SNB, which was graded as good (no supplemental anesthetic required), satisfactory (local anesthetic to the surgical site or intravenous analgesic supplementation required), or failed (general anesthesia required) had been recorded in the files and considered for the study. Additional nerve blockages (saphenous and femoral) were also considered. Pain sensation during the procedure of performing SNB had been graded using the visual analog scale (VAS) by the patients according to a scale from 0 (no pain) to 10 (worst imaginable pain). A neurological examination (assessment for paresthesia,

dysesthesia, prolonged anesthesia, or unexpected motor deficit) had been performed preoperatively and 24 hours postoperatively. Neural complications had been recorded.

First, a preliminary study was performed on the files of 20 patients. The data of the first 20 patients were used to do a power calculation, which indicated that at least 50 patients for each group were required to determine statistical significance with an alpha of 0.05 and beta of 0.2. Ordinal data were evaluated using contingency tables with χ^2 and Fisher's exact test. Student's t-test or Mann-Whitney U tests were used to compare nominal data according to data distribution. Results were documented as mean \pm SD, and a p value <0.05 was considered for statistical significance. SPSS (Version 22, IBM Corp., Armonk, NY, USA) was used to run basic statistical analyses.

Results

Data from Cadavers

The SN showed a slightly concave course, extending from points A-B to points C-D, with its concavity facing medial (Figures 1, 2 and 3). With its concavity facing medial a slightly concave line with a width of 2 cm proximally and 1 cm distally, drawn from 8 cm below the PSIS towards 2 cm lateral to the lateral border of the IT was considered to be the surface projection of the SN (Figure 3). At the exit point from the infrapiriform foramen, it was observed that

the inferior gluteal artery accompanied the SN. The distal half of the area that the SN coursed was relatively free from neurovascular structures (Figures 1 and 2). However, the proximal PCN was in this area in 90% of cases (Figure 2). Meanwhile, we did not observe small or large variants of the SN, that is, separation in the pelvic region, in the cadavers used in the study. The results of the measurements were summarized in Table 1.

Being free from any other neurovascular structures, we determined the needle insertion point for a safe approach as the point between C and D points (Figure 3). It was 13 cm distal to the PSIS and 2–3 cm (C-D points, respectively) lateral to the lateral border of the IT.

Clinical Data

There were no statistically significant differences between the two study groups for patients' demographic data (age, weight, height, sex), and duration of surgery (Table 2).

The results of the evaluated parameters of the two groups were summarized in Table 3. There was no statistically significant difference between the two approaches for the distance to reach to the nerve ($p=0.315$), and for

Table 1
Cadaveric measurements

	Mean±SD (cm)
PSIS-IT	13.1±0.6
PSIS-SN (A)	7.8±0.7
PSIS-SN (B)	9.1±0.6
IT-SN (C)	1.8±0.5
IT-SN (D)	2.9±0.6
A – B distance	2.3±0.5
C – D distance	1.2±0.3

A: the intersection point of the inferior border of the piriformis muscle with the medial margins of SN; B: the intersection point of the inferior border of the piriformis muscle with lateral margins of SN; C: the medial margin of the SN at the level of the lowermost point of IT; D: the lateral margin of the SN at the level of the lowermost point of IT; IT: ischial tuberosity; PSIS: posterior superior iliac spine; SD: standard deviation; SN: sciatic nerve.

the number of attempts to target the SN ($p=0.062$). The quality of the SNB was similar ($p=0.781$). Pain intensity during the blockages was equal between the two techniques. No neural complications were observed in the 24-hour follow-up period in both study groups. Need for

Table 2
Patient data and duration of surgery.

	Group L (n=50)	Group P (n=50)	p-value
Age (years)	43.5±14	50.9±12.6	0.23
Weight (kg)	78.7±17.2	79.6±13.4	0.43
Height (cm)	169.5±9.2	163.4±8.9	0.48
Sex (W/M) (%)	56/4	60/40	0.09
Duration of surgery (min)	61.1±14.6	65.3±19	0.32

Data are given as mean±standard deviation and %.

Table 3
Comparison of the results of the two methods (Labat's approach: Group L and parasacral approach: Group P).

		Group L	Group P	p-value
SN Depth (mm)		71.4±14	69.6±15	0.315
Number of attempts to target the SN		1.72±0.72	1.60±0.59	0.834
The time between inserting the needle into the skin to seen muscle contraction with 0.5 mAmp stimuli (seconds)		32.4±10.6	30.3±8.5	0.062
The quality of the SNB	Good	28	32	0.781
	Satisfactory	19	15	
	Failed	3	2	
Pain intensity	Moderate and severe pain (VAS ≥4)	21/50 (42%)	19/50 (38%)	0.838
Need for additional nerve blockages	Saphenous nerve blockage	26/50 (52%)	19/50 (38%)	0.017*
	Femoral nerve blockage	14/50 (28%)	9/50 (18%)	

* $p<0.05$.

additional nerve blockages (saphenous and femoral) were significantly higher in group L than in group P ($p=0.017$).

Discussion

The SNB is frequently used for surgery of the distal lower limb and foot. There are various limitations of SNB methods applied to date. Therefore, we compared two approaches used for SNB, and conducted a cadaveric study in order to suggest novel landmarks for a safe approach.

The SN is actually two nerves that are loosely connected together in the same connective tissue sheath. The tibial and the common fibular nerves usually diverge at the distal thigh, but in nearly 12.2% of people, the common fibular nerve passes through the piriformis, while in 0.5% it passes superior to the muscle.^[8] Cuvillon et al.^[9] demonstrated that single injection produces similar success rates compared with double injection. However, it is well known that the multiple injection technique for the SNB offers a higher success rate. Because the division of the SN into its components can occur at any point between the sacral plexus and the lower third of the thigh. In our study we did not observe a variation such as split SN in the cadaveric part of the study.

For the SNB procedures, clinicians usually use bony landmarks. The PSIS, the greater trochanter, and the IT are the most frequently used ones. However, identifying the greater trochanter might be difficult in some patients, e.g., obese patients. di Benedetto et al.^[10] used the GT and the IT as landmarks with the hip in flexion, but the required 90° of hip flexion might be difficult in certain patients. The subgluteus parabiiceps technique is questionable for identification of soft tissues in obese patients.^[11] Additionally, both of the studies mentioned above describe the SNB distal to the gluteal region rather than the posterior femoral area. Posterior approach for the SNB requires special positioning that might be difficult to obtain in some patients.^[2] The anterior approach to the SN has also been described and could be performed in the supine position; however, the procedure is difficult at the level of the lesser trochanter, and reaching the nerve may require leg rotation.^[12,13] Novel and easy landmarks have been developed to overcome this problem.^[14] However, needle advancement under ultrasound guidance is not feasible when using the anterior approach due to acoustic shadowing by the overlying femur. Another new supine technique proposes using the GT and the anterior superior iliac spine as landmarks for reaching the SN laterally.^[15] However, this study was conducted on a limited number of cadavers. Uz et al.^[16] described a novel anterior approach and concluded that it could be used without damaging regional vascular structures while simultaneously blocking

the femoral nerve. In our cadaveric study, we defined a safe insertion point using the PSIS and the IT as landmarks. Also, we determined the surface projection of the SN using these landmarks (**Figure 3**). A line was drawn from the PSIS to the IT. Then, a slightly concave line was drawn from the point 8 cm distal to the PSIS on the first line to 2 cm lateral to the IT (the point described above as between points C and D) to indicate the course of the proximal part of the SN. The point between C and D was then defined as the point of puncture. The advantage of the line proposed in our study is that, it also defines the course of the SN. Therefore, it provides a better orientation for choosing the optimal site for needle entry. The line describing the course of the SN in our study also provides safety margins for both sites that were determined using cadavers. The advantage of our landmarks is using clearly defined bony prominences that can be identified even on obese patients. Furthermore, our descriptions may also facilitate ultrasound-guided SNB or other imaging studies that assess the SN in the gluteal region.

Guidance by ultrasound provides basic information about the exact location of deeply located nerves and their anatomical relationships with other structures necessary to achieve nerve blockage. However, ultrasound training is not compulsory in the anesthesiology residency curriculum.^[17] In addition, insufficient knowledge about the operation of the ultrasound device, limited educational resources, the minority of teaching centers using the technique are the most important restrictions in front of the widespread use of ultrasound in the peripheral block. Therefore, the traditional method is still valid in most geographies. In the future, standard ultrasound training should be a milestone to be added to the anesthesiology specialty curriculum.

The limitation of our cadaveric study is the limited sample size. Further studies being conducted on imaging methods would be useful in order to increase the sample size.

Conclusion

Without requiring any special positioning such as hip flexion, the insertion point for SNB suggested in our study may be a significant advantage in certain patients with restricted hip joint mobility. Also, we believe that the insertion point we determined is safe and reliable being free of neurovascular structures. Prominent, fixed bony and easily detectable landmarks for determining the surface projection of the SN is the other advantage of our study.

Acknowledgments

The authors sincerely thank those who donated their bodies to science so that anatomical research could be per-

formed. Results from such research can potentially increase mankind's overall knowledge that can then improve patient care. Therefore, these donors and their families deserve our highest gratitude.

Conflict of Interest

No conflict of interest was declared by the authors.

Author Contributions

BIT: Dissections, data analysis, manuscript writing; ASC: Project development, collecting the clinical data, manuscript writing; LF: Data analysis, editing the manuscript; RST: Data analysis, editing the manuscript; AA: Collecting the clinical data, data analysis; AU: Project development, dissections, editing the manuscript.

Ethics Approval

Ethical approval was taken from the Ethical Committee of Yıldırım Beyazıt University Faculty of Medicine (2022-06). All procedures performed in studies involving human participants were in accordance with the ethical standards of the institutional and/or national research committee and with the 1964 Helsinki declaration and its later amendments or comparable ethical standards.

Funding

This research did not receive any specific grant from funding agencies in the public, commercial, or not-for-profit sectors.

References

1. Beck GP. Anterior approach to sciatic nerve block. *Anesthesiology* 1963;24:222–4.
2. Guardini R, Waldron BA, Wallace WA. Sciatic nerve block: a new lateral approach. *Acta Anaesthesiol Scand* 1985;29:515–9.
3. Raj PP, Parks RI, Watson TD, Jenkins MT. A new single-position supine approach to sciatic-femoral nerve block. *Anesth Analg* 1975; 54:489–93.
4. Waldman SD. Comprehensive atlas of ultrasound-guided pain management injection techniques. Philadelphia (PA): Wolters Kluwer; 2013. 1205 p.
5. Mansour NY. Reevaluating the sciatic nerve block: another landmark for consideration. *Reg Anesth* 1993;18:322–3.
6. Sites BD, Chan VW, Neal JM, Weller R, Grau T, Koscielniak-Nielsen ZJ, Ivani G. The American Society of Regional Anesthesia and Pain Medicine and the European Society of Regional Anaesthesia and Pain Therapy Joint Committee recommendations for education and training in ultrasound-guided regional anesthesia. *Reg Anesth Pain Med* 2010;35:S74–80.
7. Wegener JT, van Doorn CT, Eshuis JH, Hollmann MW, Preckel B, Stevens MF. Value of an electronic tutorial for image interpretation in ultrasound-guided regional anesthesia. *Reg Anesth Pain Med* 2013;38:44–9.
8. Moore KL, Dalley AF, AMR A. Lower limb. In: Moore KL, Dalley AF, AMR A, editors. *Clinically oriented anatomy*. Baltimore: Wolters Kluwer Press; 2018. p. 734.
9. Cuvillon P, Ripart J, Jeannes P, Mahamat A, Boisson C, L'Hermite J, Vernes E, de la Coussaye JM. Comparison of the parasacral approach and the posterior approach, with single- and double-injection techniques, to block the sciatic nerve. *Anesthesiology* 2003;98: 1436–41.
10. di Benedetto P, Bertini L, Casati A, Borghi B, Albertin A, Fanelli G. A new posterior approach to the sciatic nerve block: a prospective, randomized comparison with the classic posterior approach. *Anesth Analg* 2001;93:1040–4.
11. Sukhani R, Candido KD, Doty Jr R, Yaghmour E, McCarthy RJ. Infragluteal-parabiceps sciatic nerve block: an evaluation of a novel approach using a single-injection technique. *Anesth Analg* 2003;96: 868–73.
12. Ericksen ML, Swenson JD, Pace NL. The anatomic relationship of the sciatic nerve to the lesser trochanter: implications for anterior sciatic nerve block. *Anesth Analg* 2002;95:1071–4.
13. Vloka JD, Hadziç A, April E, Thys DM. Anterior approach to the sciatic nerve block: the effects of leg rotation. *Anesth Analg* 2001;92: 460–2.
14. Van Elstraete AC, Poey C, Lebrun T, Pastureau F. New landmarks for the anterior approach to the sciatic nerve block: imaging and clinical study. *Anesth Analg* 2002;95:214–8.
15. Le Corroller T, Wittenberg R, Pauly V, Pirro N, Champsaur P, Chouet O. A new lateral approach to the parasacral sciatic nerve block: an anatomical study. *Surg Radiol Anat* 2011;33:91–5.
16. Uz A, Apaydin N, Cinar SO, Apan A, Comert B, Tubbs RS, Loukas M. A novel approach for anterior sciatic nerve block: cadaveric feasibility study. *Surg Radiol Anat* 2010;32:873–8.
17. Kim TE, Tsui BCH. Simulation-based ultrasound-guided regional anesthesia curriculum for anesthesiology residents. *Korean J Anesth* 2019;72:13–23.

ORCID ID:

B. I. Torun 0000-0002-0155-7447; A. Surhan Çınar 0000-0003-2247-9764; L. Filgueira 0000-0002-2266-6650; R. S. Tubbs 0000-0003-1317-1047; A. Apan 0000-0001-9660-3276; A. Uz 0000-0002-4005-5466



Correspondence to:

Bilge İpek Torun, MD
Department of Anatomy, Faculty of Medicine,
Ankara Yıldırım Beyazıt University, Ankara, Türkiye
Phone: +90 312 906 20 83
e-mail: bilgeipek@yahoo.com

Conflict of interest statement: No conflicts declared.

This is an open access article distributed under the terms of the Creative Commons Attribution-NonCommercial-NoDerivs 4.0 Unported (CC BY-NC-ND4.0) Licence (<http://creativecommons.org/licenses/by-nc-nd/4.0/>) which permits unrestricted noncommercial use, distribution, and reproduction in any medium, provided the original work is properly cited. *How to cite this article:* Torun Bİ, Surhan Çınar A, Filgueira L, Tubbs RS, Apan A, Uz A. The course of the sciatic nerve in the gluteal region and comparison of two methods used for sciatic nerve blockage. *Anatomy* 2022;16(1):19–25.

The analysis of morphological features and ultrasonographic characteristics of Dupuytren's disease

Atilla Hikmet Çilengir¹ , Mehtap Balaban² 

¹Department of Radiology, Faculty of Medicine, Izmir Democracy University, Izmir, Türkiye

²Department of Radiology, Faculty of Medicine, Ankara Yıldırım Beyazıt University, Ankara, Türkiye

Abstract

Objectives: To detect B-Mode ultrasonography, color Doppler ultrasonography, and sonoelastography findings of the Dupuytren's disease, and to determine the differences of sonographic imaging, demographic and clinical data.

Methods: A total of 88 patients with unilateral lesion were included. Each lesion was evaluated with B-Mode ultrasonography, color Doppler ultrasonography, and sonoelastography. The location, size, morphology, and echogenicity of the lesions were analyzed by B-mode ultrasonography, the presence of vascularization by color Doppler ultrasonography, and the elasticity by sonoelastography, retrospectively. The differences between sonographic findings, demographic and clinical data were evaluated.

Results: Of the patients, 36.4% were women and 63.6% were men, with a median age of 61 (interquartile range: 9). The majority of the lesions (87.5%) were at the level of the 3rd and 4th finger/metacarpal. Median longitudinal dimension was 6.75mm (interquartile range: 4.32), mediolateral dimension was 2.5 mm (interquartile range: 1.77). Of the lesions, 67.1% were nodular shaped, 73.9% were hypoechoic, and 87.5% were hypovascular. All lesions were hard coded on sonoelastography. The cord morphology, extension to the tendon, and contracture tend to be together, and lesions with these were mostly iso-hypoechoic.

Conclusion: Dupuytren's disease lesions were mostly nodular, hypoechoic, hypovascular, and stiff. Ultrasonographic examination was sufficient and successful in the diagnosis of Dupuytren's disease.

Keywords: color doppler ultrasonography; Dupuytren's disease; morphology; sonoelastography; ultrasonography

Anatomy 2022;16(1):26–32 ©2022 Turkish Society of Anatomy and Clinical Anatomy (TSACA)

Introduction

Dupuytren's disease (DD) is a benign fibroblastic proliferation of palmar aponeurosis.^[1] It is the most common superficial fibromatosis and affects 1–2% of the population.^[2] Its frequency is geographically and racially distributed, most common in northern Europe.^[3] The frequency of DD increases in the elderly population and reaches 20% over the age of 65.^[3] Male dominance is present, it is not uncommon to be bilateral.^[2] Another name is palmar fibromatosis, and Dupuytren's contracture terminology is used in cases with flexion contracture at the fingers.^[4,5] Clinically, there are palpable painless subcutaneous nodules on the palmar face.^[1] It can grow over the years and cause retraction of the tendons, causing flexion contracture

of the fingers. It is often located at the level of the 4th and 5th metacarpal.

Although the etiology has not been clearly revealed, some reasons have been accepted. Trauma, smoking, microvascular damage, antiepileptic use, immunological and genetic factors are some of them.^[3] Fibrogenic cytokines such as fibroblast growth factor, wntless/integrated, and transforming growth factor beta released in various causes are the main cause of the disease.^[6] Therefore, DD can be seen together with other superficial fibromatoses, plantar fibromatosis (Ledderhose disease) and Peyronie's disease.^[3]

The diagnosis can usually be made easily with typical lesion localization and physical examination. Since the

differential diagnosis includes tenosynovitis, trigger finger, ganglion cyst, and other soft tissue masses, imaging should be performed even if the diagnosis is clinical. In addition, with imaging methods, information about the three dimensions of the lesion can be obtained and its relationship with adjacent tendons and neurovascular bundles can be evaluated.^[7] B-mode ultrasonography (US) is the first choice and easily accessible imaging method in superficial lesions. With US, the solid or cystic nature of the lesion can be distinguished. Its vascularity can be detected with Color Doppler US (CDUS). Sonoelastography (SEL) is a current and popular modality that provides additional contributions to tendon, ligament, muscle, and superficial masses in musculoskeletal sonographic examination.^[8,9] On SEL, the stiffness of the tissues is coded in a color scale from blue to red and transmitted to the observer. In addition to qualitative examination, quantitative stiffness measurement can be made. Superficial lesions in DD are also an ideal target for SEL examination.

There is no specific treatment for DD. Methods such as rest, topical agents, steroid injections can be tried.^[3] Lesions can be excised surgically, but since 30–40% may show recurrence, it is not preferred if there is no flexion contracture or lesion affecting daily life. The presence of a flexion contracture greater than 20 degrees in the metacarpophalangeal joint and 30 degrees in the proximal interphalangeal joint is an indication for surgery.^[10] For these reasons, treatment should be personalized on a patient basis. Therefore, imaging methods, especially ultrasound, are important in guiding the treatment. At the same time, minimally invasive treatments can be performed with ultrasound guidance (e.g., intralesional injection) and can be easily used in treatment follow-up.^[7]

Our aim in this study was to describe the US, CDUS and SEL imaging findings of DD lesions and to investigate whether these findings are differ from each other. At the same time, the differences between ultrasonographic findings and patient demographic and physical examination data was investigated.

Materials and Methods

The reports and recorded cine images of ultrasonographic examinations performed with the preliminary diagnosis of DD between June 2020 and June 2022 were retrospectively reviewed. These reports and images were reanalyzed retrospectively by a radiologist with 12 years of musculoskeletal US experience. Only patients with unilateral lesions were included in the study. In patients with multiple lesions, the dominant lesion was included. In addition, the clinical and physical examination findings of the

patients were examined. Patients with rheumatologic disease, diagnosis of malignancy, undergoing hand surgery and a history of hand trauma were excluded.

Ultrasound examination was performed while the patient was sitting, with the hand in supination in contact with the anterior thigh. The dimensions of the lesions in the transverse and longitudinal planes were measured. In all cases, B-Mode US, CDUS, and SEL examinations were performed separately for each lesion by the same radiologist, images were recorded and reported. Evaluation was done with a high resolution 5–11 MHz linear probe (GE Logiq S7 Expert, GE Healthcare, Milwaukee, WI, USA). The presence of vascularization in the lesions was evaluated in CDUS. Simultaneously, SEL examination of the lesions was performed with the same position and probe. Tissue elasticity under light compression and decompression with a probe on the lesion was evaluated according to the real-time color map on the B-Mode US image. On SEL, soft structures were coded in red, medium-hard structures in yellow, and hard structures in green and blue.

The presence of nodules or cords of DD, in which finger they were located, their size, echogenicity, extension to the flexor tendon, the presence of intralesional vascularization on CDUS, and the elasticity characteristics of the lesions on SEL were evaluated. The size of the lesions in the transverse and longitudinal planes were electronically measured on B-mode US with calipers. The echogenicity of the lesion was compared with the adjacent tendon and determined as hypoechoic, isoechoic, and hyperechoic. The extension to the flexor tendon defines the focal areas of extension of the lesions to both flexor digitorum superficialis and flexor digitorum profundus tendons. The presence of intralesional vascularization means colored areas in the lesion on CDUS examination. The elasticity characteristics of the lesions were classified on a soft to hard scale according to the color coding on the SEL examination.

Statistical analysis was performed with IBM SPSS Statistics Version 22.0 (Armonk, NY, USA) with 95 % confidence interval. The normal distribution of the quantitative variables was evaluated using the Shapiro Wilk normality test. Because the data is not normally distributed, the distribution of variables was evaluated with the chi-square test or the Mann-Whitney U test. The differences of anatomical variations were evaluated with the Mann-Whitney U test. Medians and interquartile ranges (IQR) were given because of the non-parametric tests. Results of $p < 0.05$ were considered significant.

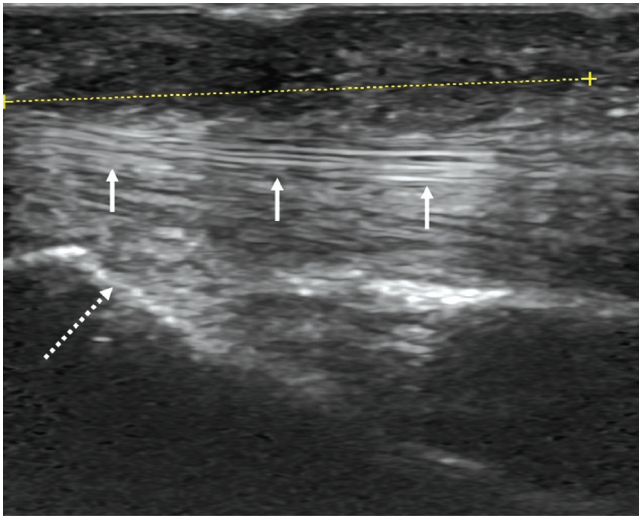


Figure 1. Hypoechoic solid nodule (longitudinal axis) of Dupuytren's disease. The dashed line indicates the longitudinal dimension of the nodule. The nodule is located in the subcutaneous tissue in the superficial neighborhood of the flexor digitorum tendons (arrows). In the deepest part, the metacarpal is observed (dashed arrow).

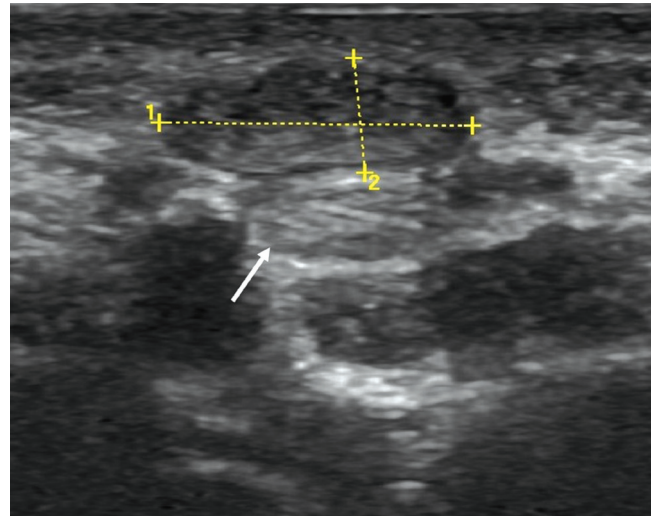


Figure 2. Hypoechoic solid nodule (transversal axis) of Dupuytren's disease. The dashed lines indicate the mediolateral and anteroposterior dimensions of the nodule. The nodule is located in the subcutaneous tissue in the superficial neighborhood of the flexor digitorum tendons (arrows).

Results

There were 88 patients (median age 61, IQR 9) meeting the study criteria. Of the patients, 32 (36.4%) were women and 56 (63.6%) were men. Fifty-six (63.5%) of the lesions were on the right hand and 32 (36.4%) on the left hand. There were 1 (1.1%) lesion in the 1st finger, 5 (5.7%) in the 2nd finger, 17 (19.3%) in the 3rd finger, 60 (68.2%) in the 4th finger, and 5 (5.7%) in the 5th finger. The lesion location ranged from the metacarpal body proximally to the middle phalanx distally. The median longitudinal dimension was 6.75mm (IQR: 4.32) and the median transverse dimension was 2.5mm (IQR: 1.77). On B-mode US examination, the lesions were hypoechoic in 65 (73.9%) patients and iso-hyperechoic in 23 (26.1%) patients (Figures 1 and 2). Lesions were nodules in 59 (67.1%) patients, and cord-shaped in 29 (32.9%) patients. Out of the total number of the patients, extension to the flexor tendon was present in 73 (82.9%) while the contracture was noted in 20 (22.7%) cases. The vascularization was present in 11 (12.5%) of the patients (Figure 3). On SEL examination, blue-green coding was found in 50 (56.8%) patients, and only blue coding was found in 38 (43.2%) patients (Figure 4). In the clinical and physical examination records of the cases included in the study, there were long-standing palpable painless stiffness in the palmar region or stiffness causing flexion deformity in the finger.

The distribution of numerical data in categorical variable groups was given in the Table 1.

There was a significant difference between lesion echogenicity and cord and contracture. Of the hypoechoic lesions, 50 have no cords and 15 have cords; of the iso-hyperechoic lesions, 9 had no cord, and 14 had cords ($p=0.001$). In addition of the hypoechoic lesions, 54 had no contracture and 11 had contractures; of the iso-hyperechoic lesions, 14 had no contracture and 9 had contracture ($p=0.029$). However, there was no significant relationship between lesion echogenicity and gender, side, localization, extension to the tendon, CDUS, and

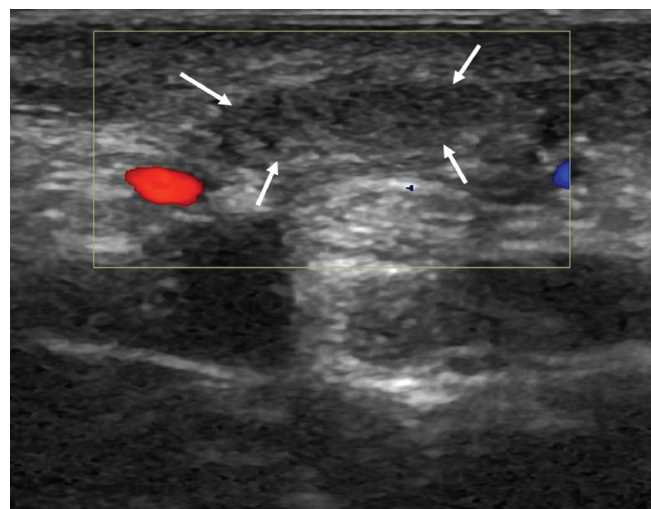


Figure 3. On the color Doppler ultrasonography examination, vascularity is not observed in the hypoechoic nodule (arrows).

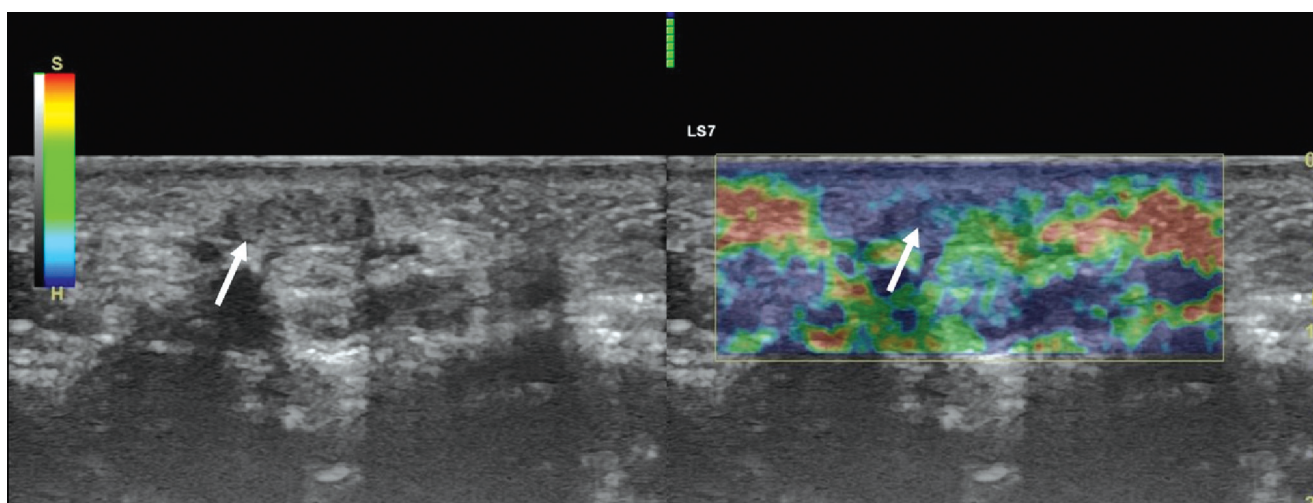


Figure 4. On sonoelastography, the hypoechoic nodule was coded blue-green (arrow), and the adjacent soft tissues were predominantly red-orange coded. Blue-green color coding indicates that the Dupuytren's disease nodule is stiff.

SEL ($p=0.854$, $p=0.854$, $p=0.271$, $p=0.553$, $p=0.660$, and $p=0.648$, respectively).

There was a significant difference between the presence of the cord and echogenicity, extension to the tendon and contracture. Of the nodular lesions, 50 were hypoechoic and 9 were iso-hyperechoic; of the cord-shaped lesions, 15 were hypoechoic and 14 were iso-hyperechoic ($p<0.001$). All 29 cord-shaped lesions had extension to the tendon, however, of the nodular lesions, 44 had extension to the tendon, 15 did not ($p<0.001$). While there was no contracture in any of the 59 nodular lesions, there were no

contractures in 9 of the cord-shaped lesions and in 20 of them ($p<0.001$). No significant difference was found between the presence of cord and gender, side, location, CDUS and SEL ($p=0.189$, $p=0.357$, $p=0.153$, $p=0.265$, and $p=0.258$, respectively).

There was a significant difference between extension to the tendon and the presence of contracture and cord. Of the lesions with extension, 20 had contracture, 53 did not; none of the 15 lesions without extension had contractures ($p=0.021$). In addition, 29 lesions with extension had cord and 44 did not. There was no cord in any of the 15 lesions

Table 1

Distribution of numerical data in categorical variable groups. Data are given as "median (interquartile range)".

	Age (year)		Longitudinal dimension (mm)		Transversal dimension (mm)	
Gender	Women: 59 (mean age:12) Men: 61 (9)	$p=0.191$	Women: 5.8 (3.6) Men: 7.3 (4.7)	$p=0.013$	Women: 1.95 (1.6) Men: 2.8 (2.1)	$p=0.001$
Side	Right: 62 (9) Left: 59 (14)	$p=0.142$	Right: 5.9 (3.9) Left: 7 (4.1)	$p=0.215$	Right: 2.4 (2.1) Left: 2.6 (1.5)	$p=0.435$
Echogenicity	Hypo: 60 (10) Iso-hyper: 65 (9)	$p=0.129$	Hypo: 7.0 (4.7) Iso-hyper: 5.6 (4.1)	$p=0.012$	Hypo: 2.4 (1.4) Iso-hyper: 2.9 (2.2)	$p=0.043$
Cord	Yes: 63 (7) No: 59 (12)	$p=0.026$	Yes: 5.6 (4.4) No: 7 (4.3)	$p=0.291$	Yes: 2.4 (1.4) No: 4.2 (4.1)	$p<0.001$
Extension	Yes: 61 (11) No: 66 (11)	$p=0.129$	Yes: 7 (5.3) No: 6.4 (4.1)	$p=0.991$	Yes: 2.5 (1.7) No: 2.5 (2.2)	$p=0.362$
Contracture	Yes: 62.5 (8) No: 60.5 (10)	$p=0.326$	Yes: 6.3 (5.2) No: 6.75 (3.8)	$p=0.580$	Yes: 5.1 (6.8) No: 2.4 (1.3)	$p<0.001$
CDUS	Yes: 57 (12) No: 61 (10)	$p=0.289$	Yes: 6.3 (3.9) No: 6.8 (4.4)	$p=0.972$	Yes: 2.2 (3.1) No: 2.5 (1.8)	$p=0.502$
SEL	Blue: 62 (8) Green Blue: 59 (12)	$p=0.024$	Blue: 5.9 (4.6) Green Blue: 7 (3.9)	$p=0.474$	Blue: 2.8 (2.3) Green Blue: 2.45 (1.7)	$p=0.899$

without extension ($p=0.012$). No significant difference was found between extension to the tendon and gender, side, location, echogenicity, CDUS and SEL ($p=0.789$, $p=0.748$, $p=0.453$, $p=0.553$, $p=0.703$, and $p=0.765$, respectively).

There was a significant difference between the presence of contracture and gender, echogenicity, the presence of a cord, and extension to the tendon. Eighteen of the contracture cases were man and 2 were woman; 38 of the non-contracted cases were man and 30 were woman ($p=0.005$). Of the lesions with contracture, 11 were hypoechoic and 9 were iso-hyperechoic; of the non-contracted lesions, 54 were hypoechoic and 14 were iso-hyperechoic ($p=0.029$). A cord was present in all 20 lesions with contracture, while 9 of non-contracted lesions had cord and 59 had no cord ($p<0.001$). All 20 lesions with contracture had extension to the tendon, while 53 of non-contracted lesions had extension and 15 did not ($p=0.021$). There was no significant difference between the presence of contracture and side, location, CDUS and SEL ($p=0.701$, $p=0.530$, $p=0.157$, and $p=0.852$, respectively).

There was a significant difference between the vascularization of the lesion and the cord and side. Of the lesions without vascularization, 50 had no cord, and 27 had cords; of the lesions with vascularization, 9 had no cord and 2 had cords ($p<0.001$). In the lesions on the right hand, vascularity was absent in 45 patients and present in 11 patients; on the left hand, vascularity was present in all 32 lesions ($p=0.028$). There was no significant difference between vascularization and gender, localization, echogenicity, extension to the tendon, contracture, and SEL ($p=0.497$, $p=0.071$, $p=0.660$, $p=0.703$, $p=0.157$, and $p=0.257$, respectively).

There was a significant difference between lesion elasticity and the side. 29 of the lesions with blue coding were on the right and 9 were on the left, 27 of the lesions with blue-green coding were on the right and 23 were on the left ($p=0.031$). There was no significant difference between lesion elasticity and gender, localization, echogenicity, extension to the tendon, cord, contracture and CDUS ($p=0.207$, $p=0.563$, $p=0.648$, $p=0.765$, $p=0.258$, $p=0.852$, and $p=0.257$, respectively).

Discussion

In this study, we revealed the ultrasonographic morphology, CDUS and SEL findings of palmar lesions in DD and also investigated their differences with each other. We revealed that men have larger lesions and contracture more frequently, hypoechoic lesions are larger but have fewer cords and contractures, older patients have more cord morphology and more stiff lesions, the mediolateral

dimension is greater in the presence of the cord and contracture, the vascularity is less in the cord morphology, the extension and contracture to the tendon is more in the cord morphology, and the contracture is more frequent in the lesions with extension to the tendon.

From these results, it can be interpreted that cord morphology, tendon extension and contracture parameters tend to be together, and lesions with these parameters are mostly iso-hyperechoic and hypovascular. Accordingly, in the presence of late signs such as contracture, the increase in echogenicity and decrease in vascularity support the increase in intralesional fibrotic tissue. In the presence of more hypoechoic and vascular lesions, early-stage DD can be considered, and treatment can be personalized accordingly.

Although the diagnosis of DD is usually made clinically, histopathological correlation may rarely be required. Distal volar localized nodules in the subcutaneous soft tissue cause shrinkage of the overlying skin as ageing. It may also result in flexion contracture due to its cord-like, palpable hard structure. Pathology does not include tendon and muscle. On ultrasound, nodules or cordlike lesions in DD may vary in scale from hypoechoic to iso-hyperechoic to tendons. However, it is generally hypoechoic compared to tendons. On CDUS, its vascularity changes, but it is mostly hypovascular. It is an important advantage that the relationship of the lesions with the tendons can be evaluated on US in real time, and it enables the exclusion of tendinous lesions in the differential diagnosis.

In the study of Morris et al.,^[1] the lesions were detected most frequently in the 3rd and 4th finger localizations. We also detected the majority of our cases (87.5%) at the level of the 3rd and 4th finger/metatarsal. In their study, 98% of the lesions were hypoechoic, and 93% of patients were hypovascular on CDUS. In our study population, again, hypoechoic and hypovascular lesions were more common, but proportionally hypoechoic (73.9%) and hypovascular (87.5%) lesions were less than them.

Cretuer et al.^[11] stated that early period DD nodules are hypoechoic compared to tendons due to their cellularity, and iso- to hyper-echoic due to the increase in collagen content in the late period. It is stated that cellular, that is, active lesions, have a higher risk of recurrence.^[4,12] Therefore, determination of lesion cellularity with imaging can be determinative in terms of prognosis and treatment. We have shown that cord morphology and stiffer lesions are common in elderly patients. This can be interpreted as the increase in fibrosis in the lesions in the late period causes the cord morphology and is coded stiffer on SEL. However, Molenkamp et al.^[13] found that hypo-

echogenicity in nodules was not a predictor of dimensional increase. No significant dimensional increase was found in the nodules that were found to be hypoechoic in their studies compared to the hyperechoic ones in their follow-up 1 year later. We also did not find a significant difference between lesion size and echogenicity.

In the study of Molenkamp et al.,^[14] a significant negative correlation was found between the echogenicity of the nodule and the myofibroblast load in histopathological examination. In addition, they found a significant negative correlation between echogenicity and hardness in their hardness examination with tonometry. These results prove that cellular nodules are more hypoechoic and stiffer. At the same time, more hypoechoic nodules can be considered to be stiffer. We did not find any significant difference between lesion echogenicity and stiffness on SEL. In the study of Ball et al.,^[15] nodules were found to be harder than normal tissue in the hardness measurement made by tonometry. In their DD case report, Ulusoy et al.^[16] described the increase in vascularization and heterogeneity in the thickening of both tendon sheaths and superficial palmar fascia in B-Mode US and CDUS. They interpreted the increase in vascularization as an early sign of nodules. On SEL examination, they found that the nodules were hard coded compared to adjacent soft tissue. They reported that this result supports fibrosis. They suggested that SEL can distinguish between acute and chronic lesions and that the efficacy of treatment can be evaluated according to lesion stiffness. Our study was not a case report, and 88 lesions were evaluated. SEL examination was performed on all lesions, and it was seen that all of them were hard coded. In addition, the lesions of the elderly patients were significantly stiffer.

There were some limitations in our study. The retrospective basis was the main limitation. Mistakes and biases may have occurred in patient selection and evaluation of images. Information from recorded images and report texts may be incomplete. Another limitation is the lack of histopathological diagnosis of the lesions. In none of our patients, lesion excision was not required since there was no excessive contracture that could be an indication for operation and the diagnosis was supported by physical examination and radiological examination. The fact that the lesions were examined by a single evaluator reduces the generalizability of the findings.

Conclusion

DD lesions is mostly hypoechoic, nodular shaped, hypovascular, and stiff. The cord morphology, tendon extension and contracture are the late stage parameters, and

lesions with these are mostly iso-hyperechoic. In the presence of a solid lesion originating from the subcutaneous soft tissue of the palmar region, DD can be diagnosed by considering the lesion location, morphology, vascularity, and degree of stiffness with a combination of US, CDUS and SEL. The DD lesions can be determined that are in the early or late stage by using morphology, echogenicity, vascularity, and stiffness data. Thus, the success of the treatment can be increased by reducing the recurrence rate.

Conflict of Interest

No conflict of interest was declared by the authors.

Author Contributions

AHÇ: project development, data management, data analysis, statistical analysis, manuscript writing/editing; MB: project development, data collection, data analysis, manuscript writing/editing.

Ethics Approval

The study was approved by Ankara City Hospital Clinical Research Ethics Committee (No: E2-20-76, Date: 30.12.2020). The study was also carried out in accordance with the Helsinki Declaration of Principles.

Funding

This research did not receive any specific grant from funding agencies in the public, commercial, or not-for-profit sectors.

References

- Morris G, Jacobson JA, Kalume Brigido M, Gaetke-Udager K, Yablon CM, Dong Q. Ultrasound Features of palmar fibromatosis or Dupuytren contracture. *J Ultrasound Med* 2019;38:387–92.
- Stewart BD, Nascimento AF. Palmar and plantar fibromatosis: a review. *J Pathol Transl Med* 2021;55:265–70.
- Murphey MD, Ruble CM, Tyszko SM, Zbojnicz AM, Potter BK, Miettinen M. From the archives of the AFIP: musculoskeletal fibromatoses: radiologic-pathologic correlation. *Radiographics* 2009;29:2143–73.
- Robbin MR, Murphey MD, Temple HT, Kransdorf MJ, Choi JJ. Imaging of musculoskeletal fibromatosis. *Radiographics* 2001;21:585–600.
- Rayan GM. Dupuytren disease: anatomy, pathology, presentation, and treatment. *J Bone Joint Surg Am* 2007;89:189–98.
- Sayadi LR, Alhunayan D, Sarantopoulos N, Kong C, Condamoor S, Sayadi J, Banyard DA, Shaterian A, Leis A, Evans GRD, Widgerow AD. The molecular pathogenesis of Dupuytren disease: review of the literature and suggested new approaches to treatment. *Ann Plast Surg* 2019;83:594–600.
- Molenkamp S, van Straalen RJM, Werker PMN, Broekstra DC. Imaging for Dupuytren disease: a systematic review of the literature. *BMC Musculoskelet Disord* 2019;20:224.

8. Botar Jid C, Vasilescu D, Damian L, Dumitriu D, Ciurea A, Ducea SM. Musculoskeletal sonoelastography. Pictorial essay. Med Ultrason 2012;14:239–45.
9. Balaban M, Çilengir AH, Idilman IS. Evaluation of tendon disorders with ultrasonography and elastography. J Ultrasound Med 2021;40: 1267–86.
10. Benson LS, Williams CS, Kahle M. Dupuytren's contracture. J Am Acad Orthop Surg 1998;6:24–35.
11. Creteur V, Madani A, Gosset N. Ultrasound imaging of Dupuytren's contracture. J Radiol 2010;91:687–91.
12. Yacoe ME, Bergman AG, Ladd AL, Hellman BH. Dupuytren's contracture: MR imaging findings and correlation between MR signal intensity and cellularity of lesions. AJR Am J Roentgenol 1993;160: 813–7.
13. Molenkamp S, Broekstra DC, Werker PMN. Echogenicity of palmar Dupuytren's nodules is not a predictor of disease progression in terms of increase in nodule size. Plast Reconstr Surg. 2019;143:814–20.
14. Molenkamp S, Song W, Bloembergen M, Broekstra DC, Werker PMN. Echogenicity of Dupuytren's nodules is correlated to myofibroblast load and nodule hardness. J Hand Surg Eur Vol 2022;47:280–7.
15. Ball C, Izadi D, Nanchahal J. Tonometry as an outcome measure for the treatment of early Dupuytren Disease. In: Werker P, Dias J, Eaton C, Reichert B, Wach W, editors. Dupuytren disease and related diseases – the cutting edge. New York: Springer; 2017. p. 205–9.
16. Ulusoy A, Tıkız C, Örgüç Ş. Dupuytren's contracture with rare bilateral thumb and little finger involvement demonstrated by ultrasound elastography. Arch Rheumatol 2015;30:357–60.

ORCID ID:

A. H. Çilengir 0000-0002-4073-9665;
M. Balaban 0000-0002-6752-6838



Correspondence to: Atilla Hikmet Çilengir, MD

Department of Radiology, Faculty of Medicine,
Izmir Democracy University, Izmir, Türkiye
Phone: +90 537 773 89 46
e-mail: acilengir@gmail.com

Conflict of interest statement: No conflicts declared.

This is an open access article distributed under the terms of the Creative Commons Attribution-NonCommercial-NoDerivs 4.0 Unported (CC BY-NC-ND4.0) Licence (<http://creativecommons.org/licenses/by-nc-nd/4.0/>) which permits unrestricted noncommercial use, distribution, and reproduction in any medium, provided the original work is properly cited. *How to cite this article:* Çilengir AH, Balaban M. The analysis of morphological features and ultrasonographic characteristics of Dupuytren's disease. *Anatomy* 2022;16(1):26–32.

The ultrasound elastography findings in lateral epicondylitis in comparison with healthy individuals

Bilge İpek Torun¹ , Serhan Eren² , Mehtap Balaban³ 

¹Department of Anatomy, Faculty of Medicine, Ankara Yıldırım Beyazıt University, Ankara, Türkiye

²Department of Radiology, Batman Kozluk State Hospital, Batman, Türkiye

³Department of Radiology, Faculty of Medicine, Ankara Yıldırım Beyazıt University, Ankara, Türkiye

Abstract

Objectives: To evaluate the ability of strain sonoelastography (SEL) in diagnosing lateral epicondylitis (LE) and to assess clinical and diagnostic efficacy of strain SEL in patients with clinically confirmed LE and in healthy volunteers.

Methods: Strain SEL was performed on 110 patients with clinical symptoms of LE and on 56 healthy participants. The common extensor tendon (CET) was evaluated with gray-scale and color Doppler ultrasonography (CDUS). The stiffness and the elasticity of the CET was divided into 2 main types and 2 subtypes as a spectrum ranging from hard for 1a to soft for 2b.

Results: The thickness of the CET in patients with LE (6.3 ± 1.06 mm) were remarkably thicker than in healthy participants (3.8 ± 0.62 mm) ($p < 0.001$). There were negative significant correlations between the thickness of the CET and lower and mean strain ratios (SR) ($r_s = [-0.666]$, $p < 0.001$ for lower SR and $r_s = [-0.358]$, $p < 0.001$ for mean SR). Thickness of the CET varied between the groups of elastographic patterns ($p < 0.001$). The SR of tendon in patients with LE (6.68 ± 2.49 mm) were remarkably lower than in healthy participants (11.16 ± 4.88 mm) ($p < 0.001$). The SR of tendon in patients with LE also varied significantly between the groups of elastographic patterns ($p < 0.001$).

Conclusion: Strain SEL is a promising sonographic technique for musculoskeletal imaging to differentiate thickening and softening of CET in LE. SR and SEL pattern findings are compatible with gray scale ultrasound and CDUS findings.

Keywords: common extensor tendon; imaging; radiologic anatomy; tendon thickness

Anatomy 2022;16(1):33–40 ©2022 Turkish Society of Anatomy and Clinical Anatomy (TSACA)

Introduction

Tendons are the ligaments that provide movement and transmit the power produced by the muscle contraction to the bones and joints.^[1] The common extensor tendon is composed of tendinous portions of the extensors carpi radialis brevis and longus, extensor digitorum, extensor digiti minimi and extensor carpi ulnaris muscles, and serve as the upper attachment for posterior extensor muscles of forearm. It originates from the lateral epicondyle of humerus.^[2] Lateral epicondylitis (LE), also called as “tennis elbow”, is a pathological condition of CET that causes pain in lateral aspect of the elbow due to repetitive stress and overuse of the CET in labor and sports activities as well as age-related degeneration. Pain, burning and

swelling of the lateral aspect of the elbow are the most common symptoms of LE. Estimated prevalence of LE is 1–3% in the general population.^[3] The diagnosis of LE is made primarily by using typical clinical manifestations and physical examination.^[4] Furthermore, a wide variety of radiologic methods are used to diagnose LE, including conventional muscle sonography and color Doppler ultrasonography (CDUS), elastography and, magnetic resonance imaging (MRI).^[5,6]

Ultrasound elastography imaging is ultrasound-based imaging method that provides information on the elasticity and stiffness properties of tissues.^[7] There are two main different techniques of ultrasound elasticity imaging: compression based strain sonoelastography (SEL) and

shear-wave SEL.^[8] Strain SEL is based on difference of stiffness and elasticity between one tissue or lesion to another by applying probe compression. Numerous clinical SEL applications and studies were found to evaluate diagnosis and assessment of changes in tissue stiffness and elasticity in pathological conditions.^[9-14] However, clinical utility of elastography has been infrequently studied in LE and has not been evaluated with tendon thickness.

The main purpose of this study was to assess clinical and diagnostic efficacy of strain SEL in patients with clinically confirmed LE and in healthy volunteers.

Materials and Methods

This study was approved by the institutional review board, and informed consent was obtained from all participants. From January 2019 to January 2022, a retrospective analysis with strain SEL was performed on total of 110 patients with clinical symptoms of LE and 56 healthy participants (103 women and 63 men, age range: 20–81 years, mean age 42.95 years). The inclusion criteria of this study were pain and discomfort of lateral aspect of humerus that compatible with LE. A clinical history of surgery, fracture, or other diseases that affect musculoskeletal system such as rheumatoid arthritis and osteoarthritis were excluded from the study. The inclusion criteria for the healthy participants were asymptomatic elbows, no previous trauma or surgery at the elbow, and no history of systemic inflammatory disorders.

The healthy participants and patients with LE were examined with gray scale and CDUS, and real-time strain based SEL (LOGIQ S7 Expert, GE Medical Systems) using a 5–11 MHz linear-array transducer by two radiologists (one radiologist with 18 years of experience and one radiologist with 5 years of experience on musculoskeletal system). In the beginning of the study, ten cases were examined together for sample consistency. All participants in our study were examined in comfortable position. All participants' arms were supported by a pillow and elbows were semi-flexed. 5–11 MHz linear array transducer was positioned parallel to the lateral epicondyle with semi-flexed elbow to investigate the CET. The CET was evaluated with gray-scale and CDUS for swelling, tendinosis, partial tear, calcification, tendon thickness, hyperemia and inflammatory changes. The thickness of the CET was measured from the longitudinal view from the antero-posterior direction. Also strain SEL images of the CET were acquired from longitudinal view of the elbow due to avoid artifacts of gray scale sonography and elastography. Strain images were obtained by freehand technique with compression and decompression. The optimal strain was

adjusted according to the visual indicator of compression. The visual indicator had six levels and strain and compressions of four or more were considered valuable. Results of the tissue elasticity distribution were showed a color map together with the B-mode image. Stiffness and elasticity of the CET were represented by the color spectrum, which was blue and green for hard, yellow for intermediate and red for soft tissue. The stiffness and elasticity of the CET was divided into 2 main types and 2 subtypes as a spectrum ranging from hard for 1a to soft for 2b: type 1a, blue predominance; type 1b, green predominance; type 2a, small yellow and red areas within green predominance; and type 2b, green areas within yellow and red predominance.

All statistical analyses were performed with SPSS software (version 28.0, IBM SPSS, IBM Corp., Armonk, NY, USA) Median and range for continuous variables were used to define feature of participants. Counts and percentages for the categorical variables were used to define feature of participants. The variables were examined with Kolmogorov-Smirnov normality test whether distributed normally or not. Continuous variables were analyzed between healthy participants and patients by using Mann-Whitney U and Kruskal-Wallis tests. Categorical variables were analyzed between healthy participants and patients by using chi-square test and Fisher exact test. The correlation between continuous variables as thickness of the CET, strain ratio (SR) and symptom duration were performed with Spearman's non-parametric correlation analysis. A p value <0.05 was considered statistically significant.

Results

Baseline characteristics of participants were summarized in **Table 1** and imaging findings of the patients are summarized in **Table 2**. There was no difference between patients and healthy participants for age ($p=0.345$).

Ultrasound examination revealed that the CET at the lateral epicondyle thickened with decreased fibrillar echogenicity, intratendinous calcification, and increased fluid in its vicinity (**Figure 1**). Intratendinous vascularization increased in CDUS (**Figure 2**). The SEL examination in the tendon showed green-weighted yellow and red coding areas consistent with soft coding (**Figure 3**).

The thickness of the CET in patients with LE (6.3 ± 1.06 mm) were remarkably thicker than in healthy participants (3.8 ± 0.62 mm) ($p<0.001$). In addition, the thickness of the CET was thicker in patients with tendinosis, partial tear, hyperemia and calcific tendinopathy than in healthy participants ($p<0.001$) (**Figure 4**). The thickness of CET increased with age ($p<0.001$). There

Table 1
Characteristics of the patients.

		Lateral epicondylitis	Control
Sex	Men	41	22
	Women	69	3428
Involvement	Right	63	28
	Left	47	52
Hand dominance	Right	99	4
	Left	11	
Age (range)		49.55±12.2 (20–81)	29.96±8.88 (20–53)

Table 2
Imaging findings of the patients.

	Lateral epicondylitis (n=110)	Control (n=56)	P-value
Gray scale findings			
Tendinosis	108	16	<0.001
Calcification	41	0	<0.001
Intrasubstance tear	68	0	<0.001
Epicondyle degeneration	35	0	<0.001
Doppler findings			
Hyperemia	50	0	<0.001
Elastographic findings			
1a	5	41	<0.001
1b	18	14	
2a	46	1	
2b	41	0	

were negative significant correlations between the thickness of the CET and lower and mean SR ($r_s = [-0.666]$; $p < 0.001$ for lower SR and $r_s = [-0.358]$; $p < 0.001$ for mean SR). The thickness of the CET also varied significantly

between the groups of elastographic patterns ($p < 0.001$) (Figure 5). But there was no difference between the thickness of the CET of 2a and 2b elastographic patterns ($p = 0.927$).

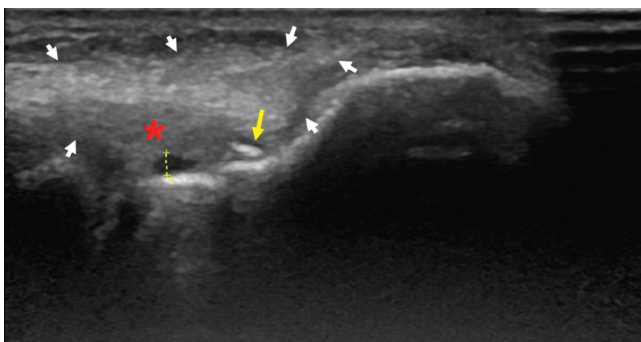


Figure 1. B-mode ultrasonography. Thickening on right common extensor tendon (white arrow heads), decrease in fibrillar echogenicity (red asterisk), adjacent anechoic fluid increase (dashed yellow line) and intratendinous calcification (yellow arrow).

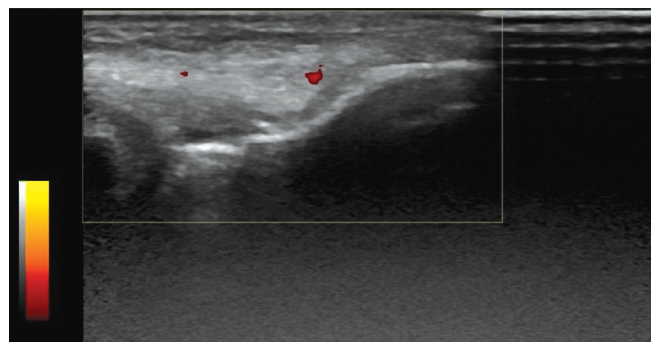


Figure 2. Increased intratendinous vascularization in the common extensor tendon.

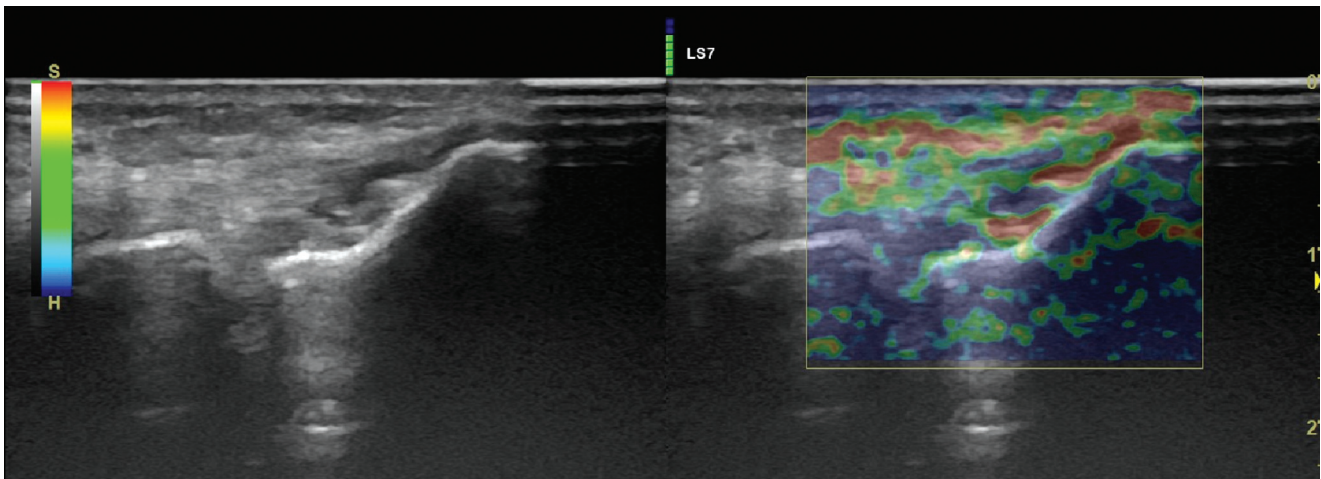


Figure 3. Green-weighted red soft coding in SEL imaging.

In 110 patients with clinical confirmed LE, right elbow involvement was 63 and left elbow involvement was 47. Intrasubstance tear was found in 68/110 (61.8%) of the patients. Calcification was present in 41/110 (37.3%) tendons. Hyperemia in the CET was found in 50/110 (45.5%) of the patients. Tendinosis of the CET was detected in 108/110 (98.2%) of the patients. Degeneration of the lateral epicondyle was found 35/110 (31.8%) of the patients.

In 56 healthy participants, tendinosis of the CET was detected in 16/56 (28%) of participants. Other B mode and CDUS findings were normal. Calcification and degenerative changes in lateral epicondyle were not involved in healthy participants.

From gray-scale ultrasonography and CDUS, intra-substance tear (Figure 6a), calcification (Figure 6b), hyperemia, tendinosis of the CET and degeneration of the lateral epicondyle were showed statistically significant differences between healthy participants and patients with LE ($p < 0.001$).

Of 166 participants, 46 (27%) showed elastographic pattern of type 1a, 32 (19%) showed elastographic pattern of type 1b, 47 (28%) showed elastographic pattern of type 2a, and 41 (24%) showed elastographic pattern of type 2b.

The SR of the tendon in patients with LE (mean: 6.68 ± 2.49 mm, min: 1.70 – max: 16.1) were remarkably lower than in healthy participants (mean: 11.16 ± 4.88 mm, min: 2.80 and max: 25.1) ($p < 0.001$) (Figures 7 and 8). The SR of the tendon in patients with LE decreased with age. There was negative significant correlation between the mean SR of tendon and age ($rs = [-0.261]$; $p < 0.001$). The

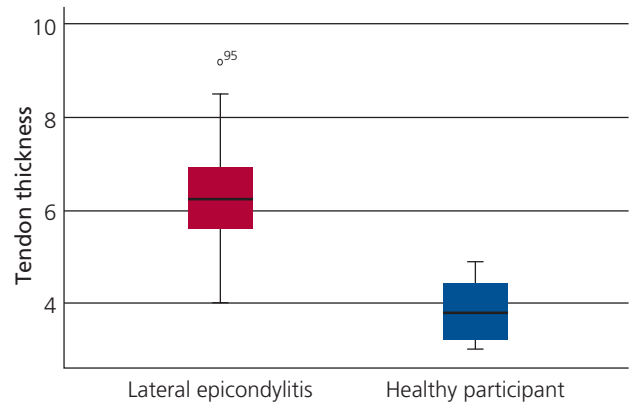


Figure 4. Plot of tendon thickness in patients with lateral epicondylitis and healthy individuals.

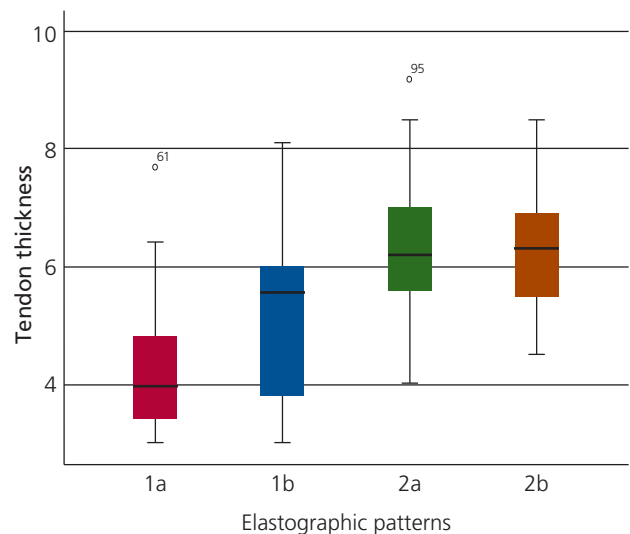


Figure 5. Elastographic patterns – tendon thickness plot.

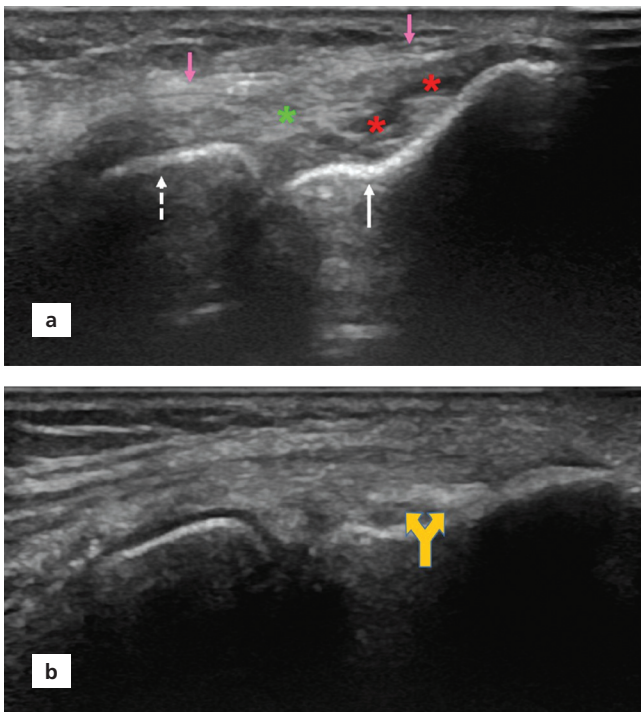


Figure 6. B-mode ultrasonography of lateral epicondyle (white arrow), distal radius (dashed white arrow), common extensor tendon (green asterisk) and upper border of the tendon (pink arrows). (a) intratendinous partial rupture (red asterisks) (b) intratendinous calcification (double-headed arrow).

SR of the tendon in patients with LE also varied significantly between the groups of elastographic patterns ($p < 0.001$) (Table 3) (Figures 9 and 10). But there was no significant difference between the mean SR of the tendon in patients with LE of 1a and 1b elastographic patterns ($p = 0.403$).

The SR of the tendon in patients with tendinosis (mean: 7.1 ± 3.07 , min: 1.7 – max: 16) were remarkably lower

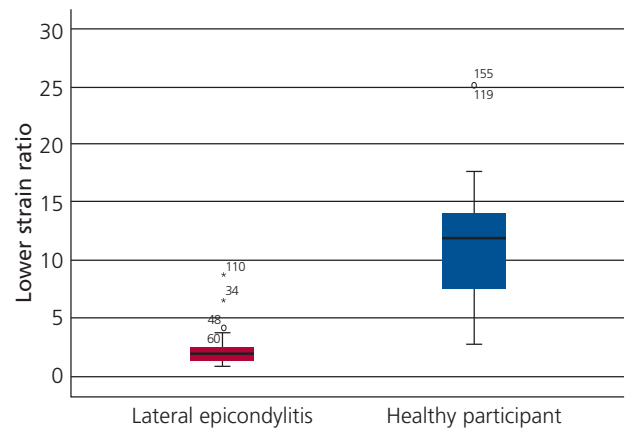


Figure 7. Plot of lower strain ratio in patients with lateral epicondylitis and healthy individuals.

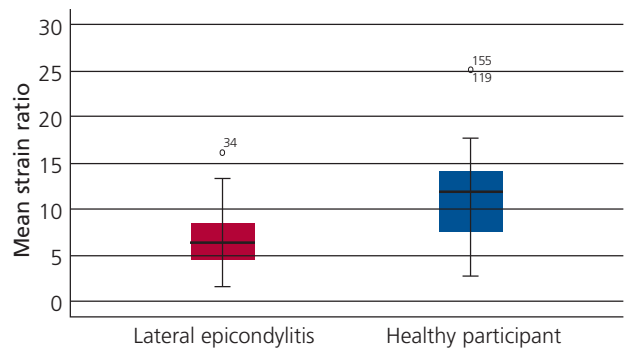


Figure 8. Plot of mean strain ratio in patients with lateral epicondylitis and healthy individuals.

than in healthy participants (mean: 11.2 ± 5.07 , min: 2.8 and max: 25.1) ($p < 0.001$). The SR of tendon in patients with intrasubstance tear (mean: 6.5 ± 2.3 mm, min: 2.5 – max: 12) were remarkably lower than in healthy partici-

Table 3

Lower and mean strain ratios of elastographic patterns.

Elastographic patterns		Lower strain ratio	Mean strain ratio
1a	Patient	4.1 ± 2.7	9.5 ± 2.6
	Control	13.3 ± 3.7	13.3 ± 3.7
1b	Patient	3.3 ± 1.1	8.9 ± 2.2
	Control	5.3 ± 1.7	5.3 ± 1.7
2a	Patient	2.2 ± 0.56	6.79 ± 2.08
	Control	3.6	4.2
2b	Patient	1.3 ± 0.3	5.2 ± 2.01
	Control	-	-

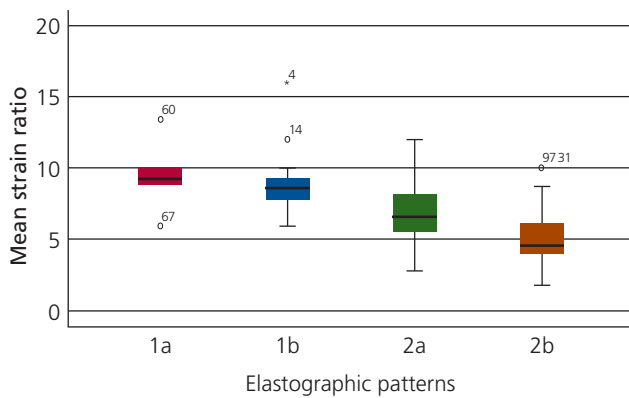


Figure 9. Elastographic patterns – mean strain ratio plot

pants (mean: 9.3 ± 4.6 , min: 1.7 and max: 25.1) ($p < 0.001$). The SR of the tendon in patients with calcification (mean: 6.9 ± 2.7 , min: 1.7 – max: 16.1) were remarkably lower than in healthy participants (mean: 8.5 ± 4.3 , min: 2.5 and max: 25.1) ($p = 0.096$). The SR of the tendon in patients with hyperemia (mean: 6.7 ± 2.25 , min: 2.7 – max: 13.4) were remarkably lower than in healthy participants (mean: 8.8 ± 4.5 , min: 1.7 and max: 25.1) ($p = 0.016$). There was no significant difference between the mean SR of the tendon in patients with lateral epicondyle degeneration (mean: 6.9 ± 2.63 , min: 2.7 – max: 16.1) and in healthy participants (mean: 8.5 ± 4.3 , min: 1.7 and max: 25.1) ($p = 0.129$).

Discussion

The mechanism of the CET injury is repetitive stress of forearm and wrist during movement of dorsiflexion and supination. Furthermore, patient characteristics, habits and activity level also affect the common extensor

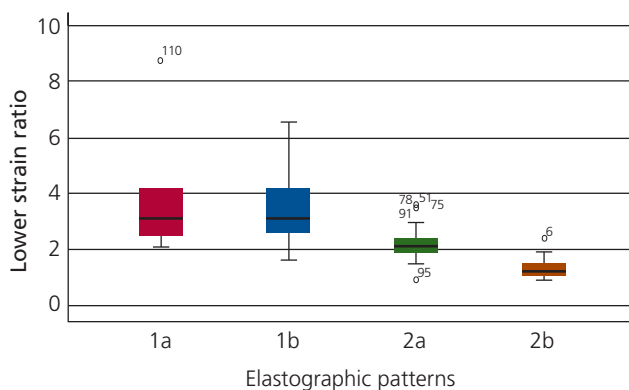


Figure 10. Elastographic patterns – lower strain ratio plot

tendinopathy.^[15,16] The diagnosis of LE is made primarily by using typical clinical manifestations and physical examination. Furthermore, a wide variety of radiologic methods is used to diagnose LE, including conventional muscle sonography, CDUS, and magnetic resonance imaging.^[16-18]

SEL provides elasticity and stiffness of tissue or lesions such as breast, liver, thyroid and tendons. In recent studies, strain SEL and shear-wave SEL have been investigated in diagnosis of LE. Gray scale and CDUS findings of LE are low echogenicity, increased thickness, intrasubstance tear, calcification and inflammation of lateral collateral ligament of elbow.^[19] Tendinosis and low echogenicity is the most common sonographic finding of LE.^[20] In our study, most gray-scale findings of the patients with clinically confirmed LE was also tendinosis and intrinsic low echogenicity. The thickness of the CET significantly increased in LE compared to the healthy participants, which is consistent with Ahn et al.^[21] and Zhu et al.^[22] In addition, thickness of the CET varied significantly between the groups of elastographic patterns, and increased with age. It was seen that the thickness of the CET increased significantly as tendon getting softer.

Khoury et al.^[23] showed that increased tendon compressibility indicative of tendon softening was a new sign of tendinopathy. De Zordo et al.^[24] showed that real-time SEL was valuable in the detection of the intratendinous and peritendinous alterations of LE. Real-time SEL images showed hard tendon structures in 96% of tendon in healthy volunteers, and softening of different grades in 67% in patients with LE, which was considered a statistically significant difference in relation to the findings. Also, Ahn et al.^[21] revealed that patients with LE had significantly lower SRs in their CET origins. In our study it was seen that the mean and lower SRs of the tendon in patients with LE were significantly lower compared to healthy participants. Furthermore, mean and lower SRs of the CET varied significantly between the groups of elastographic patterns.

Several limitations needed to be mentioned in this study. Ultrasonography and SEL imaging is highly operator dependent imaging modalities.^[25] Additionally, we did not study interobserver and intraobserver variability. To avoid of sample error, we calculated both mean and lower SRs of the CET. One sample for lower SR were taken from red color scale of tendon and second sample for mean SR were taken from all part of the CET. Another limitation is semi-quantitative calculation of SR.^[26]

Conclusion

We suggest that strain SEL is a promising sonographic technique for musculoskeletal imaging to differentiate variable etiologies that cause thickening and softening of the CET in LE. SR and SEL pattern findings are compatible with gray scale and CDUS findings. SEL findings are also compatible with degree of degeneration of the CET. Further longitudinal studies may support this consideration.

Conflict of Interest

No conflict of interest was declared by the authors.

Author Contributions

BIT: project development, collecting the clinical data, manuscript writing, editing the manuscript; SE: collecting the clinical data, manuscript writing, editing the manuscript; MB: project development, collecting the clinical data, manuscript writing, editing the manuscript. The data that support the findings of this study are available on request from the corresponding author. The data are not publicly available due to privacy or ethical restrictions.

Ethics Approval

This study was approved by the institutional review board (No: E2-20-76, date: 16.12.2021) and informed consent was obtained from all participants. All procedures performed in studies involving human participants were in accordance with the ethical standards of the institutional and/or national research committee and with the 1964 Helsinki declaration and its later amendments or comparable ethical standards.

Funding

This research did not receive any specific grant from funding agencies in the public, commercial, or not-for-profit sectors.

References

- Aslan H, Kimelman-Bleich N, Pelled G, Gazit D. Molecular targets for tendon neoformation. *J Clin Invest* 2008;118:439–44.
- Jaén-Díaz JI, Cerezo-López E, López-de Castro F, Mata-Castrillo M, Barceló-Galíndez JP, De la Fuente J, Balius-Mata Ramón. Sonographic findings for the common extensor tendon of the elbow in the general population. *J Ultrasound Med* 2010;29:1717–24.
- Whaley AL, Baker CL. Lateral epicondylitis. *Clin Sports Med* 2004;23:677–91.
- Johnson GW, Cadwallader K, Scheffel SB, Epperly TD. Treatment of lateral epicondylitis. *Am Fam Physician* 2007;76:843–8.
- Levin D, Nazarian LN, Miller TT, O’Kane PL, Feld RI, Parker LP, McShane JM. Lateral epicondylitis of the elbow: US findings. *Radiology* 2005;237:230–4.
- Potter HG, Hannafin JA, Morwessel RM, DiCarlo EF, O’Brien SJ, Altchek DW. Lateral epicondylitis: correlation of MR imaging, surgical, and histopathologic findings. *Radiology* 1995;196:43–6.
- Sigrist RM, Liao J, El Kaffas A, Chammas MC, Willmann JK. Ultrasound elastography: review of techniques and clinical applications. *Theranostics* 2017;7:1303–1329.
- Chang JM, Moon WK, Cho N, Yi A, Koo HR, Han W, Noh D-Y, Moon H-G, Kim SJ. Clinical application of shear wave elastography (SWE) in the diagnosis of benign and malignant breast diseases. *Breast Cancer Res Treat* 2011;129:89–97.
- Balaban M, Cilengir AH, Idilman IS. Evaluation of tendon disorders with ultrasonography and elastography. *J Ultrasound Med* 2021;40:1267–86.
- Dilip D, Khaladkar SM, Chanabasanavar V, Parripati SSVK. Real-time strain elastography: applications in musculoskeletal system. *J Clin Orthop Trauma* 2022;26:101784.
- Liu Q, Tang L, Chen M. Ultrasound strain elastography and contrast-enhanced ultrasound in predicting the efficacy of neoadjuvant chemotherapy for breast cancer: a nomogram integrating Ki-67 and ultrasound features. *J Ultrasound Med* 2022;41:2191–201.
- Mutala TM, Mwangi GN, Aywak A, Cioni D. Determining the elastography strain ratio cut off value for differentiating benign from malignant breast lesions: systematic review and meta-analysis. *Cancer Imaging* 2022;22:12.
- Wadugodapitiya S, Sakamoto M, Tanaka M, Sakagami Y, Morise Y, Kobatashi K. Assessment of knee collateral ligament stiffness by strain ultrasound elastography. *Biomed Mater Eng* 2022;33:337–49.
- Wang Y, Jacobson DS, Urban MW. A non-invasive method to estimate the stress-strain curve of soft tissue using ultrasound elastography. *Ultrasound Med Biol* 2022;48:786–807.
- Steinmann S, Pfeifer CG, Brochhausen C, Docheva D. Spectrum of tendon pathologies: triggers, trails and end-state. *Int J Mol Sci* 2020;21:844.
- Cha YK, Kim S-J, Park NH, Kim JY, Kim JH, Park JY. Magnetic resonance imaging of patients with lateral epicondylitis: relationship between pain and severity of imaging features in elbow joints. *Acta Orthop Traumatol Turc* 2019;53:366–71.
- Droppelmann G, Feijoo F, Greene C, Tello M, Rosales J, Yanez R, Jorquera C, Prieto D. Ultrasound findings in lateral elbow tendinopathy: a retrospective analysis of radiological tendon features. *F1000Research* 2022;11:44.
- Krogh TP, Fredberg U, Ammitzbøll C, Ellingsen T. Clinical value of ultrasonographic assessment in lateral epicondylitis versus asymptomatic healthy controls. *Am J Sports Med* 2020;48:1873–83.
- Connell D, Burke F, Coombes P, McNealy S, Freeman D, Pryde D, Hoy G. Sonographic examination of lateral epicondylitis. *AJR Am J Roentgenol* 2001;176:777–82.
- Speers CJ, Bhogal GS, Collins R. Lateral elbow tendinosis: a review of diagnosis and management in general practice. *Br J Gen Pract* 2018;68:548–9.
- Ahn K-S, Kang CH, Hong S-J, Jeong W-K. Ultrasound elastography of lateral epicondylitis: clinical feasibility of quantitative elastographic measurements. *AJR Am J Roentgenol* 2014;202:1094–9.

22. Zhu B, You Y, Xiang X, Wang L, Qui L. Assessment of common extensor tendon elasticity in patients with lateral epicondylitis using shear wave elastography. *Quant Imaging Med Surg* 2020;10:211–9.
23. Khoury V, Cardinal E. “Tenomalacia”: a new sonographic sign of tendinopathy? *Eur Radiol* 2009;19:144–6.
24. De Zordo T, Lill SR, Fink C, Feuchtner GM, Jaschke W, Bellmann-Weiler R, Klausner AS. Real-time sonoelastography of lateral epicondylitis: comparison of findings between patients and healthy volunteers. *AJR Am J Roentgenol* 2009;193:180–5.
25. Ohrndorf S, Naumann L, Grundey J, Scheel T, Scheel AK, Werner C, Backhaus M. Is musculoskeletal ultrasonography an operator-dependent method or a fast and reliably teachable diagnostic tool? Interreader agreements of three ultrasonographers with different training levels. *Int J Rheumatol* 2010;2010:164518.
26. Sowa Y, Numajiri T, Itsukage S, Nishino K. Comparison of shear-wave and strain ultrasound elastography for evaluating fat induration after breast reconstruction. *Plast Reconstr Surg Glob Open* 2016;4:e677.

ORCID ID:

B. I. Torun 0000-0002-0155-7447;
S. Eren 0000-0002-6935-4267;
M. Balaban 0000-0002-6752-6838



Correspondence to: Mehtap Balaban, MD

Department of Radiology, Faculty of Medicine,
Yıldırım Beyazıt University, Ankara, Türkiye
Phone: +90 312 906 20 00
e-mail: mehtapbalaban40@hotmail.com

Conflict of interest statement: No conflicts declared.

This is an open access article distributed under the terms of the Creative Commons Attribution-NonCommercial-NoDerivs 4.0 Unported (CC BY-NC-ND4.0) Licence (<http://creativecommons.org/licenses/by-nc-nd/4.0/>) which permits unrestricted noncommercial use, distribution, and reproduction in any medium, provided the original work is properly cited. *How to cite this article:* Torun Bİ, Eren S, Balaban M. The ultrasound elastography findings in lateral epicondylitis in comparison with healthy individuals. *Anatomy* 2022;16(1):33–40.

Retroaortic left renal vein: a clinically significant vascular variation with suggestion of a practical typological scheme

Nikolai Krastev , Yoanna Tivcheva , Lina Malinova , Lazar Jelev 

Department of Anatomy, Histology and Embryology, Medical University of Sofia, Sofia, Bulgaria

Abstract

The retroaortic left renal vein (RLRV) is a rare vascular variant with a typical position of the vein between the abdominal aorta and the vertebral column. Despite usually asymptomatic, RLRV might be associated with posterior nutcracker syndrome, other vascular pathologies and may cause major surgical complications. An existing but not expected RLRV might hamper aortic surgical dissection and to cause a life threatening bleeding. A case of a RLRV was observed during routine dissection of a formalin fixed 62-year-old female cadaver. The left kidney was found to be ectopic and located lower than usual between the level of L1 and L4 vertebra. The left renal vein was formed in the renal hilum at the level of L2/L3 intervertebral disc, and then passed obliquely downwards behind the abdominal aorta to join in the inferior vena cava at the level of upper border of L4 vertebra. The length of the RLRV was 7.5 cm. The main tributaries were the left suprarenal and left ovarian veins. Measuring the diameters of the renal vein showed slight dilation at its origin. Based on the literature review, the vascular variation reported here can be classified as Type II – RLRV draining at a lower than normal level of the inferior vena cava. An extended classification scheme of the left renal vein variations is presented here as well as an optional typological scheme.

Keywords: classification; clinical significance; renal vein collar; retroaortic left renal vein

Anatomy 2022;16(1):41–45 ©2022 Turkish Society of Anatomy and Clinical Anatomy (TSACA)

Introduction

The retroaortic left renal vein (RLRV) is rare vascular variant with a typical position of the renal vein between the abdominal aorta and the vertebral column.^[1–4] The incidence of this variation ranges from 0.4 to 9.3% in the different groups examined.^[1,5,6] The complicated embryonic development of the inferior vena cava (IVC) and its tributaries is claimed to result in formation of RLRV.^[7,8] Though this anatomical variant is often asymptomatic, the abovementioned position leads to an increase in the venous pressure and distention of the renal vein.^[9,10] The RLRV may also cause symptoms such as abdominal and left flank pain and hematuria and this to be diagnosed as posterior nutcracker syndrome.^[9,11] The RLRV is also considered one of the major vascular variations that should be taken into consideration during retroperitoneal surgery, for its accidental damage can cause severe hemorrhage, emergency nephrectomy and even death.^[1,7,10,12,13] Even though RLRV is a rare venous variant, its prompt identification and understanding of other concomitant vascular variations are essential for clinical practice.

Case Report

A case of a RLRV was observed during routine dissection of a formalin fixed 62-year-old Caucasian female cadaver. The dissection took place in the Department of Anatomy, Histology and Embryology of the Medical University of Sofia.

The anterior abdominal wall was incised and the abdominal cavity was opened wide in an anatomical way. The abdominal viscera were defined, studied and consecutively removed, as well as the posterior parietal peritoneum, in order to facilitate the dissection of the retroperitoneal space and the posterior abdominal wall. The position of the kidneys was accessed and after a meticulous blunt dissection, their vessels were exposed. The right kidney was non-totopic, with its upper pole at the level of T12/L1 intervertebral disc and its lower pole at the middle of L3 vertebra. The hilum was facing antero-medially and the vessels had a typical position and overall anatomy. The left kidney was found to be ectopic and lying lower than the right kidney (Figure 1a). Its upper pole was at the level of lower bor-

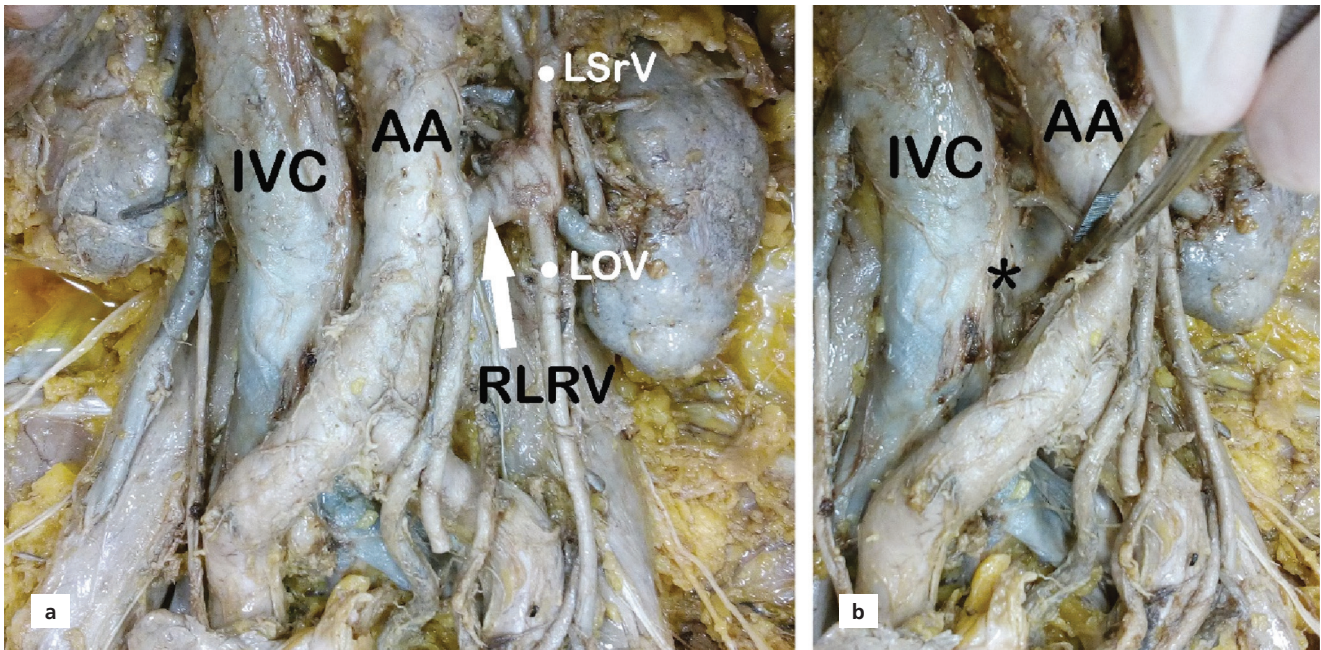


Figure 1. Photograph of the retroperitoneal space, presenting the formation and initial part of the RLRV (arrow) (a). In (b), the asterisk indicates the point where the RLRV joined the IVC behind the abdominal aorta. AA: abdominal aorta; IVC: inferior vena cava; LSrV: left suprarenal vein; LOV: left ovarian vein; RLRV: retroaortic left renal vein.

der of L1 vertebra and its lower pole – at the midpoint of L4 vertebra. The hilum was located at the level of L2/L3 intervertebral disk and was facing antero-medially. The left renal artery arose from the abdominal aorta at the level of L2 upper border and shortly after that divided into two renal arteries those are nearly of equal in size. Because of the left kidney ectopism, the two arteries descended almost vertically to reach the renal hilum. The left renal vein (Figure 1a) was formed outside the hilum by fusion of two primary tributaries. At the same confluent point, the left suprarenal vein from above and gonadal (ovarian) vein from beneath joined the left renal vein (Figure 1a). The left renal vein then passed infero-medially behind the abdominal aorta to join the IVC at the level of upper border of L4 ver-

tebra (Figure 1b). That was a point nearly 2 cm above the confluence of the common iliac veins. The length of the RLRV in our case was 7.5 cm, consistent with the findings in other studies.^[14,15] The long diameter of the vein was 2 cm at its proximal segment and 1.2 cm at the distal, suggesting a slight dilatation at its origin (normal range 1.2±0.2 cm).^[14]

Discussion

The variant left renal vein passing behind the abdominal aorta has been classified together with the anomalies of the IVC.^[1,7,8,12,13,16] Later, some classifications appeared, that grouped only the cases of an RLRV draining into a normal IVC (Figures 2a–d).^[12,17] Probably the most detailed classi-

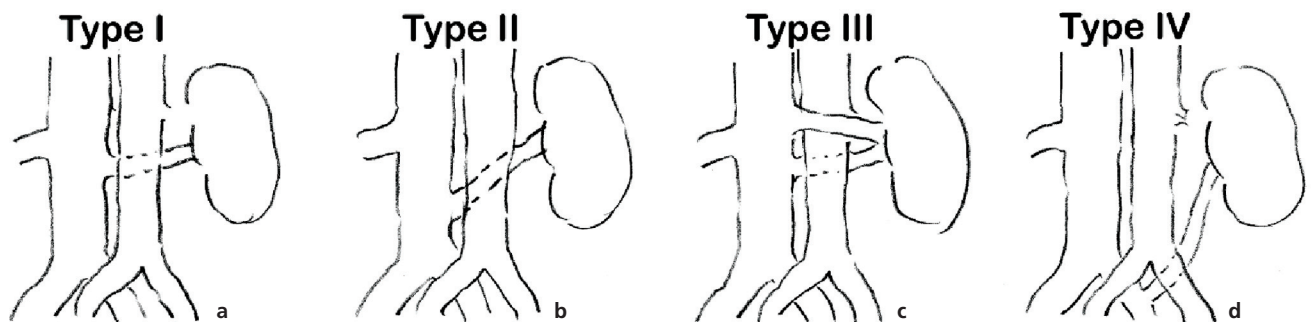


Figure 2. Current classification scheme of the RLRV: (a) RLRV Type I that drains into IVC at normal (orthotopic) position; (b) RLRV Type II that drains at a lower level of IVC (L4–L5); (c) circumaortic renal vein collar – composed of both preaortic and orthotopic retroaortic renal veins; (d) RLRV that drains much lower into the left common iliac vein.

fication of the renal vein variations is presented in the paper of Zhu et al.^[18] These authors have defined five types and many subtypes of the left renal vein variations. All these unusual venous patterns can be explained with complicated embryonic development of the veins in the retroperitoneal space between the 7th– 10th weeks of gestation.^[8,16,19,20] The main event in the development of the renal veins is formation of circumaortic renal vein collar formed from the intersupracardinal anastomosis dorsally, the intersubcardinal anastomosis and postsubcardinal anastomoses ventrally, and the suprasubcardinal anastomosis laterally. Moreover, the embryonic kidneys are drained by paired ventral and dorsal venous limbs, with the latter later regressing. The persist-

ence of the dorsal venous limb, as well as the dorsal part of the circumaortic venous collar are the possible embryological bases of RLRV development.^[8,16,20,21]

The most common classification system of RLRV includes four types (Figures 2a–d)^[1,2,13,17]: (1) RLRV Type I that drains into IVC at normal (orthotopic) position; (2) RLRV Type II that drains at a lower level of IVC (L4–L5); (3) circumaortic renal vein collar – composed of both preaortic and orthotopic retroaortic renal veins; (4) RLRV that drains much lower into the left common iliac vein. In the pertinent literature, however, some other left renal vein variations are described, that are not men-

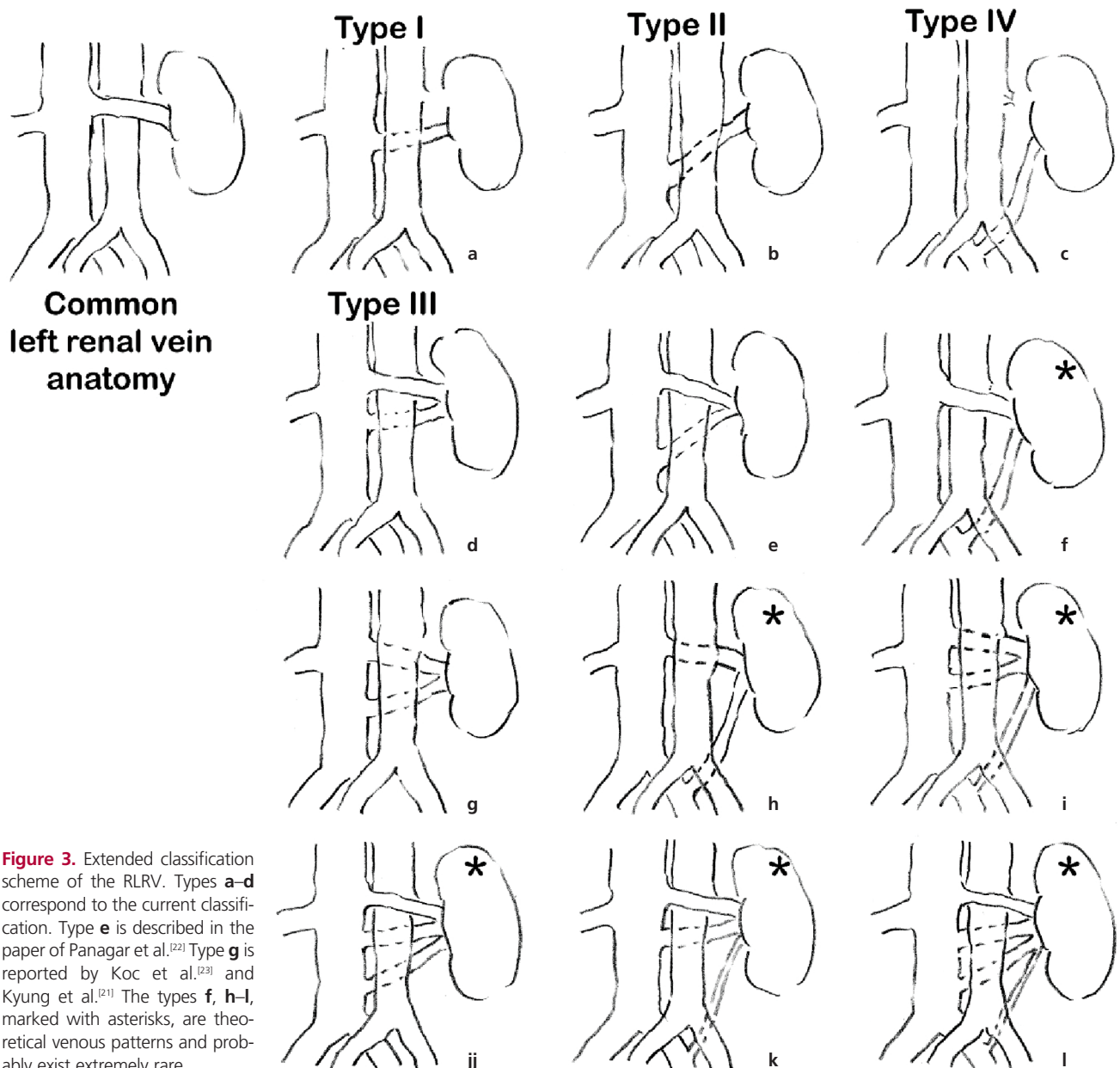


Figure 3. Extended classification scheme of the RLRV. Types a–d correspond to the current classification. Type e is described in the paper of Panagar et al.^[22] Type g is reported by Koc et al.^[23] and Kyung et al.^[21] The types f, h–l, marked with asterisks, are theoretical venous patterns and probably exist extremely rare.

tioned in this widespread classification. The circumaortic renal vein collar, for example, might be composed of preaortic renal vein and retroaortic renal veins draining at a lower level to IVC.^[22] Moreover, in the literature there are at least two reports of doubled RLRV.^[21,23] A case of tripled RLRV cannot also be excluded. All these additional variations can be explained with the developmental schemes presented in the paper of Kyung et al.^[21] Analyzing further the possible options for vascular development, much more extended classification might be presented (Figures 3a–l). After all, to memorize such an extended classification is not very practical, so instead, a typological scheme of the left renal vein variations can be extracted (Figure 4) with the following main conclusions:

- The RLRV can drain at orthotopic position to IVC, or at a lower level of IVC (L4–L5), or much lower into the left common iliac vein;
- A doubled or possibly tripled RLRV may exist with veins draining both at normal and lower levels to IVC;
- Any of the aforementioned RLRV might be accompanied by a normal pre-aortic left renal vein, thus forming a renal vein collar.

The incidence of RLRV varies greatly between the different groups examined. Karkos et al.^[1] mentioned that RLRV can be found in 0.8 to 3.7% in autopsy, on CT scans, and in surgical series. In a more detailed review of the literature with meta-analysis, Yi et al.^[6] estimated this vascular variation in 0.5–3.5% of cadaver dissections and 0.4–9.3% of clinical studies. Karaman et al.^[2] studied on MDCT angiographies the presence of RLRV in patients with urological symptoms (hematuria, abdominal/ left flank pain, varicocele on the left side) and calculated an incidence of 2.37%.

The variant left renal vein passing behind the aorta may remain unrecognized or to be named as posterior nutcracker phenomenon if an increased venous pressure, vein dilation and collateral formation is identified.^[9,24] When the dilatation becomes symptomatic, the posterior nutcracker syndrome is diagnosed.^[9,11,24] In the currently reported case, dilatation of the proximal segment of the vein was present, yet there was no data for any clinical manifestation.

The reported venous variation has a definite significance for aortic surgery.^[13,25,26] Brener et al.^[25] reported an injury to RLRV during aortic reconstruction in 40% of the operations. The complications varied from hemorrhage that can be controlled via reconstruction to nephrectomy, but such a venous injury is often fatal.^[26] To encounter an RLRV during reconstruction of abdominal aorta aneurysms is also not a rare case.^[27,28] A specific pathology is the rupture of the aortic aneurysm toward the RLRV with formation of an aorto-venous fistula.^[29–31]

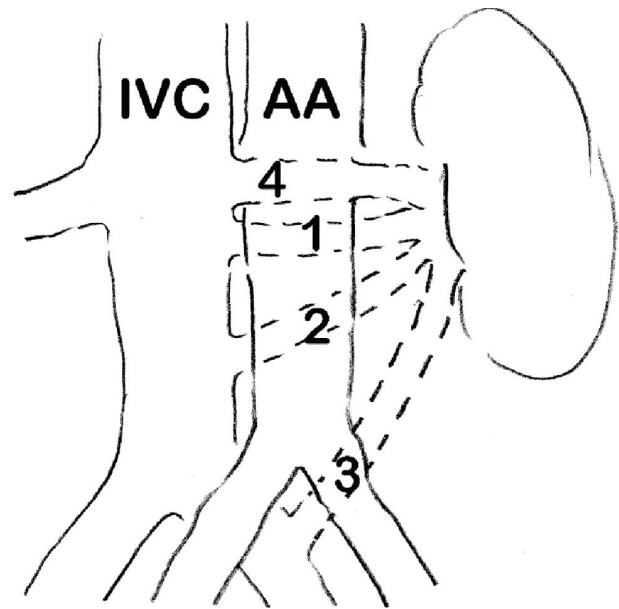


Figure 4. Typological scheme of the left renal vein variations. 1: retroaortic left renal vein draining at orthotopic level; 2: retroaortic left renal vein draining at lower level of the IVC; 3: retroaortic left renal vein draining at the level of left common iliac vein; 4: normal “preaortic” left renal vein.

Acknowledgments

The authors wish to sincerely thank those who donated their bodies to science so that anatomical research could be performed. Results from such research can potentially improve patient care and increase mankind’s overall knowledge. Therefore, these donors and their families deserve our highest gratitude.

Conflict of Interest

The authors declare no conflict of interest.

Author Contributions

NK: data collection, conception and design of the article, drafting the article, approval of the final version; YT: data collection, drafting the article, approval of the final version; LM: analysis and interpretation of the data, article revision, approval of the final version; LJ: conception and design of the article, analysis and interpretation of the data, article revision, approval of the final version.

Ethics Approval

The studies using bone or cadaver specimens are regulated by Medical University of Sofia. There were no ethical violations in the creation of this work.

Funding

The authors received no financial support for this study.

References

- Karkos CD, Bruce IA, Thomson GJ, Lambert ME. Retroaortic left renal vein and its implications in abdominal aortic surgery. *Ann Vasc Surg* 2001;15:703–8.
- Karaman B, Koplay M, Ozturk E, Basekim CC, Ogul H, Mutlu H, Kizilkaya E, Kantarci M. Retroaortic left renal vein: multidetector computed tomography angiography findings and its clinical importance. *Acta Radiol* 2007;48:355–60.
- Tatar I, Töre HG, Çelik HH, Karcaaltincaba M. Retroaortic and circumaortic left renal veins with their CT findings and review of the literature. *Anatomy* 2008;2:72–6.
- Turamanlar O, Ünlü E, Toktaş M, Horata E, Songur A. Variation of right renal artery duplication with retroaortic left renal vein: a case report. *Anatomy* 2015;9:91–3.
- Dilli A, Ayaz UY, Karabacak OR, Tatar IG, Hekimoglu B. Study of the left renal variations by means of magnetic resonance imaging. *Surg Radiol Anat* 2012;34:267–70.
- Yi SQ, Ueno Y, Naito M, Ozaki N, Itoh M. The three most common variations of the left renal vein: a review and meta-analysis. *Surg Radiol Anat* 2012;34:799–804.
- Hoeldt W, Hrubby W, Aharinejad S. Renal vein anatomy and its implications for retroperitoneal surgery. *J Urol* 1990;143:1108–14.
- Bass JE, Redwine MD, Kramer LA, Huynh PT, Harris JH Jr. Spectrum of congenital anomalies of the inferior vena cava: cross-sectional imaging findings. *Radiographics* 2000;20:639–52.
- Kurklinsky AK, Rooke TW. Nutcracker phenomenon and nutcracker syndrome. *Mayo Clin Proc* 2010;85:552–9.
- Hangge PT, Gupta N, Khurana A, Quencer KB, Albadawi H, Alzubaidi SJ, Knuttinen M-G, Naidu SG, Oklu R. Degree of left renal vein compression predicts nutcracker syndrome. *J Clin Med* 2018;7:107.
- Ali-El-Dein B, Osman Y, Shehab El-Din AB, El-Diasty T, Mansour O, Ghoneim MA. Anterior and posterior nutcracker syndrome: a report on 11 cases. *Transplant Proc* 2003;35:851–3.
- Shindo S, Kubota K, Kojima A, Iyori K, Ishimoto T, Kobayashi M, Kamiya K, Tada Y. Anomalies of inferior vena cava and left renal vein: risks in aortic surgery. *Ann Vasc Surg* 2000;14:393–6.
- Knipp B, Knechtges P, Gest T, Wakefield T. Inferior vena cava: embryology and anomalies. In: Upchurch GR Jr, Criado E, editors. *Aortic aneurysms: pathogenesis and treatment*. New York (NY): Humana Press; 2009. p. 289–307.
- Satyapal KS, Rambiritch V, Pillai G. Morphometric analysis of the renal veins. *Anat Rec* 1995;241:268–72.
- Kumaresan M, Sankaran PK, Gunapriya R, Karthikeyan G, Priyadarshini A. Morphometric study of renal vein and its variations using CT. *Indian Journal of Medical Research and Pharmaceutical Sciences* 2016;3:41–9.
- Minniti S, Visentini S, Procacci C. Congenital anomalies of the venae cavae: embryological origin, imaging features and report of three new variants. *Eur Radiol* 2002;12:2040–55.
- Nam JK, Park SW, Lee SD, Chung MK. The clinical significance of a retroaortic left renal vein. *Korean J Urol* 2010;51:276–80.
- Zhu J, Zhang L, Yang Z, Zhou H, Tang G. Classification of the renal vein variations: a study with multidetector computed tomography. *Surg Radiol Anat* 2015;37:667–75.
- Chuang VP, Mena CE, Hoskins PA. Congenital anomalies of the left renal vein: angiographic consideration. *Br J Radiol* 1974;47:214–8.
- Guttman G, Endean E. Embryology. In: Cronenwett J, Johnston W, editors. *Rutherford's vascular surgery*. Vol. 1. 7th ed. Philadelphia (PA): Saunders Elsevier; 2010. pp. 15–30.
- Kyung DS, Lee JH, Shin DY, Kim DK, Choi IJ. The double retroaortic left renal vein. *Anat Cell Biol* 2012;45:282–284.
- Panagar AD, Subhash LP, Suresh BS, Nagaraj DN. Circumaortic left renal vein – a rare case report. *J Clin Diagn Res* 2014;8:111–2.
- Koc Z, Ulsan S, Tokmak N, Oguzkurt L, Yildirim T. Double retroaortic left renal veins as a possible cause of pelvic congestion syndrome: imaging findings in two patients. *Br J Radiol* 2006;79:e152–5.
- Shin JI, Lee JS. Nutcracker phenomenon or nutcracker syndrome? *Nephrol Dial Transplant* 2005;20:2015.
- Brener BJ, Darling RC, Frederick PL, Linton RR. Major venous anomalies complicating abdominal aortic surgery. *Arch Surg* 1974;108:159–65.
- Kim MK, Ku YM, Chun CW, Lee SL. MDCT findings of right circumaortic renal vein with ectopic kidney. *Korean J Radiol* 2013;14:786–8.
- Calligaro KD, Savarese RP, DeLaurentis DA. Unusual aspects of aortovenous fistulas associated with ruptured abdominal aortic aneurysms. *J Vasc Surg* 1990;12:586–90.
- Polguy M, Stefafczyk K, Stefafczyk L. Coexistence of the aortic aneurysm with the main vein anomalies: its potential clinical implications and vascular complication. In: Kirali K, editor. *Aortic aneurysm*. Rijeka, Croatia: IntechOpen; 2017. Chapter 8. pp. 129–42.
- Mansour MA, Rutherford RB, Metcalf RK, Pearce WH. Spontaneous aorto-left renal vein fistula: the “abdominal pain, hematuria, silent left kidney” syndrome. *Surgery* 1991;109:101–6.
- Meyerson SL, Haider SA, Gupta N, O'Dorsio JE, McKinsey JF, Schwartz LB. Abdominal aortic aneurysm with aorta-left renal vein fistula with left varicocele. *J Vasc Surg* 2000;31:802–5.
- Savarese LG, Trad HS, Joviliano EE, Muglia VF, Elias Junior J. Fistula between the abdominal aorta and a retroaortic left renal vein: a rare complication of abdominal aortic aneurysm. *Radiol Bras* 2017;50:407–8.
- Stoyanova B, Nikolov N, Lukanova D, Stankev M, Atanasov A. Case report of ruptured aneurysm of the abdominal aorta to retro-aortic renal vein. [Article in Bulgarian] *Angiology and Vascular Surgery* 2017;3:42–8.

ORCID ID:

N. Krastev 0000-0002-7276-3707;
 Y. Tivcheva 0000-0002-9886-4266;
 L. Malinova 0000-0002-6928-1483;
 L. Jelevev 0000-0001-8596-7867



Correspondence to: Lazar Jelevev, MD, PhD

Department of Anatomy, Histology and Embryology,
 Medical University of Sofia, Sofia, Bulgaria
 Phone: +359-897-87-27-51
 e-mail: ljelev@abv.bg

Conflict of interest statement: No conflicts declared.

This is an open access article distributed under the terms of the Creative Commons Attribution-NonCommercial-NoDerivs 4.0 Unported (CC BY-NC-ND4.0) Licence (<http://creativecommons.org/licenses/by-nc-nd/4.0/>) which permits unrestricted noncommercial use, distribution, and reproduction in any medium, provided the original work is properly cited. *How to cite this article:* Krastev N, Tivcheva Y, Malinova L, Jelevev L. Retroaortic left renal vein: a clinically significant vascular variation with suggestion of a practical typological scheme. *Anatomy* 2022;16(1):41–45.

Rufus of Ephesus: a historical perspective on his contributions to neuroanatomy

Esra Candar¹ , İbrahim Demirçubuk² , Gülgün Şengül¹⁻³ 

¹Department of Neuroscience, Institute of Health Sciences, Ege University, Izmir, Türkiye

²Department of Anatomy, Institute of Health Sciences, Ege University, Izmir, Türkiye

³Department of Anatomy, School of Medicine, Ege University, Izmir, Türkiye

Abstract

Rufus of Ephesus (circa 1–2 AD) lived in the ancient city of Ephesus, Izmir Province of Turkey. He made significant contributions to many branches of sciences including neuroanatomy. This historical perspective manuscript focuses mainly on his neuroanatomical contributions. He described several structures, such as the pericranium, meninges, encephalon, parencephalon, varicosities, and the anatomy of the sellar region and the eye. He also coined essential terms in the nervous system such as tunica prima (dura mater), tunica altera (pia mater), spinal marrow (spinal cord), base of brain (brainstem), and choroid tunic (choroid plexus). Because of the limited number of extant works, he is not as well-known as his contemporaries. Yet, Rufus of Ephesus deserves to be recognized to the fullest for his precious and numerous contributions to neuroanatomy.

Keywords: history of science; neuroanatomy; Rufus of Ephesus

Anatomy 2022;16(1):46–50 ©2022 Turkish Society of Anatomy and Clinical Anatomy (TSACA)

Introduction

Rufus of Ephesus lived between the first and second centuries AD.^[1,2] The name of the Rufus comes from the residence in Ephesus, Izmir Province of Turkey. He practiced there and assumably in the medical center in Rome, after education at the Alexandria medical school in Egypt.^[3,4] He has worked in several fields, such as anatomy, cardiology, psychiatry, nephrology, and ophthalmology. In addition, he has used botanicals to treat various ailments.^[1,2,5,6]

Works of Rufus of Ephesus

Rufus, although he wrote more than a hundred books on several topics, is not as well known as his contemporaries because of the limited number of extant full pieces. For this reason, quotes, fragments, translations, and compilations, besides complete treatises, are especially important for his reputation and reconstruction of his works.^[2,4,7,8] His works were published in various languages such as Latin,^[9–11] Greek,^[12] French (**Figure 1a–f**).^[13,14]

Many of his works (**Figure 1f**) were collected, extracted from quotations, and translated into French in *Oeuvres*

de Rufus d'Ephèse by Charles Daremberg and Emille Ruelle in 1879. Galen (130–200 AD), Oribasius (326–403 AD), Aetius of Amida (500–550 AD), Alexander of Tralles (525–605 AD), Abu Bakr Muhammad ibn Zakaria Razi (865–925 AD) quoted the works of Rufus. Aside from the names included in this book, Rufus was cited by numerous authors such as Avicenna (980–1037), Gilbertus Anglicus (1180–1250), Ibn el Baitar (1197–1248), and Ibn Abi Usaybiah (1203–1270).^[2,7,14,15] Indeed, these indicate that Rufus of Ephesus left his mark on many cultures and geographies through the centuries.

The first anatomical terminology pioneering work is thought to be his' work *On the Names of the Parts of the Human Body*.^[9,10,12,14,16] English names of his well-known books are *On Kidneys and Bladder Diseases*,^[10–12,14] *On Satyriasis and Gonorrhoea*, *On the Interrogation of the Patient*,^[14] *Treatise on Pulses*,^[13,14] *On Melancholy*,^[17] *On Gout*,^[14] and *On Icterus*.^[18]

Because of his work on *Drug Clearance*,^[10–12] he was associated with “*pilule Ruffi*” (*Rufus' pills*) owing to his expertise in pharmacology. He was portrayed with other



Figure 1. Book covers featuring the works of Rufus of Ephesus. (a) Latin version;^[9] (b) Latin version;^[10] (c) Greek version edited by Jacques Goupyl and Adrien Turnèbe;^[12] (d) French version of Treatise on Pulses;^[13] (e) Latin version edited by William Clinch in 1726;^[11] (f) works of Rufus of Ephesus; a text collated on his manuscripts, translated for the first time into French, with an introduction / publication started by Charles Daremberg, and finished by Emile Ruelle, 1879^[14] (Cover pictures reproduced from Public Domain Materials).

medical celebrities in one of the most famous pharmacological and medical manuscripts, *De Materia Medica* (Figure 2a and b).^[19] Pedanius Dioscorides (20–70 AD) wrote *De Materia Medica* (On Medical Matters) in about 65 AD. The illustrated and alphabetical version of this pharmacopeia was accomplished about 512–525 AD in Constantinople (now Istanbul, Turkey). This volume was named “*Juliana Anicia Dioscorides*”, “*Juliana Anicia Codex*” or “*Codex Vindobonensis*”, because it was prepared for Princess Juliana Anicia, daughter of the Emperor of the Western Roman Empire, Anicius Olybrius.^[20,21]

Perspectives on Neuroanatomy

The Surgeon Anatomist

Rufus described cerebral berry aneurysms for the first time,^[22] and therefore was known as *Magister Chirurgiae*.^[21] His surgical skills developed out of his experience in dissection and knowledge of anatomy. He used primates for dissection under culturally restricted circumstances.^[23,24] In terms of anatomical features, he selected primates that sig-

nificantly corresponded to humans, and dissected animals from head to toe (*capite ad calcem*) in parallel with inspection. To compare anatomy with the exterior parts of the body, he used a slave as a human model. He described structures in considerable detail while taking account of his technique and era.^[4,25]

Neuroanatomical Contributions of Rufus

Rufus described the brain, the spinal cord, nerves, and ventricles as separate neuroanatomical structures and as parts of a whole, the nervous system.^[26,27] Thus, he identified them as connected structures with distinct anatomic components.^[28]

He named the bone membrane beneath the scalp “*pericranium*” and defined its junctions, which correspond to the coronal suture (*sutura coronalis*), sagittal suture (*sutura sagittalis*) and lambdoid suture (*sutura lambdoidea*) in today’s terminology.^[1,25,29]

Taking an integrated approach to neuroanatomy, Rufus used “osteomeninges” which is a fundamental oste-



Figure 2. Seven named physicians and botanists of the classical world. Watercolour painting. Early portraits of Greek medical celebrities from a manuscript by Juliana Anicia Dioscorides circa 500 AD, now in the Library of St. Mark’s, Venice. (a) In the middle: Galen, left with respect Crateus the botanist, Apollonius Mus, or of Pergamon, Andreas of Carystus; right: Dioscorides, Nikandros of Colophon, and Rufus of Ephesus; (b) zoom in on Rufus of Ephesus.^[19]

ology term for bones in cavities.^[1,25] According to Rufus, the membranes that surround the nervous system are defined as two types of “meninges”: the term “encephalitic meninx” for the inner part of the pericranium; and the “dorsal meninx” which is located throughout the back, and the marrow is filled it in.^[1,25,30] He mentioned that the spinal marrow descended from the encephalon as an extension, making an exit through a foramen in the skull at the occiput, which continued throughout all of the vertebrae.^[28] Rufus defined the meninges as robust in two layers with dissimilarity in thickness. The thicker is called “*tunica prima*” which is attached to the bone, and the thinner one is “*tunica altera*” which is adhered to the “encephalon”. The terms “dura mater” and “pia mater” were alluded to as earlier synonyms by him.^[25,30]

Rufus stated that the brain substance is in ash-gray color, but did not name the gray matter sections of the central nervous system.^[30] He described the spinal marrow as an extension of the brain composing of identical constituents.^[28] Yet, he did not mention a distinction between the gray matter regions and white matter tracts in the central nervous system. As a synonym for the cerebral gyri in humans, he used the term “varicosities” accounted for the cerebral cortex gray matter.^[30] He referred the upper parts of the brain with the term “varicose”, and the dorsal and lower parts with the term “base”.^[1,25,30] His definition of the “base of the brain” is possibly the first indication of the brainstem.^[30] He also referred to an extension as the “parencephalon”^[1,25] consequently stating an obvious distinction between the cerebrum and the cerebellum.^[31]

The first description of the choroid plexus was by Rufus who used the term “choroid tunic”.^[30] He defined this structure along with the ependyma,^[32] which covered the hollows inside the encephalon, and the of “*belly of the brain*” attributed to the ventricles.^[25] Rufus was well-informed concerning the ventricular system. He comprehensively clarified the lateral, third and fourth ventricles along with the aqueduct of the midbrain.^[23,31] However, Rufus is presumed to cause the misinterpretation that the pia is present in the lateral and third ventricles, but not in the fourth.^[30]

Rufus was one of the first to refer to the hypothalamic part of the third ventricle by the term “*infundibulum*”. In addition to this term, he previously used the words the “ditch” and the “hollow”. The term “*pelvis*” (“basin”, in English language) is referred to by him as the greater part of the hypothalamus, which also contains the infundibulum. The “infundibular stem” was described by Rufus, without knowledge regarding the tuberal part of the anterior lobe.^[30]

Due to his particular interest in the sellar region, he examined the neighboring structures of the ventricular system.^[23] He was among the first who identified the optic chiasm and agreed on its connection to vision, like his contemporaries Hippocrates, Herophilus, Erasistratus, and Galenus.^[23,31] Although Rufus did not give a name, he explained that fibers of the optic nerve crossed in the optic chiasm. He also did some studies on the anatomy of the eye.^[30]

Rufus is likely to be the first person who indicated the presence of an anterior chamber in the eyeball.^[33] He described the crystalline lens located very close to contact the iris.^[5] His descriptions of three ocular membranes are as follows: the first one, called the cornea, is smooth and in the form of a grape. The second choroid membrane is called “*grape-like*” due to its roughness. He named the third arachnoid membrane that surrounds the vitreous as “*crystalline*”. Rufus also cited that Herophilus named the “retina” based on its reticulated form.^[25]

Conclusion

Although most of his works are lost, the remaining fragments and quotes reveal Rufus as being ahead of his time. Consequently, Rufus deserves high credit for his unique contributions to neuroanatomy.

Acknowledgments

The authors would like to thank the Council of Higher Education (CoHE) of Turkey for funding Esra Candar under “100/2000 CoHE Ph.D. Scholarship Program” in “Translational Medicine”.

Conflict of Interest

The authors declare no conflict of interest.

Funding

The authors reported there is no funding associated with the work featured in this article.

References

1. Aciduman A, Arıtürk I, Ilgili O. Efesli Rufus’un nöroanatomi çalışmaları. *Türk Nöroşirürji Dergisi* 2010;20:64–9.
2. Eknayan G. Rufus of Ephesus and his “diseases of the kidneys”. *Nephron* 2002;91:383–90.
3. Pearce JMS. Early contribution of Alexandria medical school to the anatomy, physiology and pathology of the nervous system. *Rev Neurol* 2019;175:119–25.
4. Bujalkova M. Rufus of Ephesus and his contribution to the development of anatomical nomenclature. *Acta Med Hist Adriat* 2011;9:89–100.

5. Leffler CT, Hadi TM, Udupa A, Schwartz SG, Schwartz D. A medieval fallacy: the crystalline lens in the center of the eye. *Clin Ophthalmol* 2016;10:649–62.
6. Candar E, Şengül G. Rufus of Ephesus – the precious historical insight into neuroscience. *Anatomy* 2019;13:S78–79.
7. Pormann PE. New fragments from Rufus of Ephesus' on melancholy (24a-d) and on preferring fresh poppies. *Classical Quarterly* 2019;69:355–62.
8. Rey R. The history of pain. Cambridge: Harvard University Press; 1995. 394 p.
9. Aretaeus of C, Rufus of E. *Ruffi Ephesii de corporis humani partium appellationibus libri tres*. Grassi GP, editor. Venetiis: Apud Juntas; 1552. 240 p.
10. Aretaeus of C, Rufus of E. *Aretaei Cappadocis medici libri VIII / Ruffi Ephesii de hominis partibus libri III*. Crasso IP, editor. Paris: Apud Guilieum Morelium & Jacobum Puteanum; 1554. 600 p.
11. Rufus of E. *De vesicae renumque morbis: de purgantibus medicamentis, de partibus corporis humani*. Clinch G, editor. Cornhill: J. Bettenham; 1726. 72 p.
12. Rufus of E, Soranos of E. *Ruffi Ephesii de vesicae renumque morbis; de purgantibus medicamentis; de partibus corporis humani; Sorani de utero & muliebri pudendo*. Goupyl J, Turnèbe A, editors. Paris: Apud Adr. Turnebum Typographum Regium; 1554. 60 p.
13. Daremberg C. *Traité sur le poulx, attribué à Rufus d'Éphèse, public pour la première fois en grec et en Français, avec une introduction et des notes*. London: J. Bettenham; 1846. 47 p.
14. Daremberg C, Ruelle E. *Oeuvres de Rufus d'Éphèse: texte collationné sur les manuscrits, traduit pour la première fois en Français, avec une introduction*. Paris: Imprimerie Nationale; 1879. 678 p. [Internet] [retrieved on March 18, 2021]. Available from: <https://www.biusante.parisdescartes.fr/histmed/medica/cote?36058>
15. Bloom DA, McGuire EJ, Lapidus J. A brief history of urethral catheterization. *J Urol* 1994;151:317–25.
16. Kachlik D, Baca V, Bozdechova I, Cech P, Musil V. Anatomical terminology and nomenclature: past, present and highlights. *Surg Radiol Anat* 2008;30:459–66.
17. Pormann PE. *Rufus of Ephesus: on melancholy*. Darmstadt: Mohr Siebeck Tübingen; 2008. 331 p.
18. Ullmann M. *Die Schrift des Rufus von Ephesos über die Gelbsucht: in Arabischer und Lateinischer Übersetzung*. Göttingen: Vandenhoeck & Ruprecht; 1983. p. 87.
19. Wellcome Library. Seven named physicians and botanists of the classical world. Watercolour painting. Public Domain. London: Wellcome Library no. 543397i. [Internet] [retrieved on July 27, 2021]. Available from: <https://wellcomecollection.org/works/ggeuzb48>
20. Janick J, Stolarczyk J. Ancient Greek illustrated Dioscoridean herbals: origins and impact of the Juliana Anicia Codex and the Codex Neopolitanus. *Not Bot Horti Agrob* 2012;40:9–17.
21. Osler W. Remarks on arterio-venous aneurysm. *Lancet* 1915;185:949–55.
22. Meyermann R, Yasargil MG. Ultrastructural studies of cerebral berry aneurysms obtained operatively. Schiefer W, Klingler M, Brock M, editors. *Brain abscess and meningitis advances in neurosurgery*. Vol 9. Berlin: Springer; 1981. p. 174–81.
23. Costea CF, Turliuc Ş, Buzduga C, Cucu AI, Dumitrescu GF, Sava A, et al. The history of optic chiasm from antiquity to the twentieth century. *Childs Nerv Syst* 2017;33:1889–98.
24. Rose FC. The neurology of ancient Greece – an overview. *J Hist Neurosci* 1994;3:237–60.
25. Gersh CJ. *Naming the body: a translation with commentary and interpretive essays of three anatomical works attributed to Rufus of Ephesus [Doctorate]*. Michigan: University of Michigan; 2012. p. 210.
26. Rose FC. Cerebral localization in antiquity. *J Hist Neurosci* 2009;18:239–47.
27. Swanson LW. Quest for the basic plan of nervous system circuitry. *Brain Res Rev* 2007;55:356–72.
28. Elhadi AM, Kalb S, Perez-Orribo L, Little AS, Spetzler RF, Preul MC. The journey of discovering skull base anatomy in ancient Egypt and the special influence of Alexandria. *Neurosurg Focus* 2012;33:1–13.
29. Federative International Programme for Anatomical Terminology (FIPAT). *Terminologia anatomica*. 2nd ed. 2019. [Internet]. [revised on August 16, 2021]. Available from: <http://www.FIPAT.library.dal.ca>
30. Swanson LW. *Neuroanatomical terminology: a lexicon of classical origins and historical foundations*. New York: Oxford University Press; 2014. 1054 p.
31. Goodrich JT. Landmarks in the history of neurosurgery. Ellenbogen RG, Sekhar LN, Kitchen ND, Silva HB, editors. *Principles of neurosurgical surgery*. 4th ed. Philadelphia (PA): Elsevier; 2018. p. 1–37.e3.
32. Liddel SA. Development of the choroid plexus and blood-CSF barrier. *Front Neurosci* 2015;9:1–13.
33. Mark HH. Aqueous humor dynamics in historical perspective. *Surv Ophthalmol* 2010;55:89–100.

ORCID ID:

E. Candar 0000-0001-5408-5570;
 I. Demirçubuk 0000-0002-6574-9587;
 G. Şengül 0000-0002-5826-7379

**Correspondence to:** Esra Candar, MSc

Department of Neuroscience, Institute of Health Sciences,
 Ege University, Izmir, Turkey
 Phone: +90 535 363 15 81
 e-mail: esracandar3@gmail.com

Conflict of interest statement: No conflicts declared.

This is an open access article distributed under the terms of the Creative Commons Attribution-NonCommercial-NoDerivs 4.0 Unported (CC BY-NC-ND4.0) Licence (<http://creativecommons.org/licenses/by-nc-nd/4.0/>) which permits unrestricted noncommercial use, distribution, and reproduction in any medium, provided the original work is properly cited. *How to cite this article:* Candar E, Demirçubuk İ, Şengül G. Rufus of Ephesus: a historical perspective on his contributions to neuroanatomy. *Anatomy* 2022;16(1):46–50.

Table of Contents

Volume 16 / Issue 1 / April 2022

(Continued from back cover)

Case Report

Retroaortic left renal vein: a clinically significant vascular variation with suggestion of a practical typological scheme 41

Nikolai Krastev, Yoanna Tivcheva, Lina Malinova, Lazar Jelev

Historical View

Rufus of Ephesus: a historical perspective on his contributions to neuroanatomy 46

Esra Candar, İbrahim Demirçubuk, Gülgün Şengül

On the Front Cover:

Cancellous bone pattern of the mandibles on micro-CT images of the mandibles. (a) type I trabecular pattern; (b) type II osteoporotic pattern; (c) type III dense-irregular pattern (edentulous). **FM:** first molar; **MC:** mandibular canal; **SM:** second molar; **SP:** second premolar; **TM:** third molar; **UW:** superior wall of the mandibular canal. From Geneci F, Ocak M, Torun Bİ, Soysal H. The effect of tooth loss on the cancellous bone pattern of the mandible and on the superior bony wall of the mandibular canal: a micro-CT study. *Anatomy* 2022;16(1):1–6.

Table of Contents

Volume 16 / Issue 1 / April 2022

Original Articles

- The effect of tooth loss on the cancellous bone pattern of the mandible and on the superior bony wall of the mandibular canal: a micro-CT study** 1
Ferhat Geneci, Mert Ocak, Bilge İpek Torun, Handan Soysal
- The relationship between the body mass index and the subcutaneous adipose tissue** 7
Bilge İpek Torun, Mehtap Balaban, Ferhat Geneci, Şükrü Cem Hatipoğlu
- Sonoelastography findings of the patellar tendon in Osgood-Schlatter disease** 13
Mehtap Balaban, Sinem Sigit İkiz, İlkay S. İdilman
- The course of the sciatic nerve in the gluteal region and comparison of two methods used for sciatic nerve blockage** 19
Bilge İpek Torun, Ayşe Surhan Çınar, Luis Filgueira, R. Shane Tubbs , Alparslan Apan, Aysun Uz
- The analysis of morphological features and ultrasonographic characteristics of Dupuytren's disease** 26
Atilla Hikmet Çilengir, Mehtap Balaban
- The ultrasound elastography findings in lateral epicondylitis in comparison with healthy individuals** 33
Bilge İpek Torun, Serhan Eren, Mehtap Balaban

(Contents continued on inside back cover)